Aus dem Institut für Klinische Neuroimmunologie

der Ludwig-Maximilians-Universität München

Direktor: Prof. Dr. med. Martin Kerschensteiner

Die Dynamik des axoplasmatischen Retikulums in Modellen der Neuroinflammation und des spinalen Traumas

Dissertation

zum Erwerb des Doktorgrades der Medizin

an der Medizinischen Fakultät der

Ludwig-Maximilians-Universität zu München

vorgelegt von

Alexander Julian Scheiter

aus Herrenberg

2020

Mit Genehmigung der Medizinischen Fakultät

der Universität München

Berichterstatter:	Prof. Dr. Martin Kerschensteiner
Mitberichterstatter:	Prof. Dr. Frank Weber
	PD Dr. Stefan Kastenbauer
	PD Dr. Katharina Vill
Mitbetreuung durch den promovierten Mitarbeiter:	Prof. Dr. Thomas Misgeld
Dekan:	Prof. Dr. med. dent. Dr. h.c. Reinhard Hickel
Tag der mündlichen Prüfung:	19.05.2020

Table of Contents

List of Figures ..... **iv**

List of Tables ..... **vi**

List of Abbreviations ..... **vii**

Zusammenfassung ..... **x**

Summary ..... **xii**

1 Introduction **1**

1.1 Motivation **1**

1.2 Endoplasmic reticulum **3**

1.2.1 Neuronal ER 4

1.2.2 ER calcium homeostasis 7

1.2.3 ER stress and the UPR 10

1.2.4 ER contact sites 12

1.2.5 Structural ER dynamics 13

1.3 Axonal degeneration **15**

1.3.1 Modes of axonal degeneration 15

1.3.2 Molecular mechanisms of axonal degeneration 19

1.3.3 Axonal degeneration in MS and EAE 21

1.3.4 Traumatic axonal injury 26

1.3.5 ER calcium in axonal degeneration 27

1.4 Intravital calcium imaging **30**

1.4.1 Principles of calcium indicators 30

1.4.2 ER calcium indicators 33

1.4.3 Intravital microscopy of the nervous system 35

2 Objectives **38**

3 Materials and Methods **39**

3.1 Materials 39
3.1.1 Reagents 39
3.1.2 Tools and materials 44
3.1.3 Technical devices 47
3.1.4 Data analysis/Software 49
3.2 Methods 50
3.2.1 Molecular cloning 50
3.2.2 Experimental animals 54
3.2.3 Cell culture 54
3.2.4 AAV production and spinal cord injection 55
3.2.5 Explant imaging and laser transections 56
3.2.6 In vitro characterisation of calcium sensor 57
3.2.7 Generation of transgenic mice 58
3.2.8 Screening and immunohistochemistry of Thy-TwitchER mice 60
3.2.9 In-vivo 2-photon imaging of Thy1-TwitchER mice 62
3.2.10 Image processing and analysis 65
3.2.11 Statistical analysis 66
4 Results 67
4.1 Imaging intra-ER free calcium in single axons 67
4.1.1 Targeting and visualising the axonal ER 67
4.1.2 Twitch2B 54S+ ER can measure intra-ER free calcium 70
4.1.3 Generation and screening of Thy1-TwitchER transgenic mice 74
4.1.4 Thy1-TwitchER transgenic mice report intra-ER free calcium levels 77
4.2 Intra-ER free calcium in paradigms of axonal degeneration 78
4.2.1 ER calcium release occurs late and is not causative for FAD 79
4.2.2 ER calcium release occurs early in models of LiSCI and spinal cord contusion 83

5 Discussion 91

5.1 Imaging intra-ER free calcium in single axons: Accomplishments and limitations 91

5.1.1 Insights from structural imaging of axonal ER 91

5.1.2 Assessing the chosen ER calcium indicator 92

5.1.3 Remarks on the yielded transgenic lines 95

5.2 Discussing the role of intra-ER free calcium in paradigms of axonal degeneration 97

5.2.1 Identifying the source of detrimental calcium influx in EAE 98

5.2.2 Analysing the depletion ER calcium in traumatic axonal injury 104

5.3 Concluding remarks and outlook 106

6 References 109

7 Acknowledgements 124

8 Curriculum vitae 125

9 Affidavit / Eidesstattliche Versicherung 127

List of Figures

Figure 1: Structure of ER in soma and neurites 6

Figure 2: ER calcium signalling and CICR 9

Figure 3: Stages of FAD in EAE and MS 18

Figure 4: Cytoplasmic calcium levels predict axonal fate in neuroinflammatory lesions 25

Figure 5: Plasmid map pCMV-Twitch2B 54S+ ER 51

Figure 6: Thy-1 plasmid maps 53

Figure 7: Plasmid map pAAV-mEmeraldER 54

Figure 8: Experimental setup for in vitro sensor characterisation 58

Figure 9: Thy1-TwitchER linearisation and genotyping gels 60

Figure 10: ROI selection for data analysis 66

Figure 11: AAV-mEmeraldER spinal cord injections and explant laser transections 69

Figure 12: HEK cell ER calcium depletion and replenishment 71

Figure 13: Mutated EF hands Twitch2B control 73

Figure 14: Twitch2B 54 S+ ER expression in Thy1-TwitchER transgenic mouse lines 74

Figure 15: Twitch2B 54 S+ ER colocalisation with GRP78/BiP 76

Figure 16: Functional characterisation of the Thy1-TwitchER 481 transgenic mouse line with thapsigargin 77

Figure 17: ER calcium in EAE 80

Figure 18: Thapsigargin depletes ER calcium in EAE 81

Figure 19: Thy1-TwitchER laser transections 84

Figure 20: ER calcium in contusion model 87

Figure 21: Temporal dynamics of ER calcium in contusion model 89

Figure 22: Caffeine effect on $[Ca^{2+}]_{ER}$ and $[Ca^{2+}]_{cyt}$ 100

Figure 23: Removal of extracellular Ca^{2+} reverses cytoplasmic Ca^{2+} accumulation and prevents axon degeneration 102

Figure 24: ER calcium and fragmentation rate following spinal cord contusion 106

List of Tables

Table 1: Overview: physical properties of ER-GECIs 37

Table 2: Free-floating GRP78 BiP immunohistochemistry protocol 61

List of Abbreviations

Å	ångström, 10^{-10} m
AAD	acute axonal degeneration
AAV	adeno-associated virus
ACSF	artificial cerebrospinal fluid
AD	Alzheimer's disease
ALS/FTD	amyotrophic lateral sclerosis with associated frontotemporal dementia
AM	acetoxymethyl
AOTF	acousto optic tunable filter
APP	amyloid precursor protein
ATF4	activating transcription factor 4
ATF6	activating factor 6
ATP	adenosine triphosphate
BFP	blue fluorescent protein
CFP	cyan fluorescent protein
CICR	calcium-induced calcium release
CLAC	calcium load activated channel
CNS	central nervous system
CPA	cyclopiazonic acid
DHPR	dihydropyridine receptor
DLK	dual leucine zipper kinase
DMEM	Dulbecco’s Modified Eagle Medium
DMSO	dimethyl sulfoxide
EAE	experimental autoimmune encephalomyelitis
EGTA	ethylene glycol-bis(β-aminoethyl ether)-N,N,N',N'-tetraacetic acid
eIF2α	eukaryotic initiation factor 2α
ER	endoplasmic reticulum
FAD	focal axonal degenration
FP	fluorescent protein
FRET	fluorescence resonance energy transfer
g.s.	goat serum
GaAsP	gallium arsenide phosphide
GECI	genetically encoded calcium indicators
GFP	green fluorescent protein
GRP78/BiP	78 kDa glucose-regulated protein/ binding immunoglobulin protein
HBSS	Hank’s balanced salt solution
HHBSS	HEPES buffered Hank’s balanced salt solution
Ip3	inositol triphosphate
IP3R	inositol trisphosphate receptor
IRE1	inositol-requiring enzyme 1

K_d	dissociation constant
LiSCI	laser-induced spinal cord injury
MAM	mitochondria-associated ER membrane
MCU	mitochondrial calcium uniporter
MOG	myelin oligodendrocyte glycoprotein
MPTP	mitochondrial permeability transition pore
MS	multiple sclerosis
NAD+	nicotinamide adenine dinucleotide
NE	nuclear envelope
NMJ	neuromuscular junctions
NMN	nicotinamide mononucleotide
NMNAT1	nicotinamide mononucleotide adenyltransferase 1
nNOS	neuronal nitric oxide synthase
PBS	phosphate buffered saline
PD	Parkinson's disease
PEG	polyethylene glycol
PERK	PKR-like endoplasmic reticulum kinase
PFA	paraformaldehyde
pK_a	acid dissociation constant
PMT	photomultiplier tube
PPWM	periplaque white matter
Ptx	pertussis toxin
RER	rough endoplasmic reticulum
RNS	reactive nitrogen species
ROI	region of interest
ROS	reactive oxygen species
RT	room temperature
RyR	ryanodine receptor
SARM1	sterile alpha and TIR motif-containing protein
SCI	spinal cord injury
SER	smooth endoplasmic reticulum
SERCA	sarco/endoplasmic reticulum Ca2+-ATPase
SOCE	store-operated calcium entry
SR	sarcoplasmic reticulum
STIM	stromal interaction molecules
T	triton X-100
TAI	traumatic axonal injury
TBI	traumatic brain injury
TED	targeted-esterase induced dye loading
Thy1-TwitchER	Thy1-Twitch2B 54S+ ER
TMBIM	transmembrane BAX inhibitor motif-containing
TMCO1	protein transmembrane and coiled-coil domains 1
TPLSM	two-photon laser-scanning microscopy
UPR	unfolded protein response
VDAC	voltage-dependent anion channel

WD	Wallerian degeneration
Wld^S	slow Wallerian degeneration phenotype
XBP1	X-box binding protein 1
YFP	yellow fluorescent protein

Zusammenfassung

Kalzium ist von zentraler Bedeutung im Prozess der axonalen Degeneration. In Vorarbeiten zu der hier vorliegenden Arbeit gelang es mittels intravitaler 2-Photonen-Mikroskopie nachzuweisen, dass der Anstieg des intraaxonalen zytoplasmatischen Kalziums maßgeblich das Schicksal von Axonen in neuroinflammatorischen Läsionen beeinflusst. Axone mit erhöhtem zytoplasmatischem Kalziumgehalt zeigten eine höhere Tendenz den Degenerationsprozess der so genannten fokalen axonalen Degeneration (FAD) bis hin zur irreversiblen Fragmentierung zu durchlaufen. Als mögliche Quelle des beobachteten Kalziumanstiegs in läsionalen Axonen der experimentellen Autoimmunenzaphalomyelitis (EAE), einem Mausmodell der Multiplen Sklerose, war das endoplasmatische Retikulum (ER) mit einer Kalziumkonzentration, die das Zehntausendfache der zytoplasmatischen Kalziumkonzentration betragen kann, von besonderem Interesse.

Um Messungen der Kalziumkonzentration des endoplasmatischen Retikulums durchführen zu können, exprimierten wir zunächst den Kalziumindikator Twitch2B 54 S+ im endoplasmatischen Retikulum und charakterisierten den Sensor in HEK293-Zellen. Die Vorteile dieses Kalziumindikators liegen darin, dass er genetisch kodiert ist und ratiometrische Messungen erlaubt, welche eine Voraussetzung für die in-vivo Mikroskopie darstellen. Mit Twitch2B 54 S+ ER unter der Kontrolle des neuronalen Thy1 Promoters generierten wir transgene Mauslinien, welche wir nach für die intravitale spinale 2-Photonen-Mikroskopie geeigneten spinalen axonaler Expressionsmustern auswählten und pharmakologisch charakterisierten. Unter in-vivo Bedingungen konnte nach ER-Kalzium Depletierung durch Zugabe des SERCA-Inhibitors Thapsigargin ein Sensor-Dynamikbereich von 300 Prozent (Rmax/Rmin) ermittelt werden. Im weiteren Verlauf untersuchten wir mit den Thy1-TwitchER Mäusen auch die FAD. Eine Reduktion des ER-Kalziumgehalts konnte hier nur in irreversibel geschädigten, fragmentierten Axonen gemessen werden. Somit war es möglich, eine ER-Kalziumfreisetzung als Ursache für den in der FAD beobachteten frühen zytoplasmatischen Kalziumanstieg auszuschließen. Nachfolgende Experimente unserer Arbeitsgruppe konnten stattdessen plasmalemmale Nanoporen als Eintrittspforte des vermehrten zytoplasmatischen Kalziums in EAE-Läsionen identifizieren.

Im Unterschied zur FAD konnte in einem spinalen Kontusionsmodell sowie in spinalen Laserläsionen eine deutliche ER-Kalziumfreisetzung gemessen werden. Diese Depletierung ging mit strukturellen Alterationen in Form einer ER Fragmentierung einher. Der Prozess der ER Fragmentierung war bisher nur in Dendriten in einem Herzstillstand-Modell beschrieben. Die beobachtete traumatische ER Fragmentierung und ER Kalziumdepletierung waren über einen Zeitraum von mehreren Stunden partiell reversibel.

In der Zukunft könnte die Thy1-TwitchER Mauslinie es ermöglichen weitere neurologische Erkrankungen auf strukturelle und funktionelle ER Alterationen zu untersuchen, wie wir sie in Kontusionen und Laserläsionen nachweisen konnten, sowie deren biologische Relevanz zu evaluieren. Auch für physiologische Fragestellungen, wie zum Beispiel der Einfluss von ER-Kalzium bei der synaptischen Plastizität, stellt die Thy1-TwitchER Mauslinie ein wertvolles Modell dar.

Summary

Despite the fact that little is known about the endoplasmic reticulum (ER) in axons, it is repeatedly implicated as a potential effector in neurodegeneration. Our laboratory has demonstrated the impairment of mitochondrial structure and axonal transport in experimental autoimmune encephalomyelitis (EAE), which has raised the question of whether the ER could also be involved. Since we have established that increased cytoplasmic calcium levels determine the axonal fate in EAE, the ER (which can maintain ten-thousand-fold the cytoplasmic calcium concentration) was considered a possible source of elevated detrimental cytoplasmic calcium.

In order to measure ER calcium, the genetically encoded ratiometric and low-affinity calcium indicator Twitch2B 54S+ was targeted to the ER and characterised in cell culture. Subsequently, the novel transgenic mouse line Thy1-TwitchER was generated, screened for suitable subset axonal labelling and pharmacologically characterised via a 2-photon spinal-cord in-vivo imaging approach. A dynamic range of 300% (Rmax/Rmin) was determined by ER depletion with the sarco/endoplasmic reticulum Ca2+-ATPase inhibitor thapsigargin. Inducing EAE in Thy1-TwitchER mice revealed that axons undergoing focal-axonal degeneration (FAD) did not display a marked decrease of ER calcium unless the axonal continuity had already been disrupted. Consequently, cytoplasmic calcium elevations in FAD are not caused by ER calcium release, but rather by calcium entering the axons through plasma-membrane nanopores, as corresponding work in our laboratory concluded.

However, in the paradigms of spinal-cord contusion and laser-transection injury, a marked depletion of ER calcium could be measured. This depletion coincided with the structural alteration of ER fragmentation, which had hitherto only been described in dendrites following cardiac arrest. Traumatic axonal ER fragmentation and ER calcium depletion were demonstrated to be partially reversible over a period of several hours. In the future, the Thy1-TwitchER mouse line could be employed to screen further neuronal-disease paradigms for structural and functional ER alterations. In addition, this mouse line could serve as a valuable tool for physiological research, for example regarding the role of ER calcium in synaptic plasticity.

1 Introduction

1.1 Motivation

Many neurological diseases ultimately lead to the degeneration of neurons and their processes, namely Alzheimer's disease (AD), Parkinson's disease (PD), traumatic brain - and spinal cord injury (TBI, SCI) as well as neuro-inflammatory diseases, such as multiple sclerosis (MS) (Dziedzic et al., 2010; Trapp et al., 1998; Williams et al., 2014). Of these, MS and SCI will be in the spotlight of this thesis. Due to the central nervous system's limited capacity for regeneration, counteracting neuronal degeneration can be seen as the last line of defence to prevent irreparable damage. However, the process of neuronal degeneration is still poorly understood and thus strategies for therapeutic intervention remain scarce.

Our laboratory has been previously able to demonstrate that axonal degeneration is not a one-way street. Even morphologically severe axonal damage with localized axonal beading in neuro-inflammatory lesions, a process termed focal axonal degeneration (FAD), can potentially reverse to a configuration that appears normal, rather than undergoing complete fragmentation (Nikić et al., 2011). Consequently, a better understanding of axonal degeneration including its terminal converging pathways might help us identify promising therapeutic targets.

One common effector of degeneration is the rise of cytoplasmic calcium, which we recently showed to be an important predictor for the fate of swollen axons in FAD. High calcium favours progression to complete fragmentation, whereas reconstitution to low calcium levels favours morphological recovery of beaded axons (Witte et al., 2019). This observation combined with the abundance of calcium homeostasis related pharmacological targets puts calcium into focus for intervention strategies (Zündorf & Reiser, 2011). Therefore, it is important to identify the source of calcium elevations in degenerating axons. Feasible sources appear to be the extracellular space and/or intraorganellar stores, such as the endoplasmic reticulum (ER) and mitochondria. With regard to the high calcium level of ER in neurons, in the range of 1000 – 5000 times of the cytoplasmic calcium concentration (Berridge, 2002), we suspected ER calcium to be a likely contributor to the deleterious calcium rise seen

in FAD. Recent work has emphasised the importance of ER-derived calcium in axonal degeneration (Ouardouz et al., 2003; Stirling, Cummins, Chen & Stys, 2014; Villegas et al., 2014).

The neuronal endoplasmic reticulum spans all the way from dendrites to axons and reaches even the most distant processes as one continuous structure (M. Terasaki, Slater, Fein, Schmidek & Reese, 1994). Apart from calcium sequestration and calcium signalling it serves a plethora of functions which include the biosynthesis of membrane and secretory proteins in the rough ER, while smooth ER contributes predominantly to the secretory pathway of vesicle budding and fusion as well as lipid and sterol synthesis (Shibata, Voeltz & Rapoport, 2006). In addition, the ER interacts intricately with other organelles like the plasma membrane and mitochondria. Disturbances in the mitochondria-associated ER membranes (MAMs) have been implicated in a variety of neurodegenerative diseases including AD, PD and Amyotrophic lateral sclerosis with associated frontotemporal dementia (ALS/FTD). Diseases with MAM disruption have in common, that they all exhibit similar downstream pathological hallmarks including damage to mitochondria, defects in axonal transport and pathological ER activation patterns, such as the unfolded protein response (UPR), as well as disrupted calcium homeostasis (Paillusson et al., 2016).

Lesions in the mouse model of MS, experimental autoimmune encephalomyelitis (EAE), have been demonstrated to exhibit similar characteristics including widespread axonal transport deficits (Sorbara et al., 2014) as well as the appearance of swollen, dysmorphic mitochondria (Nikić et al., 2011). The close interrelation between ER and mitochondrial pathologies as well as the search for the source of detrimental cytoplasmic calcium elevation in axons prone to degenerate in EAE led us to investigate the role of the ER in neuro-inflammatory lesions.

Since neither ER morphology nor functional alteration had been studied before, we aimed at shedding light on both. To this end we generated a transgenic mouse line, which expresses a high K_d variant of the recently published FRET calcium indicator Twitch2B under the control of the neuronal Thy1.2 promoter (Thestrup et al., 2014). This tool allowed us to visualize the behaviour of the ER and its calcium content as surrogate for its functional state in EAE lesions. Furthermore, we evaluated the ER response in a spinal cord contusion model in comparison to EAE.

In this chapter I will outline in detail the topics of axonal degeneration, the ER, its pathological responses and interactions as well as the use of biosensors and suitable imaging methods to study the ER.

1.2 Endoplasmic reticulum

Before the advent of high-resolution imaging techniques, the outer part of the cytoplasm was described as empty ground substance or hyaloplasm, due to the lack of optically definable structures (resulting from similar optical densities between organelles and the cytoplasm). Animal-cell ER was first discovered only by the means of electron microscopy in the thin periphery of chicken-embryo fibroblasts as 'lace-like reticulum' (Porter, Claude & Fullam, 1945). The organelle was baptised endoplasmic reticulum due to its enrichment in the endoplasm, the non-spreading region of fibroblasts and relative scarcity in the ectoplasm, which defines the cytoplasm contained in fibroblasts' pseudopodia (Porter, 1953).

While Porter described the three-dimensionality of the ER and the variations in its thickness, the ER's structure has been defined much more thoroughly today. All eukaryotic cells contain ER. It consists of a network of branching tubules and flattened sacs; these enclose one continuous lumen that can constitute more than 10% of the cell volume (Alberts, Johnson, 2002). The ER consists of structurally distinct domains, including the nuclear envelope (NE), which forms the two lipid-bilayer sheets that wrap around the nucleus, the rough endoplasmic reticulum (RER), the intermediate ER and the smooth endoplasmic reticulum (SER), as well as domains that interact with other organelles, such as the subsurface cisternae, closely apposed to the axolemma. While ribosome-studded RER is characterised by flattened sheets, the SER without attached ribosomes extends to the cell periphery and is often shaped as rather dilated and convoluted small tubules (Voeltz, Rolls & Rapoport, 2002).

The RER with its membrane-bound ribosomes serves as a synthesis hub for virtually all secreted, luminal and membrane-bound proteins, except for those found in mitochondria and peroxisomes. Since all nucleated cells synthesise proteins, they all contain RER. Large amounts of RER correlate with high protein synthesis, either for secretion or for local requirements, as in neurons and pancreatic acinar cells and B cells.

An intermediate type of ER is transitional ER, which can be partly smooth and partly rough. It features Golgi exit sites, where newly synthesised proteins and lipids bud off to form vesicles directed to the Golgi apparatus.

The SER has distinct functions. Cells specialising in lipid metabolism have abundant SER, such as steroid hormone-producing cells of the adrenal cortex, since the steroid-synthesis enzymes are found in the SER membrane. Likewise, hepatocytes possess plentiful SER, which synthesises the lipid components of lipoproteins and harbors enzymes of the cytochrome P450 family for detoxification reactions. Depending on the presence of hydrophobic detoxification substrates, the amount of SER in hepatocytes is tightly regulated by lysosome-dependent autophagocytosis (Alberts, Johnson, 2002). Another example of a specialised SER function is the sarcoplasmic reticulum (SR) in muscle cells. The purpose of the SR is the sequestration of calcium ions, which can be released in a near-synchronous fashion following the process of excitation-contraction coupling. This process is dependent on two types of receptors: dihydropyridine receptors (DHPR), types of voltage-gated L-type calcium channels in the plasma membrane, and ryanodine receptors (RyR), which act as ER calcium release channels, located on the SR membrane. Depolarisation of the sarcolemma leads to a conformational change of the DHPR, which activates the RyR. The subsequent release of calcium leads to muscle contraction. The sequestration of the large amounts of SR calcium necessary for excitation-contraction coupling is enabled by the abundance of the calcium-binding protein calsequestrin (Khurana, 2006). The function of SER in neurons is less established. One hypothesis is that its endomembrane system serves as an internal-signalling organelle via a precisely orchestrated release of calcium similar to the SR (Berridge, 2002). This concept of the ER as a ‘neuron inside a neuron’ will be further evaluated in the following chapter.

1.2.1 Neuronal ER

Before addressing the intricacies of ER calcium handling, I will focus on the organisation of the ER in neurons. Neuronal ER is an internally continuous organelle. This idea was originally proposed by microscopic studies, such as from serial section electron-microscopic reconstructions of Purkinje-cell dendrites in chickens. Here, around 90% of SER profiles in the reconstructions were contained within a single network (Martone, Zhang, Simpliciano, Carragher & Ellisman, 1993). Additionally,

Terasaki et al. (Terasaki et al., 1994) demonstrated that the dye 1,1'-dihexadecyl-3,3,3',3'-tetramethylindocarbocyanine perchlorate ($DiIC_{16}$), which diffuses in strictly continuous lipid bilayers, was able to spread throughout the cell body and dendrites and into the axons of cerebellar Purkinje neurons in rats in acutely prepared brain slices. The dye clearly delineated ER in the somata as resolvable by confocal microscopy, and its distribution was independent of membrane trafficking since it also labelled fixed neurons. The neuronal ER is structurally diverse, albeit continuous. Somata and proximal dendrites possess abundant, ribosome-rich RER organised into large stacks, which is why they show Nissl bodies in the well-known aniline stain. The Nissl stain and RER alike exclude the axon hillock (Kühnel, 2003).

The ER in more distal dendrites forms an irregular network of thin tubules and variable flat, widened regions. Approximately 20% of dendritic spines are reached by at least one tubule, termed the 'dendritic spine apparatus' and characterised by the presence of the protein synaptopodin (Spacek & Harris, 1997). Dendritic ER is highly dynamic, and local ER configuration is influenced by synaptic signalling. For example NMDA-type glutamate receptors' activations can lead to the segregation of the dendritic ER into vesicular bodies (Kucharz, Krogh, Ng & Toresson, 2009), possibly leading to sequestration of functional micro-compartments or local limitation of harmful events.

Axonal ER morphology appears more organised. In the internodal parts, SER tubules run longitudinally in axons, branch occasionally and concentrate in the subaxolemmal space. Free vesicles and cisternae are rarely observed, at least in the phrenic nerve internode. At the nodes of Ranvier, cisternae-like structures are more commonly registered, and the SER is more beaded, runs straight, barely branches and forms small bundles (Tsukita & Ishikawa, 1976). Axonal ER is very narrow. In fact, tubules with a diameter between around 15 and 30 nm are the most abundant type of ER found in axons, while in non-neuronal cells, tubules are (on average) 60 nm in diameter (Terasaki, 2018). Exemplary electron microscopic depictions of ER in an axon, soma, dendrite and dendritic spine, respectively, are shown in Figure 1.

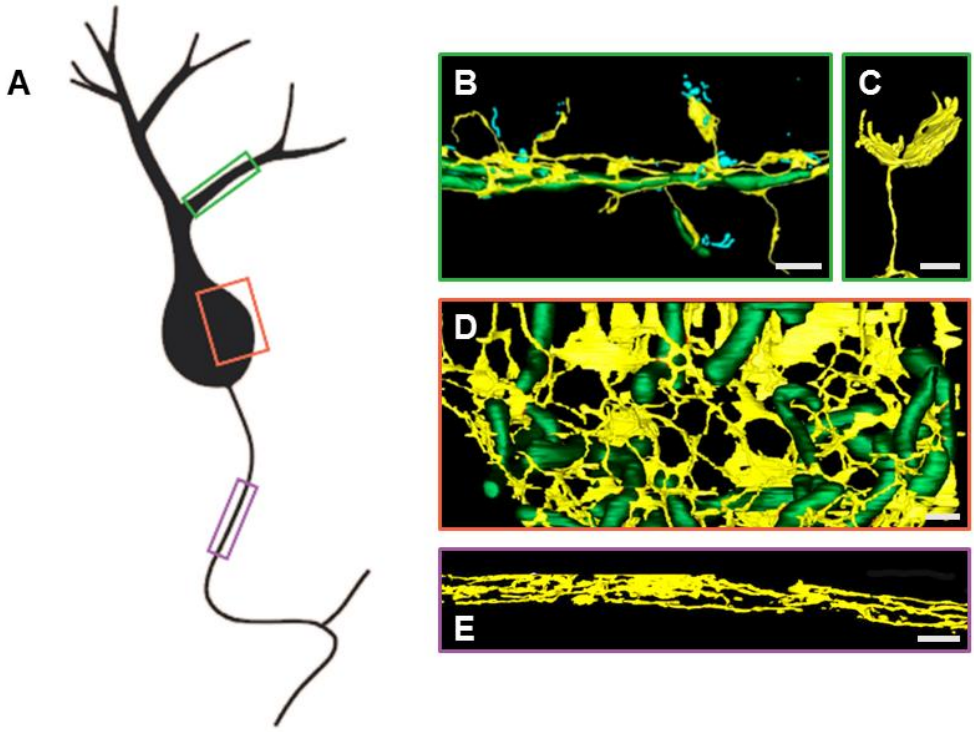

Figure 1: Structure of ER in soma and neurites

(**A**) A schematic neuron with multiple dendrites and one axon. Coloured boxes represent dendritic (green), somatic (red) and axonal (purple) regions. (**B**) Three-dimensional reconstructions of a dendrite depicting ER (yellow), mitochondria (green) and endosomes (blue) (**C**) and of an ER spine apparatus, ER (yellow) (**D**) and reconstruction of a neuronal cell body depicting ER (yellow) and mitochondria (green) in mouse nucleus accumbens, from focused ion-beam electron-microscopic image stacks. Pictures from Wu et al. (2017). (**E**) Three-dimensional reconstructions of ER (yellow) in a mouse optic-nerve axon from serial blockface scanning electron-microscopic image stacks. Picture from Yin et al. (2016). Scale bars in (**B**) 800 nm, in (**C**) 80 nm, in (**D**) 400 nm and in (**E**) 1 µm. Figure is modified from Ramirez & Couve (2011).

The axonal SER bears resemblance to its somatic and dendritic counterparts regarding its protein repertoire. The luminal ER chaperones calreticulin, BiP, ERp29 and protein disulfide isomerase – important for protein synthesis and quality control – as well as calnexin and glucose-6-phosphatase, have all been found in the three compartments, respectively (Ramirez & Couve, 2011).

In spite of the continuity of the ER and similarities in luminal-protein content, the neuronal ER is astoundingly spatially heterogeneous. The ER's capability of sorting mRNA is remarkable; for example, mRNA can be targeted to dendrites to enable

the synthesis of locally demanded proteins (Steward, 1997). The synthesis of cholesterol and phospholipids is also spatially distributed to distinct ER compartments (Verkhratsky, 2005). In contrast to the mentioned pan-neuronal ER proteins, other ER proteins have been found to be localised to SER sub-compartments, such as Inositol trisphosphate receptors (IP3R) and RyR, as well as calcium-binding proteins like calreticulin and calsequestrin (Ramirez & Couve, 2011). The neuronal ER fascinates with the dualism of localised functional sub-compartments integrated into a coherent network spanning the entire neuron. This phenomenon is especially interesting when discussing the ER's role in calcium signalling and homeostasis. One possible implication of functional sub-compartments in neurons is that the ER can act as a modular signalling system. ER in neuronal spines can release its calcium content independent of the neighbouring spines, thus being immediately interesting for spatial integration of synaptic signals (Berridge, 2002). In fact, an IP3R-mediated coincidence detection of parallel and climbing fibre input has been demonstrated in Purkinje-cell dendrites of cerebellar brain slices in rats and is discussed as the functional basis of long-term depression (Wang, Denk & Häusser, 2000).

1.2.2 ER calcium homeostasis

In order to better understand ER calcium and its role in neurodegeneration, I will outline the molecular components and their interactions in calcium homeostasis here. The ER is an essential store of calcium, which has various sinks and sources. Overall, the ER maintains a high calcium concentration reaching the millimolar range, which sets it apart from the nano- to micro-molar range of cytoplasmic calcium, thereby creating an electrochemical gradient in favour of ER calcium release (Suzuki et al., 2014). The ER is an intrinsically leaky organelle and constantly loses calcium ions through aqueous pores in the translocon complex. This basal leak is regulated by the amount of protein synthesis and, consequently, the number of ribosomes blocking the translocon pores (Lomax, Camello, Van Coppenolle, Petersen & Tepikin, 2002). The activity of the sarco/endoplasmic reticulum Ca2+-ATPase (SERCA), which pumps in calcium against the electrochemical gradient by hydrolysis of adenosine triphosphate (ATP), counteracts the constant leak. The SERCA itself is subject to different control and feedback mechanisms, which involve the ER-membrane proteins phospholamban, sarcolipin and myoregulin (Okubo,

Mikami, Kanemaru & Iino, 2018). Furthermore, calcium-buffering luminal ER proteins, including calreticulin and calnexin, regulate SERCA activity (John, Lechleiter & Camacho, 1998; Roderick, Lechleiter & Camacho, 2000). ER calcium-binding proteins and chaperones are essential for maintaining the ER's high calcium concentration and regulation of the intra-ER free calcium level. Importantly, their calcium K_d-value is in the millimolar range (e.g. calreticulin, the most abundant buffering protein, K_d~1 mM), so that intra-ER free calcium at disposal remains high and is able to diffuse unimpededly. In contrast, cytoplasmic calcium-binding proteins display high calcium affinity in the ten to several hundred nanomolar range and cause more rapid buffering. The high amount of free ER calcium allows for the generation of a large number of constant calcium signals (Berridge, 2002).

Supporting SERCA-mediated refilling, a coupling of ER calcium depletion and plasma-membrane calcium entry has recently been defined in molecular detail: store-operated calcium entry (SOCE), or capacitative calcium entry. ER calcium-sensing ER transmembrane proteins – called stromal interaction molecules (STIMs) – oligomerise upon the reception of ER calcium depletion (Brandman, Liou, Park & Meyer, 2007). The oligomers activate Orai1 calcium channels in the plasma membrane and lead to cytosolic calcium influx (Schindl et al., 2009).

Apart from the passive calcium efflux from the ER, two extensively regulated calcium channels control the active calcium release: RyR and IP3R. Both of them are found abundantly in neurons. While all three subtypes of RyR (RyR1, 2 and 3) are expressed in neurons (Mori, Fukaya, Abe, Wakabayashi & Watanabe, 2000), IP3R is predominantly expressed as subtype 1 in the central nervous system (CNS) (Furuichi et al., 1993). IP3R are activated by inositol triphosphate (IP3), in unison with cooperative calcium binding. IP3 is generated after a G_q-coupled or receptor tyrosine kinase activation of phospholipase C, caused by neurotransmitters or neurotrophins binding to their respective receptors (Berridge, 2016). RyR activation is caused by calcium ions with modulation by phosphorylation status and cytosolic factors, including reactive oxygen species (ROS). Thus, calcium entry through the plasma membrane can lead to an opening of RyR with subsequent calcium release from the ER and potentiation of the cytoplasmic calcium rise. The same principle holds true for IP3R, the opening probability of which is increased by cooperatively bound calcium in the presence of IP3. This phenomenon is called 'calcium-induced calcium release' (CICR; Verkhratsky, 2005).

A graphical summary of the proteins mentioned that are involved in ER calcium handling and an illustration of the process of CICR can be found in Figure 2.

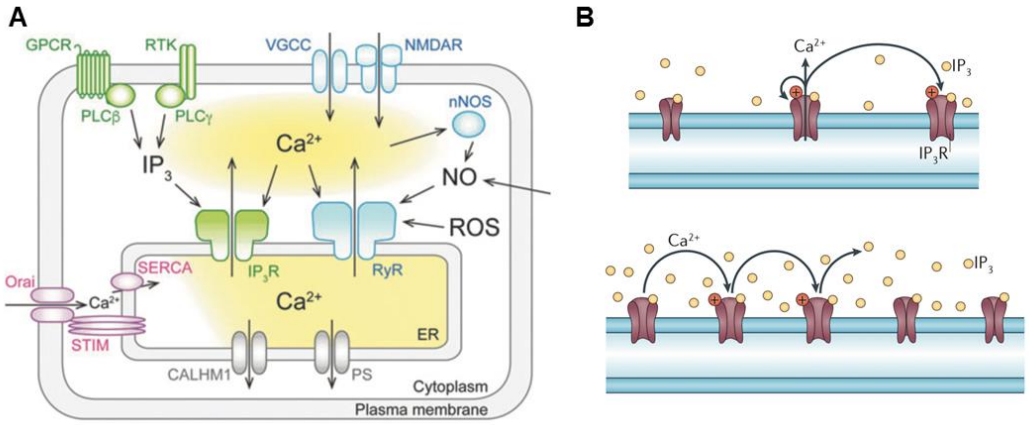

Figure 2: ER calcium signalling and CICR

(**A**) A schematic depiction of ER Ca2+ signalling and the involved channels and pumps located in ER and plasma membrane. **Additional information to text:** NO can facilitate calcium release through RYR, which is implicated in excitotoxicity. PS (presenilin) and CALHM1 (calcium homeostasis modulator 1) can form putative calcium leak channels. Mutated PS leads to ER calcium overload and impaired SOCE in AD. Figure adapted from and caption modified from Okubo et al. (2018) (**B**) Illustration of the formation and propagation of a regenerative calcium wave. Allosteric calcium binding combined with IP3 can trigger IP3 receptor opening. The released calcium ions again allosterically activate the same receptor and adjacent receptors and result in CICR, a process that is limited by the range of IP3 diffusion. Figure adapted from and caption modified from Ross (2012).

The ER's remarkable endowment with calcium regulatory proteins and its capability of positive auto-feedback via CICR have given rise to the concept of the ER as a signalling organelle. CICR allows the ER to create regenerative calcium waves, which backpropagate signals to the nucleus. IP3R-mediated calcium waves have been demonstrated in pyramidal neurons of acute cortical slices. Glutamatergic or electric dendritic stimulation first led to localised calcium waves and, with higher intensities, to a regenerative calcium increase, which reached the soma and nucleus with possible implications for gene expression (Ross, 2012).

ER calcium regulation is closely coupled to mitochondria. After calcium is released from the ER, mitochondria rapidly take up the excess of cytoplasmic calcium, buffer it and then redistribute it to the ER. Mitochondria are capable of signalling back to the ER by the means of hydrogen peroxide, which can transgress the lipid bilayer membranes and influence, for example, RyR conformation, thereby establishing a mutual communication between the two organelles. A calcium shift from the ER to

mitochondria can result in apoptosis via the induction of mitochondrial permeability transition pores (MPTP; Berridge, 2002).

ER calcium also interacts with protein homeostasis. ER resident chaperones important for protein folding rely on high luminal-calcium concentrations, so that a reduction of ER-calcium content inhibits protein synthesis (Kimball & Jefferson, 1992). The accumulation of misfolded proteins triggers the unfolded protein response (UPR), which represents an important cellular stress response and constitutes another method of ER-to-nucleus signalling. The UPR's importance is widely implied in neurodegeneration (Li, Yang, Selzer & Hu, 2013).

1.2.3 ER stress and the UPR

The ER is responsible for the synthesis, posttranslational modification and folding of about 30% of the cell's proteome. Despite the large number of chaperones and foldases involved in this process, the misfolded proteins can pile up in the ER lumen, a state called 'ER stress'. The ensuing activation of the UPR must achieve several factors in order to reconstitute proteostasis. The pro-adaptive phase of the UPR aims at a reduction of the protein translation, degradation of misfolded proteins and increases of chaperone and foldase expression. Unless these measures suffice to re-establish proteostasis, the UPR can also progress into its pro-apoptotic phase (Carreras-Sureda, Pihán & Hetz, 2017; Hetz, Chevet & Oakes, 2015).

There are three major ER type I transmembrane proteins, which transduce the UPR: activating factor 6 (ATF6), PKR-like endoplasmic reticulum kinase (PERK), and inositol-requiring enzyme 1 (IRE1). All three proteins institute different signalling cascades leading to the activation of transcription factors, which increase the expression of UPR-related genes. These include multifarious proteins like foldases and chaperones, as well as proteins involved in autophagy, quality control, lipid synthesis, secretion, amino-acid metabolism, redox metabolism and, ultimately, cell death (Peter & David, 2011).

Here, I will only outline these cascades in short. Paramount in sensing the UPR is the ER chaperone 78 kDa glucose-regulated protein, also known as binding immunoglobulin protein (GRP78/BiP), which binds to the luminal side of the three UPR-transducer proteins under normal conditions. Under ER stress however, GRP78/BiP resorts to preferential binding of misfolded proteins, due to their increased display

of hydrophobic domains and insufficient glycosylation. Thereby, GRP78/BiP loses its inhibitory effect on the three UPR transducers (Kimata & Kohno, 2011).

IRE1, one of these three UPR transducers, acts as a transmembrane endoribonuclease and leads to post-transcriptional alternative splicing of X-box binding protein 1 (XBP1) mRNA, which is located at the ER membrane. The spliced gene product is imported to the nucleus as a transcription factor. In addition, IRE1 also degrades other RNAs in a process called IRE-1 dependent decay, thereby further reducing the protein burden. PERK1 phosphorylates eukaryotic initiation factor 2α (eIF2α), leading to a shut-down of global gene expression and simultaneously increasing the expression of the activating transcription factor 4 (ATF4). ATF6 is exported to the Golgi apparatus, where its cytoplasmic fragment, a potent transcription factor, is cleaved by the proteases S1P and S2P (Hetz et al., 2015).

Calcium plays several important roles in the UPR. It sets the threshold for UPR activation by adjusting the ER chaperones' activity; it modulates ATP production via coupling to mitochondria, and it can induce apoptosis via MPTP induction (Carreras-Sureda et al., 2017). Furthermore, the activity of IP3R type 1 downregulates when GRP78/BiP and an ER resident oxidoreductase are expressed at higher levels under ER stress, possibly forming a negative-feedback loop. Reducing ER calcium efflux could help maintain a high intra-ER free calcium level, which is, in return, favourable for protein expression and maturation (Higo et al., 2010).

Convergent with the idea that excitotoxicity, oxidative stress and calcium dysregulation contribute to axonal degeneration, it has been proposed that the UPR could also be involved (Shaohua Li et al., 2013). In fact, spinal motor neurons have been shown to exhibit ER stress after ischemic injury (Yamauchi, Sakurai, Abe, Matsumiya & Sawa, 2007) and in an SCI contusion model (Penas et al., 2007). Regarding axonal injury, it has been hypothesised that ER stress might be retrogradely transmitted to the perikaryon and lead to secondary damage and degeneration of the neuron itself. In support of this idea, XBP-1 mRNA splicing following brain-derived neurotrophic-factor application has been demonstrated to occur in neurites, and activated XBP-1 was retrogradely transported to the neuronal soma (Hayashi et al., 2007). Moreover, chronic ER stress has been linked to many neurodegenerative diseases, including PD, ALS, Huntington's disease and prion-related disorders (Cabral-Miranda & Hetz, 2017).

In recent years, the UPR has become a credible pharmacological target, and potential attenuators of the ER stress response have been identified (Hetz, Chevet & Harding, 2013). An example of such substances are chemical chaperones. In an animal model of ischemia and reperfusion injury, the chemical chaperone sodium 4-phenylbutyrate conferred a neuroprotective effect by reducing ER stress signalling (Qi, Hosoi, Okuma, Kaneko & Nomura, 2004). In a model of brain ischemia, dantrolene, which can increase the load of ER calcium by acting as an RyR antagonist, was also observed to alleviate ER stress (Li et al., 2005).

Another site of UPR signalling on which current research focuses is the interface between the ER and mitochondria – the MAMs. The association between ER and mitochondria fine-tunes energy demands in UPR signalling and can ultimately induce apoptosis. AD, PD, ALS and Charcot-Marie-Tooth disease are all known to combine signs of ER stress and morphological changes of MAMs (Hetz & Mollereau, 2014). Interestingly, calcium-signalling molecules, chaperones and UPR transducers often colocalise at the MAMs, raising interest in these organelle contact sites (Carreras-Sureda et al., 2017).

1.2.4 ER contact sites

In order to exert its plentiful functions, the ER apposes tightly to other organelles' membranes and forms contacts. The contacting organelles include endosomes, peroxisomes and the Golgi apparatus (which exceed the scope of this thesis), as well as the mitochondria (MAMs) and the plasma membrane. These contact sites represent a rather localised and rapid means of interorganellar communication, in addition to classical secretory and endocytotic pathways and vesicular traffic to the plasma membrane (Wu et al., 2017).

One function of these contacts is lipid switching between the membranes. This is achieved by lipids transporting proteins without requiring vesicle fusion. This alternative way of lipid exchange is crucial for membrane homeostasis in neuronal processes far away from the Golgi apparatus, as well as for the lipid transfer to mitochondria, which are excluded from vesicular transport (Lahiri, Toulmay & Prinz, 2015). In addition to the delivery and recycling of lipids, the ER-plasma membrane contact sites are also involved in calcium signalling via SOCE (see chapter 1.2.2) and concentrate STIM1 and Orai proteins, as well as RyR (Wu et al., 2017).

Five percent to twenty percent of the mitochondrial surface is situated in a range of 10–30 nm from the ER and can thereby be classified as MAMs (Paillusson et al., 2016). At this distance, electron microscopy has shown electron-dense proteinaceous tethering structures spanning the membranes (English & Voeltz, 2013a). The MAMs facilitate phospholipid exchange between the ER and mitochondria, enabling the synthesis of phospholipids that require the enzyme repertoire of both ER and mitochondrial membranes – namely, the conversion of phosphatidylserine to phosphatidylcholine (Rowland & Voeltz, 2012). Moreover, the protein mitofusin 2 is known to localise at MAMs and act as a tether, implying the ER's involvement in mitochondrial fusion (de Brito & Scorrano, 2008).

ER-mitochondria contact sites are tightly involved in cellular calcium homeostasis. In their restricted inter-membrane space, local calcium microenvironments can form, which help to prevent the spill-over of calcium to the cytosol and lead to relatively high local calcium concentrations. Calcium is needed in the mitochondrial matrix to stimulate calcium-regulated enzymes of the tricarboxylic-acid cycle and to promote ATP synthesis (Carreras-Sureda et al., 2017). In order to channel calcium into the mitochondrial matrix, calcium first passes the IP3R in the ER membrane, traverses the small stretch of cytosol between the organelles, enters the mitochondrial inter-membrane space through the voltage-dependent anion channel (VDAC) and finally reaches the matrix via the mitochondrial calcium uniporter (MCU). Due to the MCU's low calcium affinity, calcium concentrations in the micromolar range are prerequisites for efficient calcium shuttling to the mitochondrial matrix. This highlights the pivotal role of MAMs in cellular metabolism (Patron et al., 2013). The disruption of the MAMs can lead to various neurodegenerative diseases (see chapter 1.2.4). Identification of potential tethers, functional characterisation of the calcium microdomains and the search for therapeutic targets are topics of broad current interest.

1.2.5 Structural ER dynamics

There are several proteins at work to build the complex geometry of RER and SER. The membrane curvature of ER tubules is generated by a wedge-shaped protein family called reticulons. These act in concert with members of the DP1/Yop1/REEP5/6 and REEP1-4 protein families (Shibata et al., 2010). Overexpression or depletion of reticulons result in expansion or shrinkage of ER tubules in relation to sheets, respectively (Schwarz & Blower, 2016).

The typical three-partite junctions of ER tubules are formed by the process of homotypic fusion. The protein atlastin, a dynamin-like GTPase, is essential for this process. The knockdown of atlastin results in a reduction of branch points and elongated SER tubules (Hu et al., 2009). The protein Rab10 is also involved in ER assembly and marks the position of new ER tubule growth (English & Voeltz, 2013b). Structural ER protein defects, including atlastin mutations, have been discovered in hereditary spastic paraplegia, a disease in which motor neuron axons degenerate, leading to progressive lower-limb spasticity. This is another indication of the importance of functional ER in distal neurites (Westrate, Lee, Prinz & Voeltz, 2015).

The ER is an incredibly dynamic organelle. It undergoes continuous remodelling of its network through a number of different processes. Among these are the dynein- and kinesin-dependent mechanisms of microtubule sliding, extension of tubules by the tip-attachment complex at the plus end of growing microtubules, and actin/myosin-mediated interactions (Ramirez & Couve, 2011; Westrate et al., 2015). Apart from minor remodelling, more severe kinds of ER morphology alterations have been reported. Despite the earlier notion of the ER as being a continuous organelle, there are instances, in which this continuity is disrupted. ER fragmentation, or ER fission, into small vesicles has been observed in neurons in different models. Murine primary neuronal-cell cultures instantaneously displayed a vesicular disintegration of their ER following the administration of either glutamate or NMDA in live-cell fluorescent imaging in the entire field of view. This fragmentation was not accompanied by morphological changes of the dendrite, which remained structurally intact (Kucharz et al., 2009). ER in hippocampal-slice cultures also fragmented following depolarisation with 50 mM potassium, which can likewise lead to endogenous glutamate release (Kucharz, Wieloch & Toresson, 2011a), and finally two-photon imaging of ER-targeted green-fluorescent protein (GFP) in the intact mouse brain revealed the same disintegration process of the ER, with ensuing cardiac arrest and ischemia (Kucharz, Wieloch & Toresson, 2011b).

Remarkably, this fragmentation was entirely reversible following the application of the NMDA-receptor antagonist MK-801 or removal of the depolarising medium in case of the slice and primary cultures within a time frame of 15–30 minutes. This implies a cellular coping mechanism and even the appearance of ER fragmentation as a physiological regulatory process. After fragmentation, the fragments showed a curious tendency to cluster in regularly spaced intervals, potentially by microtubular

rearrangement following extracellular-calcium influx. Interestingly, the fragmentation process was seemingly unaffected by depletion of ER calcium with the SERCA inhibitor thapsigargin and appeared to rely primarily on calcium entry through the plasma membrane (Kucharz, Wieloch & Toresson, 2013). Speculations on the function of ER fragmentation include the local sequestration of excitotoxicity by impeding the formation of CICR-mediated calcium waves and the generation of confined ER vesicles, which can exert their functions locally (for example in synaptic plasticity). However, the molecular mechanisms underlying this curious process remain unknown to date.

1.3 Axonal degeneration

Pathological loss of axons is an early hallmark of almost all neurodegenerative diseases, as well as neural injuries. It represents the primary cause of functional disability in patients (Neukomm & Freeman, 2014). This thesis explores axonal degeneration in different disease paradigms: axonal degeneration in EAE, a mouse model of MS, and axonal degeneration in spinal-cord injury induced by either blunt-force contusion or focal-laser lesioning. Accordingly, the following chapter will focus on these pathologies and provide a detailed review of the molecular processes involved.

1.3.1 Modes of axonal degeneration

A loss of axons is not only observed under pathological conditions, but is also essential for developmental remodelling of neuronal circuits through a tightly regulated process called ‘axonal pruning’. Pruning enables the nervous system to cherry-pick the best neuronal connections from an initial excess of immature processes (Luo & O’Leary, 2005). Several morphologically defined and molecularly distinct pruning processes exist. These include simple axon retraction, shedding of axosomes and local axon degeneration. Local axon degeneration is the favoured way of pruning for long-projecting axons. Morphologically, the whole axon fragment supposed for removal undergoes simultaneous granular disintegration over a course of a few hours; afterwards, the fragments are removed by the surrounding glial cells (Saxena & Caroni, 2007). Pruning has been studied extensively in vivo as well as in vitro

models induced e.g. by nerve growth-factor deprivation in microfluidic chambers (Taylor et al., 2005).

Remarkably, axonal degeneration under pathological conditions can look strikingly similar to this pruning process. Hence, there have been endeavours to identify functional similarities between these modes of axonal degeneration. The most extensively studied type of pathological axonal degeneration is called Wallerian degeneration (WD). It ensues axotomy, the most severe axonal damage, and results in synchronous pan-fragmentation of the part of the axon distal to the site of injury (Ching-Yuen, 1963). WD-matching patterns have been described in a number of diseases including AD, PD and MS (Neukomm & Freeman, 2014). The time frame of WD is very peculiar and defining. After the initial severing of the axon, the distal fragment remains structurally intact for 12 hours to 2 days, the so-called lag phase. Only after this period does the pearl-like swelling ('beads on a string') occur, followed by the explosive disintegration of the axonal portion distal to the injury site. The swelling and fragmentation likely reflect a destabilisation of the cytoskeleton by calcium-influx-dependent proteases like calpain (Misgeld, 2011).

Initially, it was hypothesised that a mere lack of trophic support from the soma could lead to the distal axonal dismantling. However, the staggering discovery of a mutated strain of mice with massively delayed WD, in which severed distal axonal portions remained intact for weeks after axotomy, completely changed the understanding of WD (Lunn, Perry, Brown, Rosen & Gordon, 1989). Since the distal axonal fragment appeared sufficiently autonomous to survive over an extended period of time without its soma, there had to be an actively regulated mechanism at work driving the axon disassembly; moreover, this mechanism can be impeded. The mouse strain is referred to as C57BL/Wld^S for slow Wallerian degeneration phenotype. Later, the mutation that corresponded to the Wld^S phenotype was identified. It results in a fusion protein consisting of the N-terminal part of E4 ubiquitin ligase Ube4b and the NAD+ scavenging enzyme nicotinamide mononucleotide adenyltransferase 1 (NMNAT1). This chimeric enzyme protects axons from WD in a dominant manner (Mack et al., 2001a). NMNAT-conferred axon protection is described in more detail in chapter 1.3.2.

Notably, Wld^S does not impede developmental pruning and consequently distinguishes it from WD, although they share morphological similarities (Hoopfer et al.,

2006). The relevance of the Wld^S mutation has been examined in many neurological-disease models. Models of traumatic nerve injury, glaucoma, toxic neuropathy or PD were alleviated by the Wld^S mutation, while hereditary spastic paraplegia and ALS were unresponsive to it (Conforti, Gilley & Coleman, 2014), and some degree of protection is assumed for EAE (Kaneko et al., 2006). The underlying theory is that spontaneous axonal transections occur in Wld^S sensitive diseases, which are instigated by local activations of axonal programs similar to WD (T. Misgeld, 2011).

Another mode of axonal degeneration precedes WD and is initiated within minutes after nerve transection: acute axonal degeneration (AAD). Here, both the proximal and distal parts of the transected axon equally undergo a rapid process of dying back over a distance of several hundred micrometres in a Wld^S-sensitive manner. This mode of degeneration might potentially deteriorate localised axonal damage, due to its ability to spread across branch points and thereby denervate initially spared side branches proximal to the lesion. Within 6 to 24 hours after the axotomy event, erratic regeneration attempts of the proximal axon tip have been observed, either by fast and straight outgrowth or by the formation of numerous lateral sprouts. However, neither method can effectively approximate the two severed ends (Kerschensteiner, Schwab, Lichtman & Misgeld, 2005). A hypothesis for the spatially restricted manner of AAD is that incipient calcium influx through the severed axolemma activates calpains locally. The cytoplasm's calcium-buffering capacity and spontaneous membrane resealing of the tip can subsequently stall the progression (Misgeld, 2011). Despite being locally destructive, AAD could also have beneficial effects on subsequent regeneration. It has been posited that destabilisation of the cytoskeleton of the proximal axon can facilitate growth-cone formation (Spira, Ruthi, Ada & Daniel, 2003). Moreover, the void created by the proximal axon's retraction could be filled by glial cells, providing a more favourable milieu for regeneration (Wang, Medress & Barres, 2012).

Another compelling mode of axonal degeneration has recently been discovered: focal axonal degeneration (FAD). It can be identified as a stereotypical process in inflammatory lesions in EAE, the mouse model of multiple sclerosis. Three morphological distinct stages have been defined: stage 0, which is morphologically unaltered; stage 1, in which the axons display one or several focal swellings but still maintain a continuous structure; and stage 2, which is characterised by the disruption of the axon's continuity. The eventual disruption of the axon membrane is often

initiated at the nodes of Ranvier and can synchronously occur at several different positions of the same axon. Importantly, congruent morphological patterns can be determined in actively demyelinating MS lesions in patients. Figure 3 shows the characteristic morphological patterns in EAE and MS.

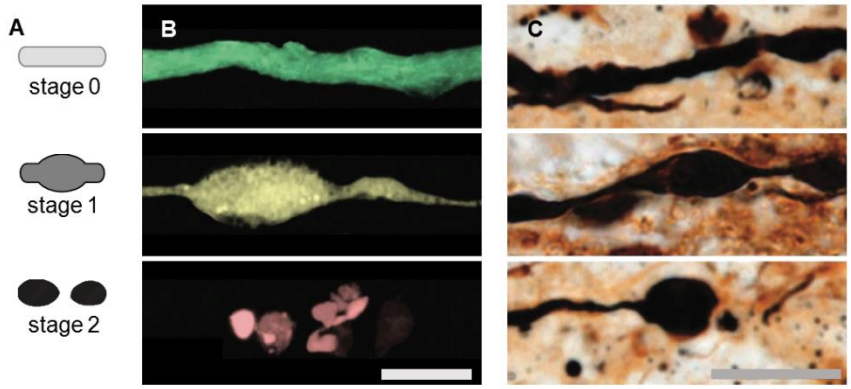

Figure 3: Stages of FAD in EAE and MS

(**A**) Schematic FAD stages used throughout this thesis. (**B**) Normal appearing (green, top), swollen (yellow, middle), and fragmented (red, bottom) axons in an EAE lesion (confocal projection images), (**C**) Exemplary axons of stages 0, 1 and 2 of FAD in a human multiple sclerosis lesion (Bielschowsky staining). Scale bars 10 µm, Figure 3B, C adapted from and caption modified from Nikić et al. (2011).

Remarkably, the swellings in the prodromal stage 1 are yet undetermined in their fate. Repeated imaging over the time course of several days showed that these swellings either persisted, progressed to complete fragmentation (i.e. stage 2) or reverted to stage 0 and recovered. The susceptibility to FAD depends on the axon diameter and favours small-calibre axons. Unexpectedly, the myelin sheath in axons undergoing FAD is generally intact, which necessitates the presence of membrane-permeable mediators of axon injury. By employing a fluorescent reporter mouse line labelling mitochondria, it can be demonstrated that stage 1 axons and even morphologically intact stage 0 axons displayed swollen dysmorphic mitochondria. These were also functionally impaired, as their membrane potential was reduced. Thus, mitochondrial damage precedes morphological alterations. Strikingly, the morphological characteristics of FAD can be reproduced in a model of ROS/RNS application on healthy spinal axons; accordingly, ROS/RNS scavenging can rescue a large proportion of stage 1 axons in EAE (Nikić et al., 2011).

1.3.2 Molecular mechanisms of axonal degeneration

In this chapter, I will focus on the molecular mechanisms of WD in particular, as the WLD^S mutation also has positive impacts on AAD. This allows us to surmise at least a similar molecular program to WD. Subsequently FAD will be treated in-depth, together with its related disease entity (see chapter 1.3.3).

Regarding the molecular mechanisms underlying WD, researchers tend to focus on disparate mechanisms, which comprise either calcium or the interplay between survival and degeneration proteins as primary effectors of degeneration. Here, I will try to interweave the two concepts and describe a common basis.

It has been established that the nicotinamide adenine dinucleotide (NAD^+) biosynthetic enzyme component NMNAT1 of the chimeric WLD^S protein confers its axoprotective function. This occurs through a gain-of-function mutation, which leads to a mistargeting of NMNAT1 to axons, instead of to its physiological nuclear localisation (Sasaki & Milbrandt, 2010). NMNAT2, which also confers axoprotection, is a more labile isoform of NMNAT1 and appears in axons physiologically (Gilley & Coleman, 2010). Consequently, it is presumed that NMNAT1 can substitute and prolong the enzymatic activity of NMNAT2, even after the proteasomal depletion of NMNAT2 in the severed axonal portion. This concept is in accordance with the theory of the loss of trophic support after denervation, since NMNAT2 or its products, which supposedly represent survival factors, cannot reach the severed distal axon and slowly deplete. Such a mechanism could serve as molecular clock and assist in explaining the lag phase in WD. However, NMNAT2 overexpression does not lead to an increased level of its product NAD^+, since the rate-limiting step in NAD^+ synthesis is the upstream conversion of nicotinamide to nicotine amide mononucleotide (MNM) (Mack et al., 2001b). Thus, the protective effect is not caused by NAD^+ levels alone.

An alternative to an axonal survival factor is a pro-degenerative program. In contrast to a gain-of-function mutation, a degenerative signal can be identified by loss-of-function mutations, which promote axonal degeneration. The first protein that could be identified as promoter of axonal degeneration was dual leucine zipper kinase (DLK) (Miller et al., 2009), which is one out of three proteins of the MAPKKK family. These all serve as degeneration triggers, and their combined knockdown leads to a robust axoprotective phenotype (Yang et al., 2015). Notably, DLK has contrary func-

tions in the axon parts proximal and distal to axotomy. While promoting degeneration in the severed part, it supports regeneration in the proximal stump. The activators of DLK discussed include disruption of the cytoskeleton and calcium influx. Downstream effectors of MAPKKK proteins are proteins of the MAPK family. Excitingly, MAPK proteins have been shown to be differentially regulated: in an inhibitory manner (by the axoprotective NMNAT2), and in a stimulatory manner (by another prodegenerative protein, SARM1, which is discussed below). This could serve as a mechanistic link between these pathways (Gerdts, Summers, Milbrandt & DiAntonio, 2016).

Sterile alpha and TIR motif-containing protein 1 (SARM1) was discovered in a large genetic screen in Drosophila (Osterloh et al., 2012). SARM1 knockout protects axons from WD for up to 14 days in mice, which is similar to NMNAT-conferred protection (Gerdts, Summers, Sasaki, DiAntonio & Milbrandt, 2013). SARM1 has been demonstrated to be functionally connected to the rapid decline of NAD^+ levels after axotomy. SARM1 negative axons display a markedly reduced loss of NAD^+. Consequently, SARM1 acts upstream of NAD^+ loss (Gerdts, Brace, Sasaki, DiAntonio & Milbrandt, 2015).

An important point to explore is the way, in which calcium fits into this complex interplay of pro-degenerative and pro-survival cues. Extracellular calcium entry was found to be both necessary and sufficient for WD induction. For this purpose, the calcium level had to reach a concentration > 200 µM. (George, Glass & Griffin, 1995). In response to the calcium elevation, the proteases of the calpain family degrade the cytoskeletal components and destroy the axonal integrity. The calpain inhibitor calpastatin, which is constitutively active, must be diminished in preparation for the axonal-dismantling process (Ma et al., 2013).

The lingering question is at which point of process the cascade calcium comes into play. It was found that the exogenous addition of calcium was sufficient to abolish protection of WLD^S, which likely positions calcium downstream of WLD^S (Glass, Schryer & Griffin, 1994).

The initial gash in the membrane is an unlikely contributor to the eventual degeneration following axotomy. In fact, the highest calcium concentrations can be found at a distance of more than 100 µm from the injury site, and the membrane cut is resealed within two minutes post-axotomy by calcium-dependent vesicular fusion (Eddleman, Ballinger, Smyers, Fishman & Bittner, 1998; Ziv & Spira, 1993).

Organellar and extracellular calcium are estimated to be more potent contributors to calcium elevation. Mitochondria can sequester calcium through selective calcium uniporters, such as the MCU. Likewise, they are capable of rapid calcium release by MPTP formation, when mitochondrial calcium reaches a certain threshold. The pharmacological and genetic targeting of cyclophilin D, which is a component of the MPTP, causes a protection of severed axons for up to four hours (Barrientos et al., 2011). In addition, ER calcium depletion is implicated as potential source for the deleterious cytoplasmic-calcium rise (see chapter 1.3.5).

Extracellular calcium has been assumed to enter primarily through L-type calcium channels, since channel blockers are capable of a potent four-day protection after axotomy (George et al., 1995). Williams et al. (2014) managed to bring another compelling mode of calcium into play, though in a model of spinal cord contusion. Axolemmal mechanopores which fail to reseal and allow the diffusion of macromolecular dyes are major contributors to elevated calcium levels. However, the exact nature of these pores and their contribution in other injury paradigms have yet to be established.

An exciting link between the NMNATs and calcium has been proposed. NAD^+ levels can influence the axonal calcium homeostasis by modulating ion-channel activity (Tamsett, Picchione & Bhattacharjee, 2009). Interestingly, a terminal decrease in NAD^+ levels has been reported prior to the deleterious calcium cascade. Although it seems appealing, this potential link between NAD^+ decrease and calcium dysregulation still requires experimental validation (Wang et al., 2012).

In summation, the puzzle of how NMNAT, SARM, MAPKKK proteins and calcium, ROS and the MPTP interact remains unsolved. It seems as though the interplay of NMNAT, SARM, MAPKKK leads to the generation of an as-yet-unknown execution signal (potentially the NAD^+ decrease), which is then answered by a downstream cascade with calcium as primary effector.

1.3.3 Axonal degeneration in MS and EAE

MS is a major cause of neurologic disability. Patients who suffer from MS experience acute episodes of neurological dysfunction, followed by often incomplete remissions, the so-called relapsing-remitting MS (RRMS). In later stages, the disease can convert to a mode of secondary progression characterised by the perfidious accumulation of disability, termed secondary progressive MS (SPMS). Approximately

10% of patients suffer from primary progressive MS (PPMS), which is ‘amputated’ from the relapsing-remitting phase that usually precedes it. Here, the disease adopts a steady functional decline with a complete lack of periods of recovery. PPMS appears to be a consequence of more diffuse immune mechanisms and neurodegeneration. Clinical symptoms of MS include, among others, paraesthesia, dysaesthesia, paresis and visual disturbances with scotoma as a consequence of optic neuritis (Lee, Taghian & Petratos, 2014; Wilkins & Scolding, 2008).

MS is characterised by inflammatory lesions, which can preferentially be found in certain CNS locations, including the paraventricular region, the callosal commissure, brain stem and optic nerve as well as subcortically (Compston & Coles, 2008). These lesions contain a large number of inflammatory cells, which comprise primarily macrophages and T-lymphocytes but also B-lymphocytes and plasma cells (Lassmann, 2013). A pathognomonic feature of these lesions is demyelination. Autoreactive lymphocytes enter the CNS via the blood-brain barrier and elicit the local production of harmful cytokines and ROS/RNS, which can impair oligodendrocyte function (Hemmer, Kerschensteiner & Korn, 2015).

Although demyelination is the classical hallmark of MS, its assumed dominance in the pathogenesis of MS has come under scrutiny in recent years. The insights gleaned from magnetic resonance imaging and histological studies demonstrate that, concomitant to inflammation, the loss of axons is an important determinant of clinical symptoms and the switch to progressive disease (Ontaneda, Cohen & Amato, 2017). Here, I will focus on the pathogenetic aspects of this axonal loss in multiple sclerosis.

Histologically, it has been shown that axonal density is significantly reduced in periplaque white matter (PPWM) as well as MS plaques (Bitsch, Schuchardt, Bunkowski, Kuhlmann & Bruck, 2000). Trapp et al. (1998) established the presence of axonal transections in MS lesions. The susceptibility to degeneration varies with the anatomical location (e.g. upper posterior column > lower posterior column) and axon diameter, where small-calibre axons (<3 μm^2) are more prone to degenerate (DeLuca, Ebers & Esiri, 2004).

Amyloid precursor protein (APP), which is transported along the axon, accumulates in disease and can be used as marker for acute disruption of axonal function. Staining against APP detected axonal damage in active and, to a lesser extent, in chronic MS lesions (Kuhlmann, Lingfeld, Bitsch, Schuchardt & Bruck, 2002). The intensity

of APP staining correlates with the number of inflammatory cells, specifically CD8-positive T-lymphocytes, macrophages and microglia (Bitsch et al., 2000).

Interestingly, many studies pointed out the reduction of axonal density in early lesion stages and even in normal-appearing white matter (Lassmann, 2013). Two alternative explanations are either that axons are locally damaged outside of the lesions or degenerate because of the result of a multi-segmental, long-standing degeneration which affects distant tracts by WD. The latter has been deemed more likely, since WD was found to be a major contributor to periplaque white-matter axonal demise (Dziedzic et al., 2010). In contrast to demyelination, which can be in part remedied by the recruitment of oligodendrocyte precursor cells (albeit with considerable inter-individual disparity) (Patrikios et al., 2006), axonal degeneration is irreversible. Hence, it is important to study the precise mechanisms of axonal degeneration in the context of neuroinflammation in order to find potential neuroprotective treatment strategies.

A broad spectrum of pathomechanisms has been suggested to contribute to axonal damage in MS. Perhaps the most obvious candidate is demyelination. Loss of trophic support from oligodendrocytes and increased energy demand due to unfavourable nerve-conduction properties are plausible. In fact, sodium channels formerly concentrated at the nodes of Ranvier become dispersed as a consequence of demyelination (Smith, 2007). This can lead to a state of virtual hypoxia, leading to increased cellular Na^+ levels as a result of reduced Na^+/K^+-ATPase activity. As a consequence, the Na^+/Ca^{2+}-exchanger can revert its function and pump Ca^{2+}-ions into the cell. Increased axonal-calcium levels can impair axonal transport, compromise mitochondria (thereby creating a vicious cycle) and ultimately prompt a degeneration cascade, which involves calpains and other calcium-dependent proteases (Haines, Inglese & Casaccia, 2011).

However, it has been demonstrated in EAE that the axonal-degeneration mode of FAD (see chapter 1.3.1) occurs in generally myelinated axons (Nikić et al., 2011). Haines et. al (2011) posited the following hypothesis: ‘Axonal damage in multiple sclerosis might be concurrent to demyelination, but not necessarily consequent to myelin destruction’. Several possible pathomechanisms independent of demyelination have been suggested. Promising candidates in an inflammatory milieu are mononuclear phagocyte-produced ROS and RNS, which are membrane diffusible and can thus permeate intact myelin. ROS/RNS have been demonstrated to induce

an FAD-like pattern of axonal degeneration, and scavenging them alleviated FAD (Nikić et al., 2011). A mechanism for RNS-mediated axonal damage is inhibition of the mitochondrial respiration (Kapoor, Davies, Blaker, Hall & Smith, 2003) and promotion of activity-dependent axonal destruction (Smith, Kapoor, Hall & Davies, 2001). ROS can derange the complex signalling at ER-mitochondria nanodomains and elicit ER calcium release (Booth, Enyedi, Geiszt, Várnai & Hajnóczky, 2016).

Equally compelling is the finding that axonal transport is markedly reduced in EAE lesions, despite intact myelination and normal morphological appearance – yet demyelination caused an increased disturbance of transport. Transport deficits again interplayed with ROS/RNS levels and could act detrimentally via reduced mitochondrial supply (Sorbara et al., 2014).

Glutamate excitotoxicity has also been posited as an axonal noxa. Glutamate is produced extensively by immune cells and can mediate both myelin and axonal damage. AMPA/kainate-types of glutamate receptors inhibition ameliorated clinical symptoms in EAE (Pitt, Werner & Raine, 2000). The downstream mechanism is again thought to involve calcium rise and Na^+/Ca^{2+}-exchanger reversal. A parallel study in my host laboratory could not, however, determine a significant amelioration of axonal calcium overload following treatment with the Na^+/Ca^{2+}-exchanger blocking agent bepridil (Witte et al., 2019).

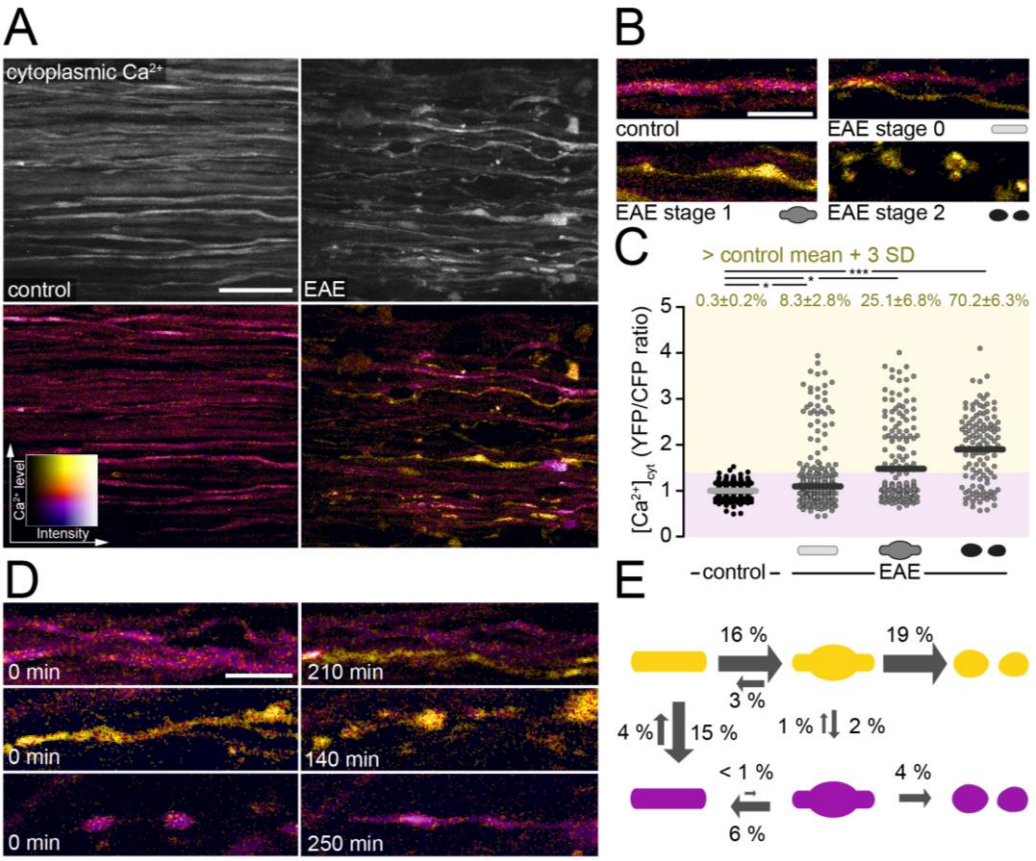

Figure 4: Cytoplasmic calcium levels predict axonal fate in neuroinflammatory lesions

(**A**) Representative in vivo 2-photon microscopy intensity projections (top, YFP channel) and the corresponding colour-coded cytoplasmic calcium ratios (bottom, YFP/CFP ratio) under control conditions (left) and subsequent to EAE induction, two days after developing symptoms (right). The images show the superficial dorsal funiculi of the spinal cord in Thy1-CerTN-L15 mice. (**B**) Exemplary images colour-coded for cytoplasmic calcium (YFP/CFP ratio) of axons under control conditions (upper left) and axons representative of the morphological FAD stages 0 (upper right), 1 (lower left) and 2 (lower right) 2 to 3 days after onset of disease following EAE induction. (**C**) Cytoplasmic calcium levels (YFP/ CFP channel) of control axons and axons representative of FAD stages 2 to 3 days after onset of EAE. The percentages on top correspond to the fraction of axons with cytoplasmic calcium > 3 times the standard deviation above the control mean value (colour-coded yellow in graph). The data is displayed as mean ± SEM (statistical testing performed per animal with n=6 control and n=11 EAE mice; Mann-Whitney U test). (**D**) Axons with colour-coding and experimental conditions analogous to (A) traced over time. Transition of a low calcium stage 0 to a high calcium stage 0 axon (top), of a high calcium stage 1 to a high calcium stage 2, fragmented axon (middle) and revorvery of a low calcium stage 1 to a low calcium stage 0 axon (bottom). (**E**) Graphical depiction of transition probabilities. Yellow = high calcium axons, purple = low calcium axons in n=307, 8 mice and 1201 axon hours. Scale bars: (A) 25 mm, (B) and (D) 10 mm. *p < 0.05; ***p < 0.001

Figure adapted from and caption modified from Witte et al. (2019). Experimenter: Adrian-Minh Schumacher

Despite not entering through a reversed Na^+/Ca^{2+}-exchanger, previous work in my laboratory established calcium as an important determinant of axonal fate in FAD by in-vivo imaging of transgenic mice which express the calcium indicator CerTN-L15 in neurons. Swollen and calcium high axons (stage 1) had a higher probability of undergoing fragmentation (stage 2) and a lower probability of recovery compared to swollen axons with normal calcium levels. See Figure 4 for a graphical summary. Consequently, elevation of cytoplasmic calcium is a potent trigger of FAD progression in neuroinflammatory lesions. Additionally, the removal of extracellular calcium by bath application of the calcium chelator ethylene glycol-bis(β-aminoethyl ether)-N,N,N',N'-tetraacetic acid (EGTA) completely blocked fragmentation in EAE lesions. The likely portal of entry was determined to be nanoruptures in the membrane present in EAE, which allowed for the diffusion of high-molecular dyes. The uptake of dyes correlated well with the axonal calcium content (Witte et al., 2019).

Assessing an additional contribution by intracellular stores, perhaps even prior to pore formation, was the primary motivation for this thesis.

1.3.4 Traumatic axonal injury

Traumatic axonal injury (TAI) can be regarded as a pathoanatomical subgroup of traumatic brain and spinal-cord injury. The amount of axonal damage is a key predictor of functional outcome and mortality following CNS trauma (Medana & Esiri, 2003). Previously unrecognised, TAI can entail progressive white-matter loss and neurodegeneration for a period of years after the injury in addition to the immediate axonal pathology (Johnson, Stewart, Begbie, et al., 2013).

Primary axotomy – albeit an import experimental paradigm which is also employed in this thesis – is, in fact, a rare finding in TAI (except for sharp-force trauma). A more common pattern of degeneration is defined by the appearance of varicosities and undulations, which can progress to ‘secondary axotomy’ (Christman, Grady, Walker, Holloway & Povlishock, 1994). These morphological alterations are generally attributed to cytoskeletal disruption. In fact, the special viscoelastic properties of microtubules can make them brittle after sudden elongations, like in the moment of impact. The following twisting and misalignment of microtubular fragments along the axon creates the beaded morphology. In an attempt to reorganise the cytoskeletal architecture, microtubules are depolymerised, leading to a temporal interruption of axonal transport, which again causes progressive swelling (Johnson, Stewart &

Smith, 2013). Special attention should be paid to the degradation of the cytoskeleton just below the axolemma (membrane skeleton). Ankyrins link the spectrin-actin complex to membrane proteins, which is crucial, e.g. for proper ion channel and -pump location at the nodes of Ranvier. Consistently, nodal and paranodal pathology with fragmentation of nodal axoplasm are prominent histological features in TAI and concur with ion channel and conductance dysfunction as well as a destabilisation of the cell membrane (Reeves, Greer, Vanderveer & Phillips, 2010). Cytoskeletal protection is a vivid field of research. Microtubule stabilisers, such as paclitaxel, have been shown to alter the rate of axonal degeneration (Kleele et al., 2014), and epothilone B has been deemed a promising neuroprotectant in spinal-cord injury (Ruschel et al., 2015).

As previously discussed, calcium dyshomeostasis also has long been implicated to be a pivotal effector of secondary axonal damage in TAI (Povlishock, 1992). Notably, several studies indicate that initial calcium dysregulation in TAI is caused by release from intra-axonal calcium stores, such as the ER (Staal et al., 2010; David P. Stirling et al., 2014). Later, a more gradual and lasting calcium dysregulation ensues. This implies that ER calcium release is upstream of the influx of extracellular calcium. However, the significance of calcium entry from the extracellular space also has a solid experimental foundation. Williams et al. (2014) demonstrated that axons can exist in a metastable state for hours after spinal-cord contusion. Meanwhile, the accumulation or buffering of elevated intracellular calcium determines these axons' fate. They can either progress to secondary axotomy if their calcium remains high, or they can recover. The source of this calcium was proven to be membrane mechanopores by dye-loading experiments, like my host laboratory found in EAE. Hence, the study of membrane-sealing agents is of high therapeutic interest. Candidates include polyethylene glycol (PEG), Mitsugumin 53 (a tripartite motif protein) and Kollidon VA64, which has proven promising in rodent TBI (Hill, Coleman & Menon, 2016; Miller et al., 2014). Nevertheless, a preceding contribution of intraorganellar calcium is still plausible (vide infra).

1.3.5 ER calcium in axonal degeneration

In this chapter, I will list a number of studies that implicate the role of ER-derived calcium in axonal degeneration.

The most solid foundation of experimental evidence for ER calcium release can be found in the models of anoxia and ischemia. Notably, there is a significant overlap between ischemia and other axodegenerative-injury paradigms (Stys, 1998). In ischemic axons, a rise of intracellular calcium can be detected, even when extracellular calcium is absent or chelated, and the intracellular calcium sources have been shown to sufficiently trigger the degenerative cascade without extracellular calcium influx (Ouardouz et al., 2003). Particularly ischemia, which is more severe than anoxia since it also involves a reduction of nutrient supply, has been demonstrated to recruit ER calcium stores in addition to extracellular calcium influx. The latter has been validated in the optic nerve of rats and spinal-cord explants in vitro (Stirling & Stys, 2010).

Stys et al. (2010) developed a fascinating mechanistic model of ER calcium involvement in axonal degeneration. They postulate the existence of so-called intermodal nanocomplexes, which are clusters of molecules involving GluR5- and GluR6 containing kainate receptors. These could potentially be activated by glutamate release from inflammatory cells or the reversal of axonal glutamate transporters under injury. GluR5-dependent ER calcium release is triggered by a G-protein-coupled activation of phospholipase C, which catalyses the generation of IP3. IP3 acts on IP3Rs to release intraorganellar calcium. GluR6 kainate receptors, however, lead to a depolarisation-induced excitation-contraction coupling-like release of calcium through RYRs. NO generated the neuronal nitric-oxide synthase (nNOS), which has been posited as an important modulator of this coupling mechanism. The molecules mentioned occur in close proximity to each other by means of immunoprecipitation assays and immunoelectron microscopy and have therefore been termed ‘nanocomplexes’ (Ouardouz et al., 2009; Stirling & Stys, 2010). Indeed, glutamate excitotoxicity has been determined not only to be important in grey-matter pathology, but also in white-matter degeneration. Accordingly, kainate receptor agonists and glutamate can cause axonal injury experimentally and elicit a lasting cytoplasmic-calcium rise (Li & Stys, 2000; Matute, 1998). If, in turn, kainate receptor antagonists are administered (in this example, NBQX), the rise in cytoplasmic calcium can be blocked efficiently. Another way to diminish glutamate-mediated calcium flux is blocking RyR with ryanodine, while a calcium-free perfusate was also an efficient way to reduce cytoplasmic-calcium rise. This points at an interdependence of extra-

cellular calcium influx and RyR activation, just as it is known for excitation-contraction coupling (Ouardouz et al., 2009). Internodal nanocomplexes could thus promote focal cytoplasmic calcium accumulation in an ER-enhanced manner and contribute to secondary axotomies. Primary axotomies (silk suture of spinal nerves in rats) were also reported to result in ER-calcium depletion, which was assessed by the surrogate marker of the reduction of caffeine-evoked ER calcium release. Furthermore, ER calcium was measured directly, employing the low-affinity calcium indicator mag-Fura-2-AM (Rigaud et al., 2009). In a model of stretch injury, a biphasic increase of cytoplasmic calcium could be detected. The rapid, primary increase was dependent on intracellular calcium sources, while the smaller and delayed secondary increase was attributed to extracellular sources, since it was diminished in a calcium-free medium (Staal et al., 2010).

Villegas et al. (2014) found that calcium release through RYRs and IP3Rs entails the activation of MPTP, which can be triggered by mechanical and toxic insults. ER calcium channel blockers had an inhibitory effect on injury-induced axonal degeneration. Accordingly, the genetic knockdown of ER calcium release channels had the same effect. In response to the attenuation of ER calcium release, mitochondrial swelling and dysfunction could also be significantly delayed.

Finally, a recent study by Stirling et al. (2014) established a deleterious role of ER calcium depletion in secondary-bystander axon degeneration in a whole spinal-cord explant laser-lesioning model. ‘Bystander degeneration’ indicates that some axons which are not transected by the initial laser lesioning still succumb to secondary degeneration. The study found that removal of extracellular calcium was completely ineffective in attenuating bystander degeneration in laser-induced spinal-cord pathology, which led to the investigation of intracellular calcium pools. A RyR gain of function mutant mouse line exhibited more severe bystander degeneration, while bystander degeneration (in wildtype and mutant lines) was attenuated by the pharmacological blockade of RyRs and IP3Rs with the respective antagonists ryanodine and 2-APB.

Combined, all of these studies clearly raise interest in the contribution of ER-calcium release to the axodegenerative cascade – especially with regard to other pathologies such as neuroinflammation, which is one of the main objectives of this thesis.

1.4 Intravital calcium imaging

Osamu Shimomura, Martin Chalfie and Roger Y. Tsien were awarded the Nobel Prize in Chemistry in 2008 ‘for the discovery and development of the green fluorescent protein, GFP’. GFP was later tweaked and modified to generate a mesmerising portfolio of variants, which today spans the entire spectrum of visible light and beyond (Ehrenberg, 2008).

In addition to the diversified spectral properties, improved brightness and photostability, fluorescent proteins (FP) soon entered the realm of biosensing. Today, more than a hundred biosensors have been developed, which allow for the detection of ions, redox conditions, enzymatic reactions and specific molecules (Palmer, Qin, Park & McCombs, 2011). ‘Such sensors, can be targeted to specific locations within a cell, expressed within specific cell types in a transgenic organism, and incorporated into organisms for long-term imaging’ (Palmer et al., 2011). These benefits of biosensors have all been explored in this thesis, in which I measured calcium in a subcellular compartment (the ER), in cell types of interest (neurons) and I created a transgenic organism (a mouse line) for 2-photon imaging.

1.4.1 Principles of calcium indicators

The design of genetically encoded calcium indicators (GECIs) based on FP-variants has followed two distinct pathways: GECIs containing a single FP, and GECIs which consist of two different FPs that interact via a process called fluorescence resonance energy transfer (FRET, vide infra).

The single-FP-type sensors are based on circularly permutated FPs in combination with a calcium-responsive element. The underlying mechanism depends on the alteration of the fluorophores by the degree of protonation. The protonation state changes with the conformation of the calcium-responsive element (often calmodulin-derived). This type of calcium sensor is generally characterised by a high dynamic range and a narrow range of excitation and emission wavelengths. Consequently, two or more of these indicators with different wavelengths can be monitored independently in the same experiment. This single FP-type of GECI is typically intensiometric, which means that the intensity of the signal is proportional to the amount of bound calcium. The readout is a single-channel measurement. However, there are confounding factors which influence intensity, such as expression levels

and movements of the specimen. Therefore, it is difficult to determine the resting-state calcium level using intensiometric sensors. Intensiometric calcium sensors are, however, superior in measuring temporal dynamics in stable specimens and feature a large dynamic range (Palmer et al., 2011; Thestrup et al., 2014). The most popular single-FP sensors include the green G-CaMPs (Nakai, Ohkura & Imoto, 2001), their red counterpart R-CaMP (Akerboom et al., 2013) and GECOs (Zhao et al., 2011).

The opposite of intensiometric sensors are ratiometric sensors – in particular, emission ratiometric sensors, which allow one to determine the calcium level by the ratio of two FPs' intensities, thereby providing a relative measure. These sensors are advantageous in imaging moving specimens and resting-state calcium levels, since they are not influenced by changes in optical-path length, excitation-light intensity and GECI-expression level. These factors combined with the superior baseline brightness make FRET-based GECIs the sensors of choice for transgenic organisms and intravital imaging. The archetypal ratiometric calcium sensors are the cameleons, which are the oldest and most optimised GECIs. Cameleons consist of two spectrally overlapping fluorescent proteins (mostly YFP and CFP variants), which are tethered together by a calcium-sensitive domain – in this case, calmodulin – and the M13 peptide from myosin light-chain kinase (Miyawaki, Griesbeck, Heim & Tsien, 1999). Upon calcium binding, a conformational change in the calcium binding domain occurs, and the two FPs approximate. Within a distance of 5–100 Å, the spectrally overlapping FPs transfer energy via FRET. In the case of a CFP-YFP couple, CFP acts as donor and YFP as acceptor of this radiation-less energy transfer. With decreasing distance of the FPs, CFP emission is increasingly quenched, and YFP emission is sensitised. Apart from the donor-acceptor distance, the efficiency of the energy transfer also depends on the dipole orientations of donor and acceptor, and the environmental factors which influence dipole interactions, such as types of solvents, degree of hydration, pH and temperature. The practical consequence of FRET is that it can serve as a nanoscale ruler, which translates submicroscopic distances into varying fluorescence intensities (Murphy & Davidson, 2012; Palmer et al., 2011; Schumacher, 2015).

Cameleon calcium indicators underwent a notable history of improvements and modifications. The earliest cameleon included the FP's blue-fluorescent protein

(BFP) and S85T GFP. However, a spectral red shift was favourable for cellular imaging, due to reduced phototoxicity of the excitation light, as well as diminished light scattering and auto-fluorescence. Thus, the spectrally red-shifted pair of ECFP and EYFP replaced BFP and S85T GFP and became known as the YC family of cameleons (creating truly red FRET-based GECIs for deeper-tissue penetration is an ongoing endeavour to date; however, they still suffer from poor dynamic ranges) (Miyawaki et al., 1997; Palmer et al., 2011). The FPs were further improved to increase photostability as well as folding at 37°C and reduce pH and chloride-sensitivity (Griesbeck, Baird, Campbell, Zacharias & Tsien, 2001). However, each sensor features its individual advantages, and there is an abundance of choice. For example, EYFP V68L/Q69K containing GECIs have reduced chloride and pH-sensitivity, but have less-efficient maturation at 37 °C and are dimmer than their counterparts, venus and citrine. Venus and citrine, in turn, are more susceptible to chloride and pH-influences (Griesbeck et al., 2001). These characteristics are important to consider when designing an experiment involving GECIs. Subsequently, circularly permuted FPs have been integrated into FRET GECIs. Here, the original N- and C-termini of the original FPs are fused together, and new termini are defined. This leads to an altered dipole orientation, and it can increase the dynamic range drastically (Nagai, Yamada, Tominaga, Ichikawa & Miyawaki, 2004). The calcium-sensitive linker has become another target for modifications. Instead of calmodulin and the M13 peptide, troponin C has been incorporated into GECIs. This was a necessary step, since calmodulin has abundant interactions with cellular proteins which can hamper an experiment. In both troponin C- and calmodulin-based linkers, the calcium-binding linker consists of two globular domains with two calcium-binding sites on each. This can lead to abundant calcium buffering and nonlinear kinetics (Palmer et al., 2011; Thestrup et al., 2014). In an effort to reduce the complexity of the calcium-binding site, Thestrup et al. (2014) created GECIs with a minimal calcium binding domain of toadfish (Opsanus tau) troponic C with fewer calcium-binding sites and improved dynamic ranges. These sensors were called Twitch-sensors; they possess a superior Hill coefficient and are less likely to interfere with calcium buffering. A low-sensitivity Twitch variant (Twitch2B 54S+) was used to measure ER calcium in this thesis.

1.4.2 ER calcium indicators

Since the majority of GECIs was destined for cytoplasmic measurements, enhancing their sensitivity has been a primary focus in the evolution of calcium indicators. This allowed, for example, the measurements of fast synaptic transients in neurons. However, the amount of calcium differs over several orders of magnitude in different subcellular environments. This renders high-sensitivity calcium indicators with a low-dissociation constant (K_d) useless in the ER, where the free calcium concentration can be up to 10.000 times the cytoplasmic concentration. Moreover, the ER has a more oxidising environment, which allows disulphide bond formation and proteins in the ER, including GECIs, are subject to covalent modifications, such as glycosylation (Gerasimenko, Petersen & Gerasimenko, 2014).

Consequently, ER calcium indicators had to be specialised in order to function in this unique milieu. Initially, intra-ER free calcium could only be measured by dye-loading techniques. Mostly acetoxymethyl (AM) esters of low-affinity calcium dyes (Mag-Fura-2 and others) were used, which accumulated in the ER and other organelles. After dye loading, cytosolic dialysis using patch-clamp techniques is required, so that imaging under physiological conditions is precluded (Gerasimenko et al., 2014; Suzuki, Kanemaru & Iino, 2016). An elegant way to circumvent the necessity of cellular dialysis is targeted esterase-induced dye loading (TED). Here, the esterification of the AM-ester is carried out directly in the ER lumen by a genetically encoded, ER-targeted carboxylesterase. This obviates the need of cytoplasmic dialysis, since the remaining dye can be easily washed out (Samtleben et al., 2013).

However, GECIs are still the indicators of choice for intravital imaging. Recent advances in ER environment-optimised GECI design have proven the feasibility of this concept. The first ER-targeted GECIs were YC3er and YC4er. Their K_d-value was raised to the low micromolar range by inserting point mutations into the calmodulin domain. Still, a K_d-value of 4.4 µM in case of YC3er is too low to faithfully report ER calcium alterations. YC4er was better suited and offered a K_d-value of 700 µM (albeit biphasic) but had the drawback of a limited dynamic range (Miyawaki et al., 1997). Further improvements yielded the sensor D1ER, which was engineered to be insensitive to interactions with endogenous calmodulin and offered an increased dynamic range (Palmer, Jin, Reed & Tsien, 2004).

Moreover, single-FP calcium indicators have been engineered to enable ER calcium measurements. One such sensor is CatchER, containing charged residues close to the fluorophore in EGFP, which act as calcium-binding moiety. CatchER offers the benefits of being excitation-ratiometric and having a high dynamic range of 230 %. This sensor was demonstrated to be capable of measuring calcium fluxes in mouse myofibre SR (Tang et al., 2011). Another attractive alternative is the CEPIA family of GECIs. CEPIA indicators are based on GECOs with inserted point mutations in the calmodulin domain. Spectral properties of CEPIAs match those of GECOs. Consequently, red and green CEPIA variants are available – even an emission-ratiometric CEPIA variant, GEM-CEPIAer. These sensors offer superb dynamic ranges (470 %–2100 %) and have been successfully employed to visualise the process of ER calcium replenishment following synaptic input in Purkinje cells in mice (Okubo et al., 2015; Suzuki et al., 2014). Further alternatives in this group of single-FP ER-GECIs have been designed and include ER-LAR-GECO1 (Jiahui Wu et al., 2014) and GCaMPer (Henderson et al., 2015). Finally, erGAP1 is based on a fusion of aequorin and GFP. Despite including aequorin, it is independent of the cofactor coelenterazine. It is believed that aequorin serves as a calcium-sensing element and influences the fluorophore in GFP by conformational changes. This indicator is also excitation-ratiometric and has been successfully used in transgenic mice, where ER calcium release could be measured in acute hippocampal slices (Navas-Navarro et al., 2016; Rodriguez-Garcia et al., 2014).

An overview of the physical properties of this enumeration of ER-targeted GECIs can be found in Table 1. Also included in this table is the eventual choice that we made for measuring ER-calcium dynamics in a transgenic mouse line. For intravital imaging, we needed an emission-ratiometric sensor which would compensate for differences in expression levels, optical-path-length differences and movements. Transgenic mice expressing FRET indicators TN-XXL and CerTN-L15 were successfully used in my host laboratory previously to measure cytoplasmic axonal calcium dynamics in transgenic mice (Schumacher, 2015). Thus, we sought indicators with similar spectral properties. Due to the reported low dynamic range and brightness of D1ER and D4ER FRET GECIs, we chose to target a high-K_d variant of the improved Twitch sensors to the ER, Twitch2B 54S+ (Thestrup et al., 2014). The emission-ratiometric, high dynamic range indicator GEM-CepiaER could have been a suitable alternative as well. However, we could only generate very low intensities

in peripheral nerves in a virus-based expression system, which were also subject to rapid photobleaching. The physical properties of Twitch2B54S+ (originally determined without the ER retention tag KDEL) are included in Table 1.

1.4.3 Intravital microscopy of the nervous system

Two important concurrent developments made in-vivo microscopy of the nervous system possible: the advent of new imaging techniques – namely, two-photon laser-scanning microscopy (TPLSM) – and the development of transgenic technologies, allowing the labelling of single neurons (Misgeld & Kerschensteiner, 2006).

The labelling of individual neurons was achieved with the so-called Thy1-XFP mice, where XFP indicates any fluorescent protein or fluorescent functional indicator under the control of the modified Thy1-promoter. The Thy1-promoter is a pan-neuronal regulatory element, which gives rise to a strong neuronal expression with a variable extent. Dependent on the chromosomal integration site, the reporter expression can be restricted to a small percentage of neurons and can thereby create a Golgi-like staining pattern (subset-labelling), or the expression can include all neurons (full-labelling). Subset-labelling is particularly desired for intravital imaging, since it reduces the density of the structures of interest (e.g. axons, dendrites) and allows easier tracking over time (Misgeld & Kerschensteiner, 2006). The first Thy1-XFP transgenic mice were created by Feng et al. (2000) and contained a number of spectral variants with individual expression patterns (among others GFP, YFP, CFP, DsRed). Subsequently many more reporters have been established in Thy1-trangenic lines, which enabled the assessment of organelle transport and distribution, synaptic release and spiking activity as well as mitochondrial redox state (Marinkovic, Godinho & Misgeld, 2015). Neuronal calcium concentrations could also be measured by placing GECIs under the control of the Thy1-promoter, which resulted in the transgenic line CerTN-L15 (Heim et al., 2007). This line was used to determine calcium as a key contributor to axonal degeneration in FAD (Witte et al., 2019).

The potential of these transgenic lines could only be fully exploited when TPLSM became widely accessible. This imaging technique uses very high intensities of longer-wavelength light to excite FPs, instead of their characteristic lower peak-excitation wavelengths. Key to this excitation process is that two photons of longer

wavelength arrive at the fluorophore nearly simultaneously, thereby adding their energies together. This requires intense light pulses from an ultra-fast laser. Thereby, excitation is limited to the focal point, which obviates the need for a pinhole to exclude out-of-focus light, as it is used in confocal microscopy (intrinsic optical sectioning of TPLSM). Consequently, even scattered-emission light can be used for detection, since it must have originated in the focal point. This accounts for the practicality of TPLSM for intravital imaging, together with the facts that the infrared excitation light can penetrate tissue easily and that out-of-focus bleaching and phototoxicity are kept at low levels (Lichtman & Fraser, 2001; Misgeld & Kerschensteiner, 2006). From the beginning, TPLSM has been used to shed light on calcium dynamics in neurons. Initially, vital dyes (calcium green) were loaded to dendrites in neocortical neurons and faithfully reported calcium rises in coincidence with sodium action potentials, which proved the practicality of this novel imaging technique (Svoboda, Denk, Kleinfeld & Tank, 1997). Today, by making use of the abundant arsenal of GECIs in conjunction with modern TPLSM, even in-vivo measurements of calcium in organelles as small as the axonal ER are feasible, as will be demonstrated in this thesis.

.

Illustration	Name	Type	Tag	K_d for Ca^{2+}	Dynamic range	Hill coefficient	Ca2+-responsive elements	Fluorophores	Excitation peak (nm)	Emmission peak (nm)
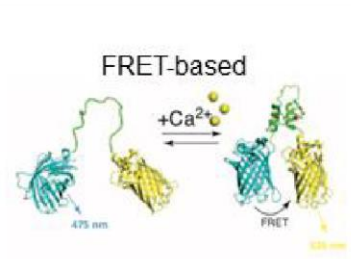	YC3er	FRET	Calreticulin, KDEL	4.4 µM	—	0.76	CaM, M13	ECFP, EYFP	433	475, 527
	YC4er	FRET	Calreticulin, KDEL	0.083, 60 µM,	—	1.5, 0.87	CaM, M13	ECFP, EYFP	433	475, 527
	D1ER	FRET	Calreticulin, KDEL	0.081, 60 µM,	—	1.18, 1.67	CaM, M13	ECFP, Citrine	433	475, 529
	D4ER	FRET	Calreticulin, KDEL	195 µM	—	—	CaM, M13	ECFP, Citrine	433	475, 529
	Twitch2B 54S+ ER	FRET	Immunoglobulin Vh,KDEL	174 µM	3.2	—	Troponin (Opsanus), minimal domain	mCerulean3 cpVenusCD	433	475, 528
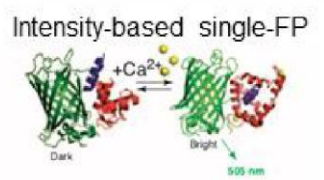	G-CEPIA1er	Intensio	Immunoglobulin Vh,KDEL	672 µM	4.7	1.95	CaM, M13	cpEGFP	497	511
	R-CEPIA1er	Intensio	Immunoglobulin Vh,KDEL	565 µM	8.8	1.7	CaM, M13	cpmApple	562	584
	ER-LAR-GECO1	Intensio	Calreticulin, KDEL	24 µM	10	1.3	CaM, M13	cpmApple	561	589
	GCaMPer(10.19)	Intensio	Calreticulin, KDEL	400 µM	14	1.9	CaM, M13	cpEGFP	496	513
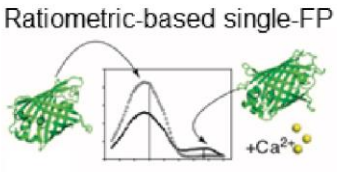	GEM-CEPIA1er	Ratio	Immunoglobulin Vh,KDEL	558 µM	21.7	1.37	CaM, M13	cpEGFP	391	462, 510
	CatchER	Ratio	Calreticulin, KDEL	180 µM	2.3	0.94	Created Ca^{2+}-site	EGFP	398, 490	510
	erGAP1	Ratio	Calreticulin, KDEL	12 µM	2.7	1	Aequorin	EGFP	403, 470	510

Table 1: Overview: physical properties of ER-GECIs

GECIs with a single FP can be divided into: intensiometric and ratiometric indicators. Single-FP-type GECIs and FRET-type GECIs are illustrated schematically. Twitch2B 54S+ ER which is used in this thesis and its physical properties are highlighted in yellow. Illustrations adapted from Palmer et al. (2011). Table adapted and modified from Suzuki et al. (2016).

2 Objectives

The preceding work has demonstrated calcium to be the fate-determining mediator of focal axonal degeneration in neuroinflammatory lesions and in the model of spinal-cord contusion (Schumacher, 2015; Williams et al., 2014). Moreover, mechano- or nanopores in the membrane were established as important paths of entry for calcium from the extracellular space in both models (Bewersdorf, 2017; Williams et al., 2014). Recent studies also implicate that calcium from a major organellar store, the ER, can be sufficient to trigger the axonal degeneration cascade (Ouardouz et al., 2003; Stirling et al., 2014). Such a contribution of ER calcium deregulation is a compelling finding, since numerous methods of pharmacological manipulation of the ER calcium homeostasis exist. Consequently, this thesis aims to shed light on ER calcium dynamics (perhaps even as an upstream regulator) in neuroinflammatory lesions and in the traumatic spinal-cord injury models. The following questions were specifically addressed:

1. **Is there a modality for in-vivo imaging of intra-ER free calcium in single axons?**
   - 1.1. Can the axonal ER be targeted, visualised and morphologically characterised using fluorescent reporters?
   - 1.2. Is there a calcium indicator that can generate a conclusive readout of intra-ER free calcium, and can we ascertain that it actually measures calcium?
   - 1.3. Can this indicator of intra-ER free calcium be stably expressed in a transgenic mouse line with expression patterns, levels and locations applicable to in-vivo imaging of the spinal cord?
   - 1.4. If such a transgenic line can be generated, does the indicator report intra-ER free calcium adequately upon pharmacologic manipulation in an in-vivo setting of the spinal cord?
2. **How is intra-ER free calcium affected in paradigms of axonal degeneration?**
   - 2.1. Can changes of intra-ER free calcium or ER morphology be detected in lesions of acute EAE, and, if so, do these influence the axonal fate in the degeneration process?
   - 2.2. Can changes of intra-ER free calcium or ER morphology be detected in traumatic spinal-cord injury paradigms?

3 Materials and Methods

3.1 Materials

3.1.1 Reagents

3.1.1.1 Reagents for surgery and in vivo imaging

Agarose	Sigma-Aldrich® Chemie GmbH, 82024 Taufkirchen, Germany
Bepanthen Augen- und Nasensalbe 5 g (eye ointment)	Bayer Vital GmbH, Leverkusen, Deutschland
Cutasept F Lösung 250 ml (disinfectant spray)	Bayer Vital GmbH, Leverkusen, Germany
Ethanol 70%	CLN GmbH, 85416 Niederhummel, Germany
Forene (Isoflurane)	Abbott AG, Baar, Switzerland
Ketamine hydrochloride 10% (Ketamine)	Bremer Pharma GmbH, Warburg, Deutschland
Ringerlösung Fresenius KabiPac (Ringer's solution)	Fresenius KaBI Dtl., Bad Homburg, Deutschland
Sterile artificial mouse cerebrospinal fluid (aCSF)	Solution A: 8,66 g NaCl (Merck) 0,224 g KCl (Merck) 0,206 g CaCl2 · 2H2O (Sigma-Aldrich) 0,163 g MgCl2 · 6H2O (Sigma-Aldrich) Solution B: 0,214 g Na2HPO4 · 7H2O (Merck) 0,027 g NaH2PO4 · H2O (Merck) dH20 ad 500 ml Mixture of solutions A and B in a 1:1 ratio
Xylariem 20 mg (Xylazine)	Riemser Arzneimittel AG, Greifswald-Insel Riems, Germany
Midazolam B. Braun 5mg/ml	B. Braun Melsungen AG, Melsungen, Germany
Domitor® (Medetomidin) 1mg/ml	Orion Pharma Corporation, Espoo, Finland

Fentanyl B. Braun 0.1mg	B. Braun Melsungen AG, Melsungen, Germany
Dimethylsulfoxid (DMSO)	Sigma-Aldrich Chemie GmbH, 82024 Taufkirchen, Germany
Thapsigargin	Merck KGaA, 64293 Darmstadt, Germany

3.1.1.2 Reagents for cell and explant imaging

Ionomycin, Calcium Salt (1:1)	Life Technologies GmbH, 64293 Darmstadt, Germany
10x Normal Ringer's solution	Made in Konnerth labortatory, Munich, Germany $NaHCO_3$ 21.84g NaH2PO4* H2O 1.72g KCl 1.86g NaCl 73.05g Dissolved in dH2O. 1 l total volume.
1x Normal Ringer's solution	2ml CaCl2, 1M 1ml MgCl2, 1M 100ml Ringer solution (10x) 3.6g Glucose dH2O ad 1l prepared in house
HBSS (10X), calcium, magnesium, no phenol red	Thermo Fisher Scientific Inc. Waltham, Massachusetts, USA
HHBSS (1x)	50ml 10x HBSS 1 g Glucose 2.38 g HEPES dH20 ad 500 ml adjust pH to 7.4
HHBSS (1x) with 10mM calcium	50ml 10x HBSS 1 g Glucose 2.38 g HEPES 0.485 g $CaCl_2$ dH20 ad 500 ml adjust pH to 7.4

3.1.1.3 Reagents for tissue processing/ immunohistochemistry

Phosphate Buffer (PB) 0,2 M	27,598 g NaH2PO4· H2O, 35,598 g Na2 HPO4· 2H2O dH2O ad 1l
Phosphate Buffered Saline (PBS), 10x 103,23 mg Na2HPO4 · H2O	103,23 mg Na2HPO4 · H2O 26,52g Na2HPO4 · 2H2O 40g NaCl H2O bidest. added to 1l Prepared in house.
PFA (paraformaldehyde) 4%	8% PFA (Sigma-Aldrich) in dH2O, heated up to 55 °C and stirred additional 10 min, filtrated and mixed in a 1:1 ratio with 0,2 M PB (Phosphate buffer), pH adjusted to 7,2-7,8
Gibco Goat Serum	Invitrogen GmbH, Darmstadt, Germany
Sucrose	Sigma-Aldrich® Chemie GmbH, 82024 Taufkirchen, Germany
TBS 10x (Tris buffered saline), pH=7,6	61 g Tris base (121,14 g/mol), (Sigma- Aldrich) 90 g NaCl dH2O ad 1l
Tissue Tek optimal cutting temperature (O.C.T.)	akura Finetek Europe B.V., Alphen aan den Rijn, The Netherlands
Triton X-100	Sigma-Aldrich® Chemie GmbH, 82024 Taufkirchen, Germany
Vectashield Mounting Medium, Fluorescence H-1000	Vector Labs, Burlingame, CA 94010, USA
Rabbit polyclonal to GRP78 BiP antibody (ab21685)	Abcam, Cambridge, MA 02139-1517, USA
Alexa Fluor® 647 Goat Anti-Rabbit IgG (H+L) Antibody	Life Technologies GmbH, 64293 Darmstadt, Germany

3.1.1.4 Reagents for molecular cloning and cell culture

T4 DNA Ligase Buffer (10X)	New England Biolabs, Ipswich, Massachusetts 01938, USA
Nuclease-free water	New England Biolabs, Ipswich, Massachusetts 01938, USA

T4 DNA Ligase	New England Biolabs, Ipswich, Massachusetts 01938, USA
10x CutSmart® Buffer	New England Biolabs, Ipswich, Massachusetts 01938, USA
10x NEBuffer 4	New England Biolabs, Ipswich, Massachusetts 01938, USA
DNA Polymerase I, Large (Klenow) Fragment	New England Biolabs, Ipswich, Massachusetts 01938, USA
Phusion® High-Fidelity DNA Polymerase	New England Biolabs, Ipswich, Massachusetts 01938, USA
5X Phusion HF and GC Buffer	New England Biolabs, Ipswich, Massachusetts 01938, USA
10 mM dNTPs	New England Biolabs, Ipswich, Massachusetts 01938, USA
BamHI-HF	New England Biolabs, Ipswich, Massachusetts 01938, USA
NotI-HF	New England Biolabs, Ipswich, Massachusetts 01938, USA
ClaI	New England Biolabs, Ipswich, Massachusetts 01938, USA
HindIII-HF	New England Biolabs, Ipswich, Massachusetts 01938, USA
PvuI-HF	New England Biolabs, Ipswich, Massachusetts 01938, USA
EcoRI-HF	New England Biolabs, Ipswich, Massachusetts 01938, USA
XhoI-HF	New England Biolabs, Ipswich, Massachusetts 01938, USA
Qiagen Plasmid Maxi Kit	Qiagen, Venlo, Netherlands
Qiagen Plasmid Mini Kit	Qiagen, Venlo, Netherlands
Pronucleus Injection Buffer	Tris 5mM EDTA 0.1 mM Adjust pH to 7.6, filter sterilize and store at 4°C, prepared in house
MfeI-HF	New England Biolabs, Ipswich, Massachusetts 01938, USA

NheI-HF	New England Biolabs, Ipswich, Massachusetts 01938, USA
BlpI	New England Biolabs, Ipswich, Massachusetts 01938, USA
SacI-HF	New England Biolabs, Ipswich, Massachusetts 01938, USA
Lipofectamine™ 2000 Transfection Reagent	Life Technologies GmbH, 64293 Darmstadt, Germany
NEB® 5-alpha Electrocompetent E. coli	New England Biolabs, Ipswich, Massachusetts 01938, USA
Sodium hydroxide solution	Life Technologies GmbH, 64293 Darmstadt, Germany
SOC Outgrowth Medium	New England Biolabs, Ipswich, Massachusetts 01938, USA
AccuTaq™ LA DNA Polymerase with 10x buffer (used for genotyping)	Merck KGaA, 64293 Darmstadt, Germany
Ethidium bromide	Sigma-Aldrich Chemie GmbH, 82024 Taufkirchen, Germany
Alkaline Phosphatase, Calf Intestinal (CIP)	New England Biolabs, Ipswich, Massachusetts 01938, USA
Dulbecco's modified Eagle medium (DMEM)	Invitrogen, Carlsbad, California, USA
Fetal Bovine Serum, certified, heat inactivated, US origin	Thermo Fisher Scientific Inc. Waltham, Massachusetts, USA
Penicillin/Streptomycin solution	Sigma-Aldrich® Chemie GmbH, 82024 Taufkirchen, Germany
Poly-L-lysine hydrobromide	Sigma-Aldrich® Chemie GmbH, 82024 Taufkirchen, Germany
Lipofectamine 2000 Transfection Reagent	Invitrogen, Carlsbad, California, USA
QIAquick Gel Extraction Kit	Qiagen, Venlo, Netherlands

3.1.1.5 Reagents for immunization

Myelin Oligodendrocyte Glycoprotein (MOG)	Stock solution, produced by laboratory of Martin Kerschensteiner, 82152 Planegg, Germany

M. tuberculosis H37 RA	Sigma-Aldrich® Chemie GmbH, 82024 Taufkirchen, Germany
Incomplete Freund Adjuvans (IFA)	Sigma-Aldrich® Chemie GmbH, 82024 Taufkirchen, Germany
Pertussistoxin (Ptx) from Bordetella pertussis, inactivated	Sigma-Aldrich® Chemie GmbH, 82024 Taufkirchen, Germany
Sodium acetate (3mM, pH 3)	Merck KGaA, 64293 Darmstadt, Germany

3.1.2 Tools and materials

3.1.2.1 Tools and materials for surgery and in vivo imaging

Wella contura W7807 (Hair clipper)	Wella, Darmstadt, Germany
BD Plastipak Hypodermic luer slip syringe 1 ml (syringe for Ketamine/Xylazine and Ptx injection)	Becton, Dickinson and Company, Franklin Lakes (New Jersey), USA
Feather stainless steel blade (surgical blade)	pfm medical ag, Cologne, Germany
Noyes Spring Scissors (Large spring scissors)	Fine Science Tools GmbH, Heidelberg, Germany
Vannas-Tübingen Spring Scissors (Small angled spring scissors)	Fine Science Tools GmbH, Heidelberg, Germany
Dumont Mini Forceps – Inox Style 5	Fine Science Tools GmbH, Heidelberg, Germany
Hypodermic Needles BD Microlance 3 30 Gauge (0,3 mm, yellow) for subcutaneous injection of Ptx and anesthesia	Becton, Dickinson and Company, Franklin Lakes (New Jersey), USA
Hypodermic Needles BD Microlance 3 23 Gauge (0,6 mm, blue) for subcutaneous emulsion immunization	Becton, Dickinson and Company, Franklin Lakes (New Jersey), USA
BD Plastipak hypodermic luer slip syringe 1 ml (syringe for injection of Ptx, anesthetics)	Becton, Dickinson and Company, Franklin Lakes (New Jersey), USA

Ethicon Ethilon monofil 6-0 size, 667H (skin suture)	Johnson & Johnson Medical GmbH, Norderstedt, Germany
Ethicon Vicryl 4-0 size, MIC101H (intracorporal suture)	Johnson & Johnson Medical GmbH, Norderstedt, Germany
Sugi (absorbent triangles)	Kettenbach GmbH & Co. KG, Eschenburg, Germany
Spongostan special (hemostatic gelatin sponge)	Ethicon Inc. Somerville, New Jersey, USA
Metal plate	Custom-made
Cast Alnico Button Magnets	Eclipse Magnetics Ltd, Sheffield, UK
Rubber bands	
Infinite Horizons Impactor	Precision Systems and Instrumentation, Fairfax Station, VA 22039, USA
P-30 Vertical Micropipette Puller	Sutter Instruments, Novato, California, USA
Safety-Multifly-Set 21Gx3/4” TW (0,8 x 19 mm)	Sarstedt AG & Co., Nümbrecht, Germany
51500D Digital New Standard Stereotaxic, Rat and Mouse	Stoelting Europe, Terenure, Dublin D6WY006, Ireland
Thin wall Borosilicate Glass Micropipettes	Sutter Instrument, Novato, CA 94949, USA
Support cushion	

3.1.2.2 Tools and materials for cell and explant imaging

minuten pins (0.2-mm diameter, shortened to 4 mm), FST: 26002-20	Fine Science Tools GmbH, Heidelberg, Germany
10 cm plastic petri dishes	Sigma-Aldrich Chemie GmbH, 82024 Taufkirchen, Germany
15 cm glass petri dish	Sigma-Aldrich Chemie GmbH, 82024 Taufkirchen, Germany
Metal plate	

3.5-cm tissue culture dish filled with Sylgard polymer	Dow Corning Inc., Midland/Michigan, USA
.Tubing to oxygenate explants during the dissection procedure	Warner Instruments, Holliston, MA 01745, USA
Vacuum system with suction tube	Warner Instruments, Holliston, MA 01745, USA
Warner W4 64-0704 22 mm Coverslips square	Warner Instruments, Holliston, MA 01745, USA
Warner Large closed Diamond Bath RC-21B	Warner Instruments, Holliston, MA 01745, USA
Flow Valve	Warner Instruments, Holliston, MA 01745, USA
Syringe Holder, eight 60 cc syringes	Warner Instruments, Holliston, MA 01745, USA
Heating ring for 3.5-cm dishes	Warner Instruments, Holliston, MA 01745, USA
Vaccum grease	Warner Instruments, Holliston, MA 01745, USA

3.1.2.3 Tools and materials for for tissue processing/ immunohistochemistry

12-Well Microtiter plates	Becton, Dickinson and Company, Franklin Lakes, New Jersey, USA
15 ml and 50 ml Falcon tubes	Greiner Bio-One GmbH, Frickenhausen, Germany
Transparent nail varnish	
Microscope slides 76x26 mm	Gerhard Menzel Glasbearbeitungswerk, GmbH & Co. KG, Braunschweig, Germany
Microscope cover slips 24x60 mm	Gerhard Menzel Glasbearbeitungswerk, GmbH & Co. KG, Braunschweig, Germany
Parafilm	Brand GmbH & Co. KG, Wertheim Germany

Pipettes, pipette tips and tubes (2ml and 1,5 ml)	Eppendorf AG, Hamburg, Germany
Tissue Tek Cryomold Standard, 25x20x5 mm	Sakura Finetek Europe B.V. , Alphen aan den Rijn, The Netherlands
Tissue Tek Cryomold Biopsy, 10x10x5 mm	Sakura Finetek Europe B.V. , Alphen aan den Rijn, The Netherlands

3.1.2.4 Tools and materials for molecular cloning

Gene Pulser®/MicroPulser™ Electroporation Cuvettes	Bio-Rad, California 94547, USA
MicroPulser™ Electroporator	Bio-Rad, California 94547, USA
Kanamycin or Ampicillin containing selective plates	Produced and sterilized in house
Falcon 25cm, Rectangular Canted Neck Cell Culture Flask with Vented Cap	Corning GmbH, 65189 Wiesbaden
Real-Time PCR Detection System	Bio-Rad, California 94547, USA
Paper filters (185 mm Ø circles)	Whatman Schleicher & Schuell GmbH, Dassel, Germany

3.1.3 Technical devices

3.1.3.1 Technical devices for surgery and in vivo imaging

Olympus KL 1500 LCD (cold light source for stereomicroscopy)	Olympus Deutschland GmbH, Hamburg, Germany
Olympus Stereo Microscope SZ51	Olympus Deutschland GmbH, Hamburg, Germany
FST 250 Hot Bead Sterilizer (sterilizer for surgical instruments)	Fine Science Tools GmbH, Heidelberg, Germany

T/Pump (Heating pad)	Gaymar Industries, Orchard Park (New York), USA
100W infrared lamp	Beurer GmbH, Ulm, Germany
Spinal Cord Clamps	NARISHIGE INTERNATIONAL LIMITED, London, U.K.

3.1.3.2 Technical devices for microscopy

Olympus FV1200 MPE multiphoton microscope x25/1.05 water immersion objective	Olympus GmbH, Hamburg, Germany
Olympus FVMPE-RS multiphoton microscope x25/1.05 water immersion objective	Olympus GmbH, Hamburg, Germany
MaiTai Deep See® Titanium:sapphire Laser	Newport/ Spectraphysics, Irvine, California, USA
Olympus FV1000 confocal system mounted on BX61 vertical microscope, equipped with x10/0.3 dry, x20/0.85 oil and x60/1.42 oil immersion objectives	Olympus GmbH, Hamburg, Germany
Manual XY translation stage	Luigs & Neumann Feinmechanik und Elektrotechnik GmbH, Ratingen, Deutschland parts by Thorlabs Inc Newton (New Jersey), USA
Upright fluorescence microscope Olympus BX51WI, equipped with long-working distance objectives: 20x/0.5 water-immersion dipping-cone objective; 100x/1.0 water-immersion dipping-cone objective for explant imaging. And Olympus UAPO 40x/ 1,15 water immersion objective with correction collar for cell imaging	Olympus GmbH, Hamburg, Germany

3.1.3.3 Technical devices for cell and explant imaging

(Kerschensteiner, Reuter, Lichtman & Misgeld, 2008)

Olympus SZ51 dissection microscope equipped with Schott KL 1500 LCD	Olympus GmbH, Hamburg, Germany

Two-channel temperature control system (one output for the in-line heater and one output for the heating ring; input for a temperature probe)	Warner Instruments, Holliston, MA 01745, USA
Fast shutter and filter wheel	Sutter Instrument Company, Novato, CA 94949, USA
Warner TC-324B Temperature controller	Warner Instruments, Holliston, MA 01745, USA
Warner W4 64-1561 Platform, heated, magnetic	Warner Instruments, Holliston, MA 01745, USA
Tube Pump	Watson-Marlow Fluid Technology Group Wilmington, MA 01887, USA

3.1.3.4 Technical devices for for tissue processing/ immunohistochemistry

HISTO LEICA Vibratome VT1200S	Leica Microsystems GmbH, Wetzlar, Germany
Leica CM1850 Cryostat	Leica Microsystems GmbH, Wetzlar, Germany
KERN EW 150-3M (Scale)	Kern & Sohn GmBH, Balingen-Frommern, Germany
Laboratory pH-meter inoLAB	WTW Wissenschaftliche-Technische Werkstätten, Weilheim, Germany
Magnetic stirring hotplateMR 3001K and stirring bars	Heidolph Instruments GmbH & Co. KG, Schwabach, Germany
Vortex-Genie 2	Scientific Industries, Inc., Bohemia, New York, USA
Olympus IX71 inverse fluorescence microscope (initial assessment of stainings and expression)	Olympus GmbH, Hamburg, Germany

3.1.4 Data analysis/Software

Adobe Creative Suite 6 (Photoshop, Illustrator)	Adobe Systems, Inc., San Jose, California, USA

ImageJ/ FIJI	General Public License http://rsbweb.nih.gov/ij/download.html
Graphpad Prism	GraphPad Software, La Jolla, California, USA
Microsoft Office (Powerpoint, Excel, Word)	Microsoft Corporation, Redmond, Washington, USA
µManager	Open source microscopy software (Edelstein et al., 2014)
SnapGene software	GSL Biotech; available at snapgene.com

3.2 Methods

3.2.1 Molecular cloning

The GECI source plasmid pRSETB-Twitch2B-54S+ was kindly provided by Dr. Oliver Griesbeck (Max Planck Institute of Neurobiology, Martinsried, Germany). It encodes Twitch2B-54S+, consisting of mCerulean3, a low-calcium-affinity toadfish Troponin C-minimal domain linker (1 functional EF-hand) and cpVenus^{CD} (Thestrup et al., 2014). Suitable endonuclease-cleavage sites were generated by overhang PCR using the custom-made upstream primer L-BamHI-pRSETB and downstream primer R-pRSETB-NotI (synthesised by metabion international AG, 82152 Planegg, Germany). The pCMV G-CEPIA1er was a gift from Masamitsu Iino (Addgene plasmid # 58215) (Suzuki et al., 2014) and is itself based on pShooter^{TM} Vector pCMV/myc/ER (Invitrogen, Carlsbad, California, USA). The pCMV G-CEPIA1er was used as a backbone for the assembly of the eukaryotic ER-targeting vector pCMV-Twitch2B 54S+ ER by restriction with BamHI and NotI-enzymes and subsequent ligation. Special attention in vector design was paid to an expression-enhancing intron sequence in the backbone's 5'-region and to in-frame cloning with mouse immunoglobulin V_h-signalling sequence, as well as the ER retention peptide KDEL and myc-tag. Transformation was performed, either by heat shock or electroporation, using standard molecular-cloning protocols. Minipreps of positively ampicillin selected E. coli cultures and – following restriction digest verification – maxipreps were

carried out using Qiagen kits. pCMV-Twitch2B 54S+ ER coding sequence was confirmed in maxipreps by sequencing (Eurofins Genomics, 85560 Ebersberg, Germany). A negative control of pCMV Twitch2B 54S+ER was created by synthesis of a linker domain, which replaced all amino acids implicated in calcium binding in the functional EF-hand 1 and the EF-hand 2 (which is notably already crippled by the 54S insertion) (Dotson & Putkey, 1993) by randomly chosen aliphatic amino acids. The synthesis of the mutated-linker DNA fragment was carried out by Eurofins Genomics (85560 Ebersberg, Germany). The mutational-linker DNA was used to replace the functional linker domain using the restriction enzymes BlpI and SacI. A schematic representation of pCMV-Twitch2B 54S+ ER can be found in Figure 5.

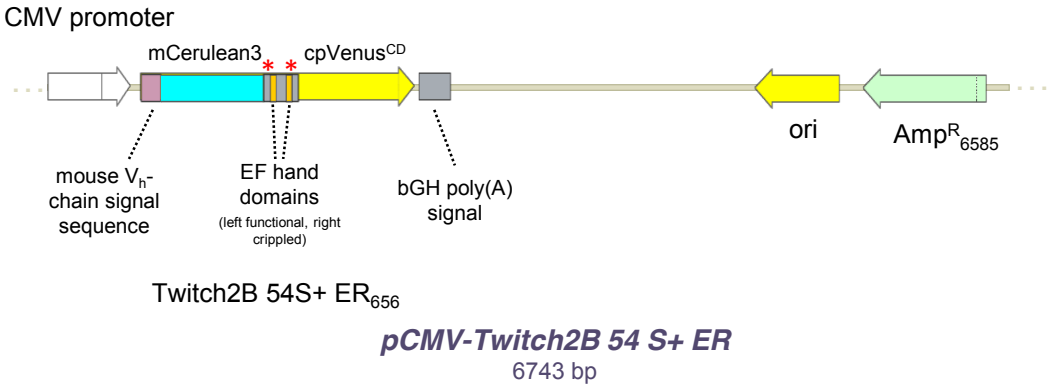

Figure 5: Plasmid map pCMV-Twitch2B 54S+ ER

Schematic representation of pCMV-Twitch2B 54S+ER plasmid. Locations of fluorescent proteins, linker site and EF hand domains are annotated. Red asterisks indicate the sites of mutation in pCMV-Twitch2B mutated linker plasmid.

The pCMV-Twitch2B 54S+ ER plasmid was used for transfection of HEK cells (see chapter 3.2.3) and for the generation of the Thy-1 Twitch2B 54S+ ER plasmid, from which transgenic mouse lines were generated (see chapter 3.2.7). The Thy-1 expression vector is derived from a gene that encodes a small immunoglobin superfamily member, Thy-1 (Ingraham, Lawless & Evans, 1986), which is endogenously expressed in many cell types, including immune cells and neurons (Marinkovic et al., 2015; Morris, 1992). By identifying the cis-acting elements which control neuronal expression and removing the elements which control thymus expression, specific neuronal expression can be achieved (Vidal, Morris, Grosveld & Spanopoulou, 1990). The Thy-1 backbone vector used in this thesis was originally described by Caroni (1997) (Marinkovic et al., 2015). A schematic representation of the neuron specific Thy-1 vector and its regulatory elements can be found in Figure 6A. In order

to allow linearisation after the assembly of the Thy-1 vector with the Twitch2B 54S+ ER insert, the Thy-1 vector backbone needed to be modified. The original prokaryotic-expression cassette (including an ampicillin-resistance gene and origin of replication) was replaced by the prokaryotic-expression cassette from pmTurquoise2-mito (including kanamycin resistance and origin of replication). The pmTurquoise2-Mito was a gift from Dorus Gadella (Addgene plasmid #36208). Suitable endonuclease-cleavage sites were generated by overhang PCR using the custom-made upstream primer L-PvuI-MfeI-Backbone and downstream primer R-Backbone-BmtI-EcoRI (synthesised by metabion international AG, 82152 Planegg, Germany). The steps to yield maxipreps are the same as described above. This Thy-1(modified) plasmid was subsequently used as backbone for the generation of the Thy1(modified)-Twitch 2B 54 S+ ER plasmid. Again, endonuclease cleavage sites were generated by overhang PCR using the custom-made upstream primer L-XhoI-Twitch2B54S+ER and downstream primer R-Twitch2B54S+ER-XhoI (synthesised by metabion international AG, 82152 Planegg, Germany). Thy1(modified) plasmid backbone and the insert Twitch2B54S+ER with resulting overhangs were cleaved using XhoI. The backbone was dephosphorylated using CIP-enzyme to avoid religation in blunt-ended cloning. The resulting Thy1(modified)-Twitch 2B 54 S+ ER plasmid was confirmed by sequencing (Eurofins Genomics, 85560 Ebersberg, Germany), and a schematic representation can be found in Figure 6B.

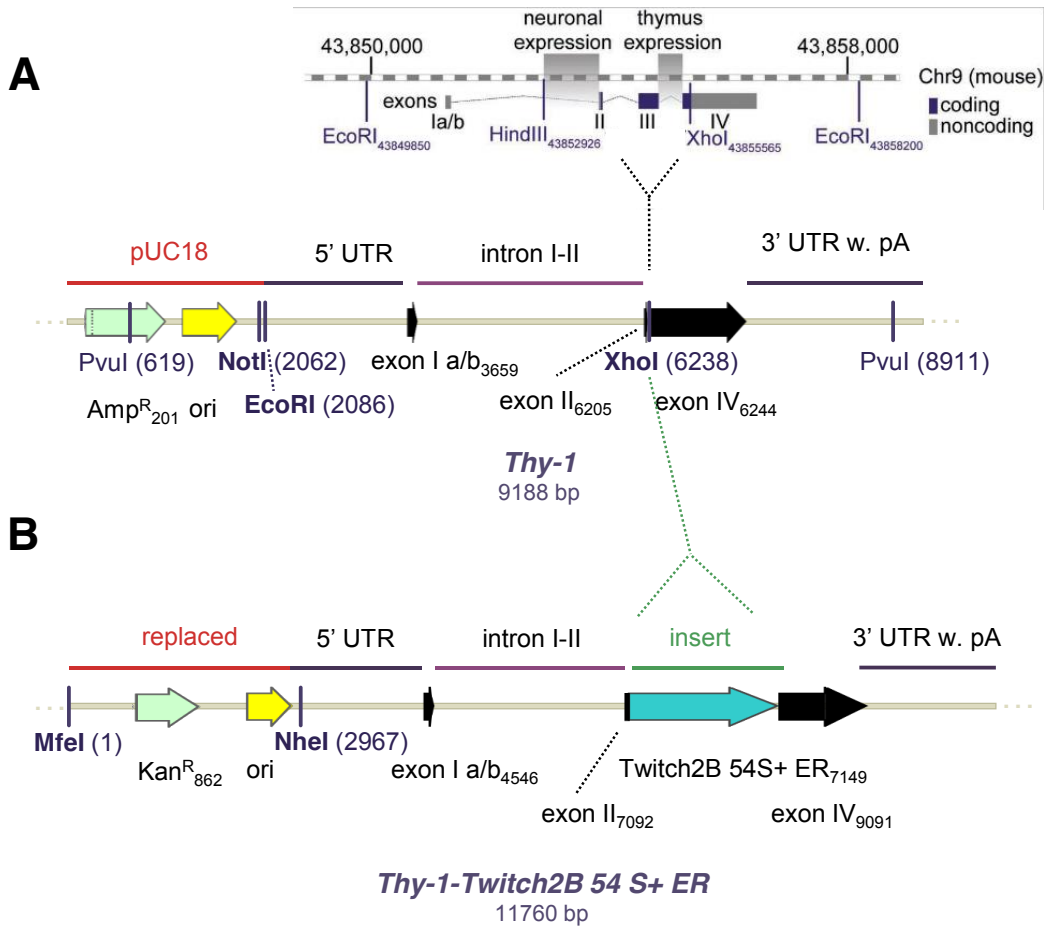

Figure 6: Thy-1 plasmid maps

(**A**) On top: Thy1 regulatory cassette with indication of omitted thymus expression elements. Below: Schematic representation of original Thy-1 plasmid with XhoI restriction site for insert integration. Modified from (Caroni, 1997; Marinkovic et al., 2015). (**B**) Scheme of Thy-1-Twitch2B 54S+ER assembled plasmid. Note that the pUC18 prokaryotic expression cassette has been replaced. Twitch2B 54S+ ER coding sequence is integrated at XhoI site.

The plasmid pAAV-mEmeraldER was required for the production of an adeno-associated virus (AAV) (see chapter 3.2.4) in order to express a bright, photostable structural marker in the neuronal ER. The insert was generated from the mEmerald-ER-3 plasmid, which contains a calreticulin-signalling sequence and a KDEL-retention sequence. The mEmerald-ER-3 plasmid was a gift from Michael Davidson (Addgene plasmid #54082), and endonuclease cleavage sites were added by overhang PCR using the custom-made upstream primer L-ClaI-mEmeraldER and downstream primer R-mEmeraldER-HindIII (synthesised by metabion international AG, 82152 Planegg, Germany). The AAV-MCS backbone plasmid was kindly provided by Dr. Florence Bareyre. Both insert and backbone were cut using HindIII and ClaI restriction enzymes, ligated and transformed to bacteria. The resulting plasmid was

confirmed by sequencing (Eurofins Genomics, 85560 Ebersberg, Germany). A schematic representation is shown in Figure 7.

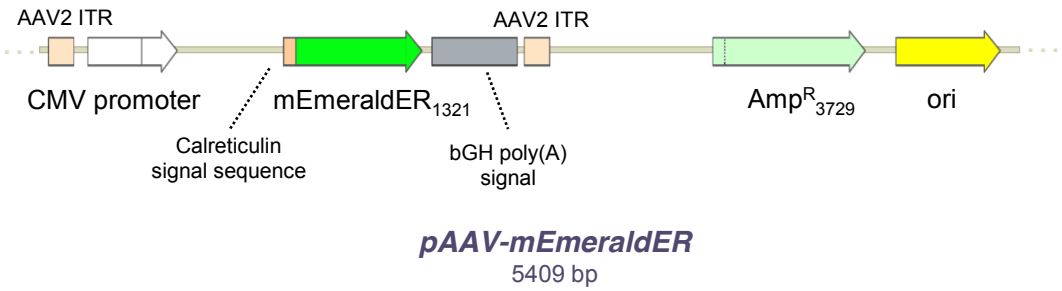

Figure 7: Plasmid map pAAV-mEmeraldER

Schematic representation of pAAV-mEmerald ER plasmid. ITR= Inverted terminal repeats.

The SnapGene software was used to plan cloning strategies. All corresponding sequence files are available upon request.

3.2.2 Experimental animals

C57BL/6JRj mice obtained from Janvier Labs (53940 Le Genest-Saint-Isle, France) were used for virus-injection experiments. Transgenic mouse lines include Thy1-TwitchER lines generated by the group of Ronald Naumann in the Transgenic Core Facility of the Max Planck Institute of Molecular Cell Biology and Genetics (01307 Dresden, Germany) (see chapter 3.2.7). All experimental mice were kept and bred under standard conditions, i.e. they were held in Eurostandard Type II long cages 365x207x140 mm cages (Tecniplast, Hohenpreißenberg, Germany) and stored in an IVC rack system in 12 h light/dark cycles. The maximum number of mice was limited to five per cage. The animals were fed autoclaved food (regular food 'Maus' from Ssniff, Soest, Germany) and water ad libitum (Bewersdorf, 2017; Schumacher, 2015). All animal work was approved by the Animal Study Committee of the Regierung von Oberbayern.

3.2.3 Cell culture

Hek-293 cells were cultured under standard conditions. The cells were grown in Dulbecco's Modified Eagle Medium (DMEM), substituted with 10 % fetal bovine serum and 1 % penicillin/streptomycin. For in-vitro characterisation of Twitch2B 54S+

ER sensor in the pharmacological ER depletion and replenishment experiment ~50.000 Hek-293 cells were seeded on poly-l-lysine coated glass coverslips in 6-well titer plates. The next day, for transfection, 500 ng plasmid DNA of the pCMV-Twitch2B 54S+ ER construct was diluted in 500 µl sterile PBS, mixed with 0.5 µl lipofectamine and incubated at room temperature for 10 minutes. The mixture was added on the cells dropwise, and the medium was exchanged with 3 ml fresh medium after two to five hours. Afterwards, the cells were grown for one to two days to express the construct sufficiently before imaging.

For the negative-control cell experiment, 60–100 µl of dense cell suspension was seeded on 3–6 cm petri dishes. Hek-293 cells were transfected the next day with 2-4 µg of pCMV-Twitch2B 54S+ ER or pCMV-Twitch2B mutated linker construct respectively using a standard calcium-phosphate transfection protocol. Cells were subsequently imaged using the FVMPE-RS Olympus 2-photon microscope after expression was confirmed using an epifluorescence microscope.

3.2.4 AAV production and spinal cord injection

The production of AAV from the AAV-mEmeraldER-expression constructs was kindly assisted and instructed by Charlène Granier (PhD student, Bareyre lab, LMU) and Anja Schmalz (technician, Kerschensteiner lab). An AAV 1/2 production was performed using standard techniques. Briefly, $6 \cdot 10^6$ AAV-293 cells were seeded in 14 cm plates with 10 ml DMEM on each. Cells were transfected with AAV-mEmeraldER and Helper plasmid DNA on day 2 using a standard calcium-phosphate transfection protocol. After additional three days of growth, the virus was harvested using extremely low protein-binding cellulose acetate membranes. Afterwards, the crude lysate was purified with Amicon-ULTRA centrifugation filters. The AAV-mEmeraldER virus titer was determined to be $9.79 \cdot 10^{10}$ copies /ml by quantitative PCR, using primers specific to the pAAV Cag vector according to an established protocol (Veldwijk et al., 2002).

Spinal-cord injections of the virus were carried out in order to label axons in intercostal nerves, which are accessible to imaging by preparation of triangularis sterni explants (see chapter 3.2.5). To this end, AAV particles were stereotactically injected into the mouse cervical and/or upper thoracic spinal cord. Shortened glass pipettes produced with a vertical pipette puller were filled with 1 µL of AAV mEmeraldER solution diluted to 1:2 in 1x sterile PBS. C57BL/6JRj mice older than six

weeks were anaesthetised using MMF (15 µL/ mouse g) and a one-level laminectomy was performed of cervical vertebra 7 (identified by prominent spinous process). The dura was removed using a hooked needle tip in the space between C7 and Th1. The coordinates for the bilateral injection were chosen to be 0.5 mm lateral of the central vein and 0.9 mm below the dorsal surface in order to reach α-motor neurons in the ventral horn. The neck muscles were loosely adapted to cover the injection site by suturing, and the skin was closed with metal clips. Animals were subsequently allowed to recover in a pre-heated chamber and monitored daily for signs of discomfort or neurological deficit. Triangularis sterni explants were prepared six to eight weeks after the injection. The protocol was modified from Breckwoldt (2014). To verify the injection protocol, transverse spinal cord sections of the injection site were examined by confocal microscopy using an FV1000 confocal system. The staining of α-motor neurons and morphological signs of toxicity were assessed.

3.2.5 Explant imaging and laser transections

For the preparation of triangularis sterni muscle explants, mice were euthanised six to eight weeks after AAV-mEmeraldER, with spinal-cord injections using isoflurane. The rib cage, which contains intercostal nerves and the triangularis sterni muscle, was isolated using paravertebral cuts, cleaned of muscles attached to the rib cage externally, and then pinned into Sylgard-coated dishes using minuten pins. Afterwards, the rib cage was placed on a heated stage (32-35 °C) in normal Ringer solution and bubbled with carbogen gas (95% O_2, 5% CO_2) (Breckwoldt et al., 2014; Kerschensteiner et al., 2008). Recordings were performed in the middle part of intercostal nerves, which contained mEmeraldER-labelled axons.

For structural imaging, a BX51 wide-field microscope was used equipped with x20/0.5 N.A. and x100/1.0 N.A. dipping-cone water immersion objectives, a filter wheel with a shutter, a 525/50 nm emission filter (AHF Analysentechnik AG, 72074 Tübingen, Germany), a 470/40 nm excitation filter (F47-526 AHF Analysentechnik AG, 72074 Tübingen, Germany) and a cooled CCD camera in order to image mEmeraldER green fluorescence.

For laser transections of intercostal nerves in explants, confocal imaging was performed using an FV1200 system with an attached confocal unit. For laser transections, the Mai Tai 2photon laser was tuned to 760–800 nm, a circular region of interest on a labelled axon was defined. Subsequently, this region was illuminated at

60–80% laser transmission in the ‘whirl mode’ for 3 to 10 seconds. The lesion site was observable by a rise of autofluorescence in the region of interest. Subsequently, the light path was changed to confocal imaging. The 488 nm laser line was used for excitation, while light from 500–600 nm was detected. The interval was set at ‘free-run’. The focus was continuously adjusted during recording.

3.2.6 In vitro characterisation of calcium sensor

For the pharmacological ER depletion and replenishment experiment, glass coverslips with pCMV-Twitch2B 54S+ ER transfected Hek-293 cells (see chapter 3.2.3) were transferred to a heated (37 °C) Warner Instruments flow chamber by using forceps. The chamber was continuously perfused with carbogen-gassed HEPES buffered Hank’s balanced salt solution (HHBSS). Pharmacological solutions consisted of carbogen-gassed HHBSS containing either 3 µM thapsigargin for ER depletion or 10 mM $CaCl_2$ + 5 µM ionomycin for ER replenishment. These were directed to the heated flow chamber through a tubing system with a flow valve upon opening of a luer lock. Imaging was performed with a widefield BX-51 Olympus epifluorescence microscope equipped with a water-immersion Olympus UApo 40x/1.15 N.A. objective with correction collar to adjust for the variable thickness of the coverslip glass. CFP (exposure 300 ms) and YFP-FRET channels (exposure 150 ms) were alternately recorded at a frequency of 1 Hz. A FRET CFP/YFP filter set (F46-052 AHF Analysentechnik AG, 72074 Tübingen, Germany) was used, which contains the excitation bandpass filter 436/20 and the dichroic mirror 455LP to remove excitation light from the emission-light path. The emission filters, CFP bandpass 480/40 nm (F47-480 AHF Analysentechnik AG, 72074 Tübingen, Germany) and YFP bandpass 535/30 nm (F47-535 AHF Analysentechnik AG, 72074 Tübingen, Germany), were alternated with a fast-moving filter wheel. The images were recorded with a cooled CCD camera.

The experiment was conducted with 10 frames (=20 s) pre-run with HHBSS perfusion, after which the luer lock to the thapsigargin solution was opened. Thapsigargin perfusion was maintained for 300 frames (=10 min), after which the luer lock was closed again. In an immediately following second-recording, 10 frames (=20 s) pre-run were acquired, followed by the opening of the luer lock to the ionomycin + $CaCl_2$ solution. Next, another 300 frames (=10 min) were recorded. A photograph of the experimental setup can be seen in Figure 8.

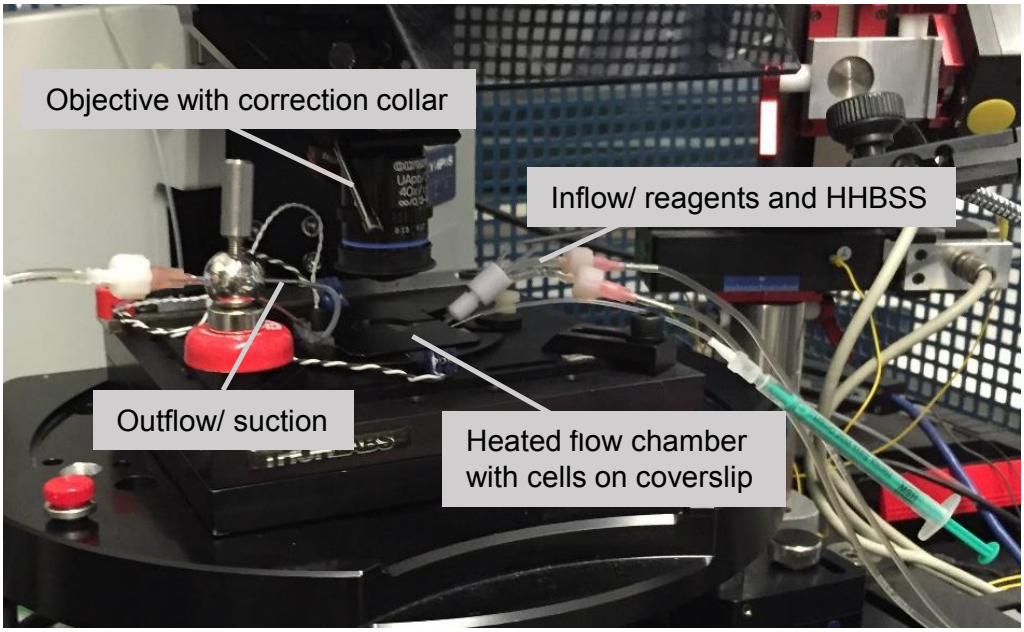

Figure 8: Experimental setup for in vitro sensor characterisation

For the negative control experiment, transfected cells (either with pCMV-Twitch2B 54S+ ER or pCMV-Twitch2B mutated linker DNA) were imaged directly in 6 cm petri dishes using an Olympus FVMPE-RS 2photon microscope equipped with a x25/1.05 N.A. water-immersion objective after replacing the medium with 3 ml prewarmed (37 °C) HBSS without phenol red. Seventy images were acquired every 10 seconds, and the focus was continuously adjusted. A total of 1 ml of 20 µM prewarmed (37 °C) thapsigargin stock solution in HBSS was gently pipetted into the petri dish after 10 time points to yield 5 µM thapsigargin concentration. The imaging settings were as follows: GaAsP1 detector: 500 V, GaAsP2 detector: 550 V, Insight laser tuned to 840 nm with variable AOTF between experiments. The emission filter cube FV30-FCY (CH1: BA410-455 / SDM475 / CH2: BA495-540; Olympus GmbH, Hamburg, Germany) was inserted.

3.2.7 Generation of transgenic mice

Thy1-Twitch2B 54S+ ER transgenic mice (abbreviated as Thy1-TwitchER) were generated by pronuclear injection into a C57Bl6 background in cooperation with Ronald Naumann (Transgenic Core Facility of the Max Planck Institute of Molecular Cell Biology and Genetics, Dresden, Germany). To prepare the DNA for pronuclear injection, 10 µg of the Thy1(modified)-Twitch 2B 54 S+ ER plasmid were linearised

using the restriction endonucleases NheI HF and MfeI HF. The DNA was run on an ethidium bromide free 1 % agarose gel and loaded without loading dye. The respective band with a calculated size of 8794 bp was cut out. In order to achieve this without inducing UV damage to the DNA, an outlying control lane with a small amount of the cut plasmid was stained individually with ethidium bromide and used as reference for the cut-out site (Figure 9A). The cut-out gel fragments were purified using the QIAquick Gel Extraction Kit. The DNA was eluted in pronuclear injection buffer. The eluted DNA's concentration was determined to be 57.5 ng/µl using a Nanodrop (ThermoFisher Scientific, Waltham, Massachusetts, USA) spectrometer. Pronuclear injection was carried out by the Naumann laboratory. Specific PCR primers and a corresponding thermocycler program were designed to generate a band of 235 bp in the presence of the Thy1-Twitch2B 54S+ ER insert:

Myc2_Fwd: 5' CCGAGGTGAAATTCGAAGGG 3' 20bp, Tm= 58,63 °C

Myc2_Rev: 5' TCTTCTGAGATGAGTTTTTGTTCTG 3' 25bp, Tm= 57,51 °C

Thermocycler program: 1: 94 °C 1 min 2: 94 °C 10 s 3: 55,5 °C 5s

4: 72 °C 15 s 5: GOTO 2 Repeat 29 times 6: 72°C 10 min 7: 4 °C forever

From 43 tails sent by the Naumann laboratory, 11 were tested positive using this genotyping PCR. The corresponding agarose gel can be seen in Figure 9B. The offspring of these 11 mice represented the founder lines, which were subsequently screened for expression patterns and brightness of the Twitch2B54S+ ER GECI insert.

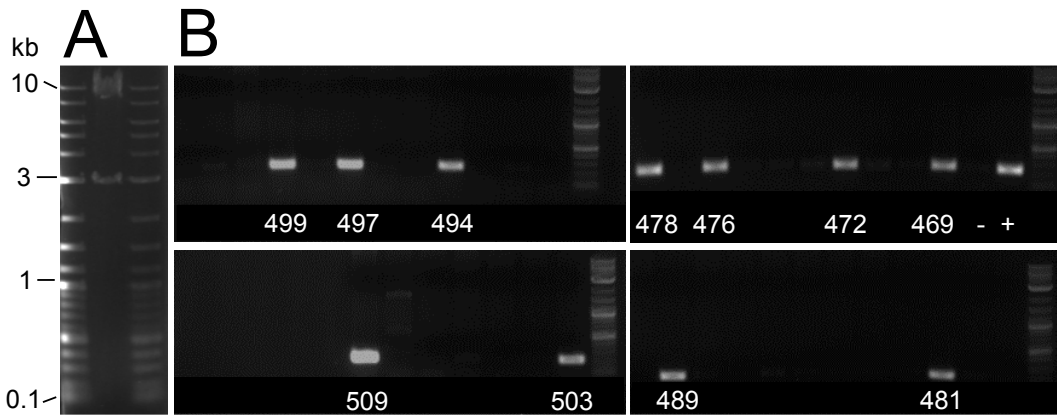

Figure 9: Thy1-TwitchER linearisation and genotyping gels

(**A**) Linearisation digest gel (NheI HF, MfeI HF) of Thy1-Twitch2B 54S+ ER plasmid for pronuclear injection, control lane. Upper band of 8794 bp was cut from aligned neighbouring unstained gel section. (**B**) Agarose gel from genotyping PCR. 11 Thy1-Twitch2B 54S+ ER positive lanes are labelled with founder line number. The plus sign indicates positive control (5 ng of Thy1-Twitch2B 54S+ ER plasmid); the minus sign indicates negative control (water). The same 2-log DNA ladder as labelled in (A) was used on all gels.

3.2.8 Screening and immunohistochemistry of Thy-TwitchER mice

Offspring of the 11 founder lines were screened as previously described (Marinkovic et al., 2015). Explants were prepared and imaged as described in chapter 3.2.5 in order to assess expression in intercostal nerves and neuromuscular junctions (NMJs). After extraction of the rib cages, animals were transcardially perfused with 4 % wt/vol paraformaldehyde (PFA) diluted in 1x phosphate buffered saline (PBS) and then post-fixed in 4 % PFA in PBS for 24 hours. Afterwards, spinal cord, brain and eyes were micro-dissected under an Olympus Stereo Microscope SZ51. Eyes and spinal cord were incubated in 30 % sucrose in 1x PBS for a minimum of 24 hours for cryoprotection. Cryoprotected samples were embedded in O.C.T. and rapidly frozen in an ethanol-dry-ice bath. Some 30-50 µm sections were prepared using a Leica CM1850 cryostat. A total of 50-100 µm brain sections were cut using a HISTO LEICA vibratome VT1200S. The samples were mounted on microscope slides; a drop of Vectashield was applied and cover slips were gently placed on top. The edges were sealed using nail varnish. Subsequent imaging was performed with an Olympus FV1000 confocal microscope. The 515 nm laser line was used for excitation with a 440/515/635 excitation dichroic mirror placed in the light path. The emission light was sent through a 535-565 nm bandpass filter and collected with a

photomultiplier tube (PMT). The PMT voltage was adjusted to prevent oversaturated pixels. x10/0.3 N.A. dry, x20/0.85 N.A. oil-immersion and x60/1.42 N.A. oil-immersion objectives were used. Mosaic scans of brain slices were produced using the x20/0.85 N.A. oil-immersion objective and 20 % overlap between images. Images were stitched in Image J. Expression of the GECI construct was assessed in the cortex, hippocampus, cerebellum, spinal cord, dorsal root ganglia and retina.

To validate the sensors' localisation in the ER, immunostainings of the ER resident chaperone GRP78/BiP were performed on cryoprotected lumbar spinal cords. Some 50 µm-thick sagittal sections were cut using a cryostat. Sections were stained with the free-floating immunohistochemistry protocol shown in Table 2. Stained samples were mounted in Vectashield and sealed with nail varnish. The stainings were analysed using an Olympus FV1000 confocal microscope exciting with 488 nm and 635 nm laser lines and a 405/488/559/635 excitation dichroic mirror. A 535-565 nm bandpass filter was used to collect FP fluorescence in channel 1. An SDM 640 dichroic mirror was used to collect AF 647 infrared-emission light in channel 2.

Based on the in-vitro and in-vivo (vide infra) screening results, two transgenic lines were selected for further breeding: Thy1-TwitchER 481 because of a particularly bright subset labelling in the dorsal spinal column apt for in vivo imaging, and Twer 489, because of a full labelling, which also includes cerebellar Purkinje cells.

Step	**Temperature**	**Time**	**Medium**
1 Washing	Room temperature (RT)	3 x 10 min	1x PBS
2 Blocking	RT	1 h	10% goat serum (g. s.)/0.5 %Triton X-100 (T)/PBS
3 Primary antibody	4°C, shaker	overnight	1:200 rabbit polyclonal to GRP78 BiP antibody (diluted in 1 % g.s./ 0.5 % T/ PBS)
4 Washing	RT	4 x 10 min	0.5 %T/ PBS
5 Secondary antibody	RT	3 h	AF 647 goat anti rabbit 1:1000 (diluted in 1 % g.s./ 0.5 % T/ PBS)
6 Washing	RT	3 x 30 min	PBS

Table 2: Free-floating GRP78 BiP immunohistochemistry protocol

3.2.9 In-vivo 2-photon imaging of Thy1-TwitchER mice

Thy1-TwitchER mice were used for 2-photon imaging of the spinal cord's dorsal column. Surgery was performed according to an established protocol (Kerschensteiner et al., 2005; Nikić et al., 2011; Romanelli et al., 2013). Mice were anaesthetised by intraperitoneal injection of MMF (a mixture of 0.5 mg/kg medetomidin, 5 mg/kg midazolam and 0.05 mg/kg fentanyl) and kept in a heating pad for approximately 15–30 min in order to ensure sufficient depth of anaesthesia. The fur above the spinal cord was shaven; animals were fixed on a metal plate with their limbs outstretched using elastic rubber bands and magnets. A median incision was made above the lower lumbar spinal segments with a surgical blade. Using spring scissors, tissue was removed down to the autochthonous back musculature, which was carefully dissected to allow access to the lateral processes and laminae of the lumbar vertebrae L4 and L5. Bilateral laminectomies were performed, and the laminae were gently removed by applying tension on the spinous process and attached muscles. Bleeding was controlled by using triangular cotton swabs (sugis) and a hemostatic sponge material (spongostan) drenched in artificial cerebrospinal fluid (ACSF). The exposed spinal cord was repeatedly rinsed with ACSF. The dura mater was punctually incised with a hooked 30-gauge hypodermic needle tip, pinched with a Dumont mini forceps (size 5) and carefully stripped off. For immobilisation of the spinal cord, the vertebrae adjacent to laminectomy were clamped using a Narishige clamping device, and the animal's tail was fixed. Subsequently, a 2 % agarose well was constructed surrounding the laminectomy site in order to keep the immersion liquid, ACSF, at a sufficient level for imaging.

In-vivo microscopy of exposed dorsal column axons was performed using an Olympus FV1200-MPE 2-photon microscope equipped with a femto-second pulsed titanium-sapphire laser (Mai Tai HP-DS). The laser was tuned to 840 nm, a wavelength which has been validated for CerTN-L15 mice, which also express a CFP/YFP containing fluorescent GECI (Schumacher, 2015). The laser was modulated in intensity with an acousto optic tunable filter (AOTF). Emission was detected using gallium arsenide phosphide (GaAsP) detectors, which were generally set at a voltage of 640 V for the CFP channel and 500 V for the YFP channel, unless otherwise indicated. We used 455-490 and 526-557 nm emission bandpass filters to detect CFP and YFP channels. Images were acquired at 12 bits with a 25x/1.05 N.A. dipping cone water-immersion objective. Volume stacks were acquired penetrating up to 60 µm

into the tissue from the dorsal surface. During imaging, animals were kept under constant anaesthesia with regular assessment of breathing and reflexes. Animals were euthanised with isoflurane after imaging.

3.2.9.1 In-vivo 2-photon imaging of pharmacological ER depletion

For pharmacological characterisation of the Thy1-TwitchER 481 line, the ER-depletion agent thapsigargin was applied on the exposed spinal column. One pre-application stack was acquired with GaAsP1 detector voltage at 600 V and GaAsP2 detector voltage at 500 V. All other parameters matched the description above. The ACSF in the agarose well was then replaced by 10 µM thapsigargin in ACSF. For this purpose, a 1 mM thapsigargin dimethyl sulfoxide (DMSO) stock solution was diluted in ACSF 1:100, thereby keeping the DMSO concentration at 1 %. The specimen position was adjusted to match the pre-stack location. Subsequently, the spinal cord was imaged in 10 min intervals under continuous thapsigargin bath application. At least 5 stacks were recorded.

3.2.9.2 In-vivo 2-photon imaging of EAE lesions

EAE was induced in mice older than six weeks using a standard protocol (Abdul-Majid et al., 2000). Mice were immunised with 250 µl of an emulsion containing 400 µg of purified recombinant myelin oligodendrocyte glycoprotein (MOG, N1-125, produced in E. coli) and incomplete Freund's adjuvant with 5 mg/ml mycobacterium tuberculosis H37 Ra. Animals were anaesthetised with KX (mixture of 87 µg/g body weight Ketamine and 13 µg/g body weight Xylazin) and received three subcutaneous injections of the described emulsion, 50 µl at the base of the tail and 100 µl in both flanks. On the day of immunisation and 48 hours later, 350 ng of pertussis toxin (Ptx) were administered intraperitoneally. Following the immunisation, the animals' weight and neurological status was assessed on a daily basis. A standardised EAE scoring scale for evaluation of neurological deficits was employed: 0, no detectable clinical signs; 0.5, partial tail weakness; 1, tail paralysis; 1.5, gait instability or impaired righting ability; 2, hind-limb paresis; 2.5, hind-limb paresis with partial dragging; 3, hind-limb paralysis; 3.5, hind-limb paralysis and fore-limb paresis; 4, hind-limb and fore-limb paralysis; 5, death. Only animals with a score ≥ 2 were used for experiments, since at these stages, confluent lesions can be found in the superficial dorsal spinal cord (Sorbara et al., 2014). Animals were imaged at two days (+/- 1 day) after the onset of neurological symptoms, i.e. a score > 0.

Regions were selected for imaging based on the density of cellular infiltrates, which were detectable by autofluorescence and based on the presence of axonal degeneration stages (Nikić et al., 2011). Four or more stacks were acquired of each mouse. Imaging one region twice was avoided by meandering through the sample in a stereotypical way. The stacks were acquired with a z-step size of 1 µm, zoom 2, 1024x1024 pixels and a pixel dwell time of 2 µs.

3.2.9.3 In-vivo 2-photon imaging of laser-induced spinal-cord injuries

The Thy1-TwitchER line 509 was used for a laser-induced spinal-cord-injury experiment (LiSCI) (breeding of this line was later discontinued). In order to transect bundles of axons, the 2-photon laser was tuned to 760 nm wavelength, and an elliptic area traversed by >10 axons was illuminated for 10s at 70–100 % laser transmission in the whirl mode. This reliably led to a local transection of the superficially passing axons, while sparing adjacent regions, which remained structurally unaltered. Transected axons could be identified by fragmentation of the ER, which progressed from the lesion site. The lesion was visible by autofluorescence.

One pre-lesion stack was recorded. After laser lesioning, the field of view was moved cranially, so that the lesion site was directly adjacent to the imaging region, in order to avoid damaging the GaAsP detectors by the bright autofluorescence. Stacks were acquired at 2 min intervals for at least 14 min. Standard imaging parameters described above were used.

3.2.9.4 In-vivo 2-photon imaging following spinal-cord contusion

The Thy1-TwitchER line 509 was used for contusion experiments. An established protocol was adapted (Williams et al., 2014). In contrast to the other imaging experiments, the dura mater was not removed in order to prevent obscuration by capillary bleeding. Contusions were administered using the Infinite Horizons impactor with the impact force set to 40 kDynes. Animals with significant subdural bleeding were excluded.

For two time-point experiments, mice were imaged before and after the contusion. The stage coordinates were noted, and drawings were made of the vascular patterns, as seen under epifluorescence illumination. After impacting, the well was refilled with a sufficient amount of ACSF for objective immersion, and the clamping device was reaffixed to the stage. The pre-position or, if obscured, the positions

directly adjacent to it were set. This process of administering the contusion and re-positioning the mouse correctly took approximately five minutes. The post-contusion stack was acquired using the same imaging parameters as in the pre-contusion stack. Occasionally, the laser intensity had to be slightly reduced, in order to avoid saturation of pixels in brightly labelled ER fragments. For the contusion time-series experiment, z-stacks of the same region were acquired at 15 min intervals for 1 hour.

3.2.10 Image processing and analysis

Images were post-processed using the open-source image-analysis software, ImageJ/Fiji as well as Adobe Photoshop. In Fiji, the YFP(FRET) channel – with a generally better signal-to-noise ratio than the CFP channel – was visualised in a grey-scale look-up table. In the case of spinal-cord in-vivo imaging data, regions of interest (ROIs) of individual axons (only 1 ROI per axon was selected), as well as directly adjacent non-axonal background regions with similar size, were encircled as exemplified in Figure 10. Regions with saturated pixels were avoided. Mean grey values of axonal and non-axonal background ROIs were measured in the CFP and YFP(FRET) channels and subtracted in Microsoft Excel. The YFP(FRET)/CFP ratio of background corrected regions of interest was calculated. Background-corrected YFP(FRET)/CFP ratios were interpreted as proxy of ER-calcium concentration, as has been established previously for FRET-based GECIs (Mank & Griesbeck, 2008). For baseline characterisations, all axons crossing a virtual medio-lateral line were measured. The YFP/CFP ratios were normalised either to the mean of control mice or to the mean of the first time point of an experiment, as indicated. Only axons that could be tracked over all frames were included to time-series analyses. The same principles apply to cell experiments (1 ROI per cell plus adjacent cell-free background region were selected). For EAE experiment evaluation, each axon was assigned an FAD stage from zero to two based on visual-morphology assessment. In order to assign stage 1, a clear continuity of the beaded axon had to be detectable, as opposed to stage 2 axons, where the axonal continuity had to be visually disrupted (Nikić et al., 2011).

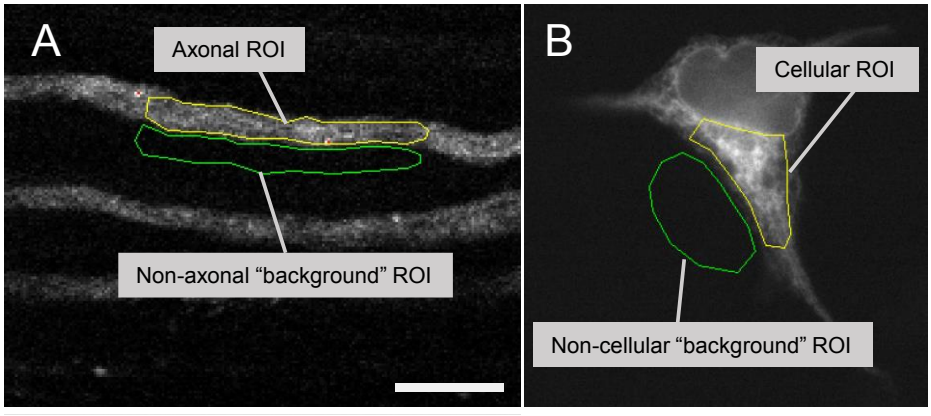

Figure 10: ROI selection for data analysis

(**A**) Exemplary selection of axonal ROI (yellow) and non-axonal ‘background’ ROI (green) in Thy1-TwitchER transgenic mouse YFP channel in greyscale (saturated pixels red). Scale bar 10 µm (**B**) Exemplary selection of cellular ROI (yellow) and non-cellular ‘background’ ROI (green) in pCMV-Twitch2B 54 S+ ER transfected Hek-293 cell YFP channel in greyscale.

Ratiometric images presented in this thesis were generated as follows: maximum-intensity projections of single channels were created, and a binary-threshold mask of axonal/cellular structures was generated from the YFP(FRET) channel. Projection images were multiplied by the binary mask, and the resulting images were divided by each other (YFP(FRET)/CFP). This image was displayed with a custom look-up table, which represents the highest ratios as yellow and the lower ratios as violet or black. The boundary values for this look-up table were determined individually for each experimental setup. A despeckle filter was applied in Photoshop to a projection of the YFP(FRET) channel. The generated ratiometric RGB images were blended with this greyscale YFP(FRET) channel projection image using the ‘Overlay’ layer function. These images were only used for presentation purposes and not for analyses.

3.2.11 Statistical analysis

GraphPad Prism version 7.01 was used to calculate statistical significance. Unpaired t-tests were employed where normal distribution could be confirmed using the Shapiro-Wilk normality test. The Mann-Whitney U test was used when normal distribution could not be confirmed. The data was considered significant when p values were <0.05. Significance levels are indicated in the figure legends and discussed in the corresponding passage.

4 Results

The structure of this chapter is based on the previously set objectives (chapter 2). I will demonstrate that intra-ER free calcium can be reliably measured in single axons and that intra-ER free calcium is dynamically altered in paradigms of axonal degeneration.

4.1 Imaging intra-ER free calcium in single axons

4.1.1 Targeting and visualising the axonal ER

The axonal ER is very narrow – with a diameter that can vary between 15 and 30 nm – and can be relatively sparse dependent on the neuronal subtype (Mark Terasaki, 2018). Therefore, it was necessary to validate that a concentration of FPs sufficient for imaging could be achieved in the peripheral axonal ER. Previously, neurite ER targeting and imaging of FPs in transgenic or virus-injected mice had only been accomplished with dendrites (Kucharz et al., 2011b; Okubo et al., 2015).

A neurotropic AAV1/2 was produced which encodes for mEmeraldER, an ER-targeted version of the bright, photostable GFP-variant mEmerald with an N-terminal calreticulin ER-signalling peptide and a C-terminal KDEL ER-retention sequence (see chapter 3.2.1). The calreticulin ER-signalling peptide and KDEL ER-retention sequence was used before to achieve dendritic ER expression in Thy1-EGFP-ER transgenic mice (Kucharz et al., 2011b).

For preliminary validation of AAV-mEmeraldER, Hek-293 cells were infected with the virus, and an ER fluorescence pattern was visible. Next, spinal-cord injections of AAV-mEmeraldER were performed at levels C7/Th1 in C57BL/6JRj mice to yield fluorophore expression in intercostal nerve axons. Regional ER pattern expression at the injection site could be verified in 4 % PFA-fixed spinal-cord slices (prepared four weeks post-injection) by confocal microscopy (Figure 11A, B). The fluorescence pattern in neuronal somata was reminiscent of rough ER sheets; a nuclear envelope was also visible. Tubular ER fluorescence could also be detected in dendrites and axons, with bundles of labelled axons emerging from the ventral horns. Neurons appeared vital, and the regional damage caused by the injection was minimal. To

assess intercostal nerve mEmeraldER labelling, explants were prepared and imaged by widefield epifluorescence microscopy. Labelling of intercostal nerve axons was achieved with varying labelling densities. At 100x magnification, dense tubular ER could be visualised with prominent, bright subsurface cisternae-like structures. At the nodes of Ranvier, ER tubules become more sparse, and subsurface ER features are more subtle (Figure 11C). Time-series imaging revealed occasional, brightly labelled, distally bound 'comets' reminiscent of vesicular structures, which moved rapidly and straight along the axon. One could hypothesise that these represent either a vesicular ER subcompartment for rapid supply of distal ER regions or mEmeraldER mistargeted to other vesicular organelles, or mere proteinaceous aggregates of mEmeraldER. The tubular axonal ER also displayed some motility in the sense of small, translational movements of tubules and the wobbling of loosely attached end-standing tubules/vesicles.

To study potential ER response patterns following laser induced axonal injury, morphological response patterns have been demonstrated for mitochondria, which swell and round up (Breckwoldt, 2014). Laser transections of single axons in intercostal nerves were carried out using punctual high-energy 2-photon laser illumination. Confocal imaging was employed. Indeed, a disintegration of the tubular ER into small, optically resolvable vesicular fragments was detected immediately proximally and distally to the injury site. Subsequently, the fragments seemed to fuse and create larger vesicular bodies with bright mEmeraldER fluorescence. Notably, mEmeraldER fluorescence concentrated in the fragments, which indicates that the integrity of the ER membrane during the fragmentation remains intact and does not allow dissipation of molecules as large as FPs (~27 kDa). A representative time series can be seen in Figure 11D. The fragments were highly mobile, potentially indicating a detachment from the cytoskeleton, and concentrated in spatial intervals, where they often formed large clusters. The extent of vesicularisation spread over a maximum of several hundred micrometres from the injury site. Vesicularisation of the ER in response to injury of the plasma membrane has been described before in cell culture (Raeymaekers & Larivière, 2011). ER fragmentation in dendrites has also been described in paradigms of glutamate excitotoxicity and ischemia (see chapter 1.2.5). In this thesis, axonal ER fragmentation could be established as a consistent and stereotypical morphological response to laser-induced injury and was considered as an indicator of ER-effective trauma in the following experiments.

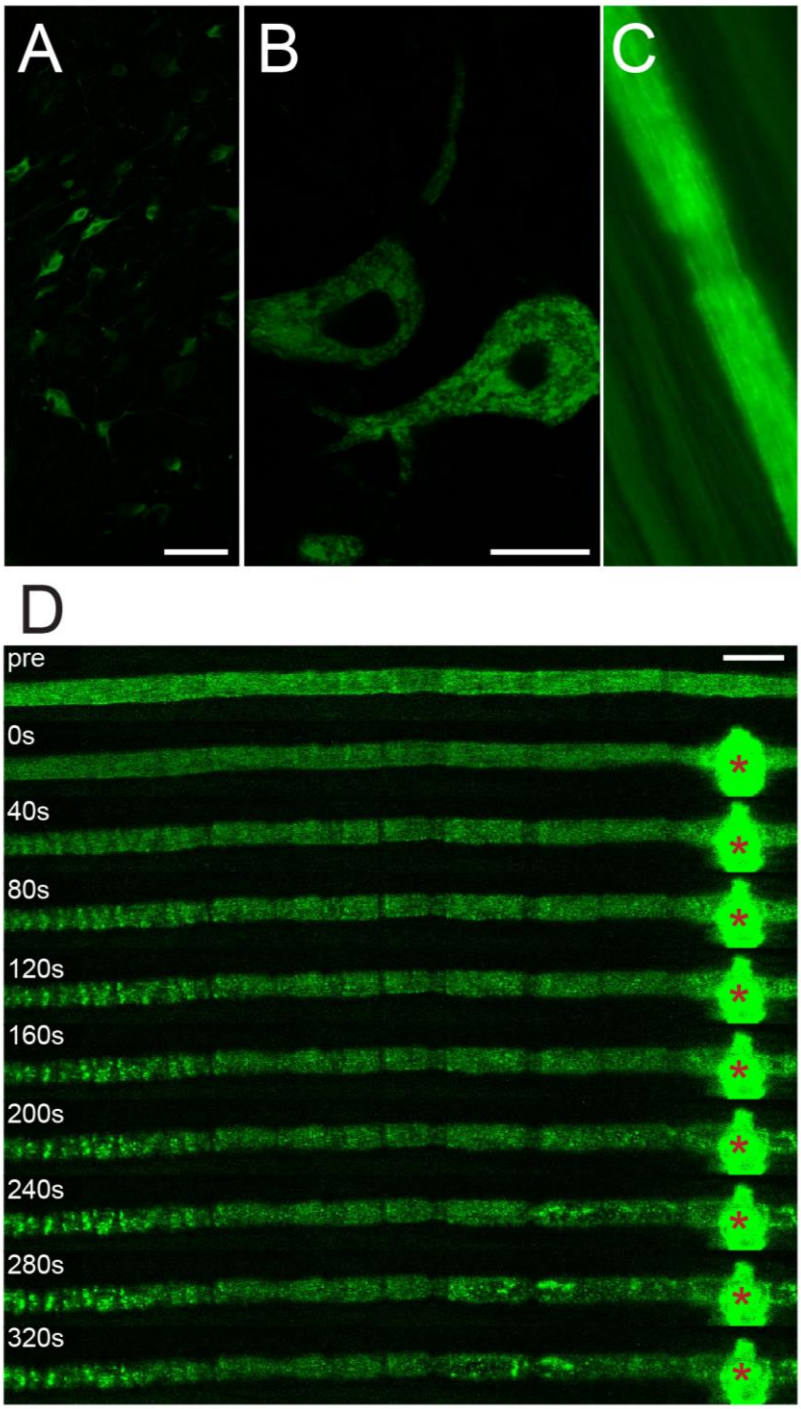

Figure 11: AAV-mEmeraldER spinal cord injections and explant laser transections

(**A**) Confocal image of spinal cord transversal section close to AAV-mEmerald ER injection site at 20x magnification; (**B**) at 60x magnification (α-motor neurons). (**C**) Widefield epifluorescence image of intercostal nerve axon at 100x magnification, rib cage explant of mouse injected with AAV-mEmeraldER. (**D**) Intercostal nerve axon laser-induced injury. Red asterisks indicate site of laser lesion. Confocal time series, rib-cage explant of mouse injected with AAV-mEmeraldER. Scale bars 25 µm.

4.1.2 Twitch2B 54S+ ER can measure intra-ER free calcium

Finding a suitable ratiometric calcium indicator was a prerequisite for reliability in vivo intra-ER free calcium measurements. Reasons for this are manifold: expression of individual axons can vary over time; movement artefacts can cause apparent changes in fluorescence intensity; and one time-point measurements, i.e. baseline characterisation, were required for the assessment of FAD stages in EAE. These requirements precluded the use of intensiometric ER-calcium indicators, despite their higher dynamic ranges. Obvious candidates which remained were GEM-Cepia1er and ER-targeted FRET-based cameleons (see chapter 1.4.2). GEM-Cepia1er was also analysed in cell culture and in intercostal nerves after GEM-Cepia1er AAV injections. Owing to similar emission maxima as in FRET-based cameleons (for which corresponding filter cubes were available), the usage of GEM-Cepia1er was, in theory, feasible. However, cellular imaging of GEM-Cepia1er required much higher excitation intensity than its cameleon counterparts, and the fluorescence yielded in both cells and explants was meagre (data not shown). Moreover, the excitation maximum is located at 391 nm wavelength, i.e. in the UV spectrum, which could account for considerable phototoxicity (Suzuki et al., 2014). Consequently, it was opted against GEM-Cepia1er, despite its beneficial ratiometry, high dynamic range and high K_d-value (558 µM). Alternatively, Twitch2B 54S+ was cloned in frame with an N-terminal mouse immunoglobulin V_h-signalling peptide and a C-terminal KDEL ER-retention sequence (see chapter 3.2.1). Notably, this ER-targeting approach had been successful before for labelling dendrites in cerebellar Purkinje cells in mice (Okubo et al., 2015). Twitch2B 54S+ ER had originally been generated in a screening for high dynamic range, minimal domain CFP/YFP-derivative-based FRET indicators (Twitch indicators) by Thestrup and colleagues (Thestrup et al., 2014). While the primary incentive of this screening was the search for highly sensitive calcium sensors with linear response kinetics, a number of low-affinity calcium sensors were also yielded. Among these was Twitch2B-54S+ ER, with a high Kd-value of 174 µM and a dynamic range of 320%. This indicator was selected for further in-vitro characterisation for several reasons: First, resting axonal $[Ca^{2+}]_{ER}$ had been determined to be on average ~150 µM (de Juan-Sanz et al., 2017), which ideally matched the K_d of Twitch2B-54S+ER and would, in principle, enable ideal-response kinetics. Secondly, the sensor belongs to the family of FRET-based (CFP/YFP derivative containing) ratiometric indicators, for which all filters

were readily available and 2-photon excitation spectra and corresponding phototoxicity had been determined beforehand (Schumacher, 2015). Thirdly, the FPs comprising the indicator (cpVenus^{CD} and mCerulean3) offer high quantum yields and photostability, which is especially beneficial concerning the limited volume of axonal ER, which can only accommodate small amounts of sensor and restricts diffusion of new sensor molecules. Fourthly, FRET-based ER-calcium indicators that had previously been described suffered from low dynamic ranges. Lastly, Dr. von Blume (Max Planck Institute of Biochemistry, Martinsried, Germany) had made successful use of low-affinity calcium indicators of the Twitch family in the Golgi apparatus, which also constitutes a high calcium-content organelle (personal communication).

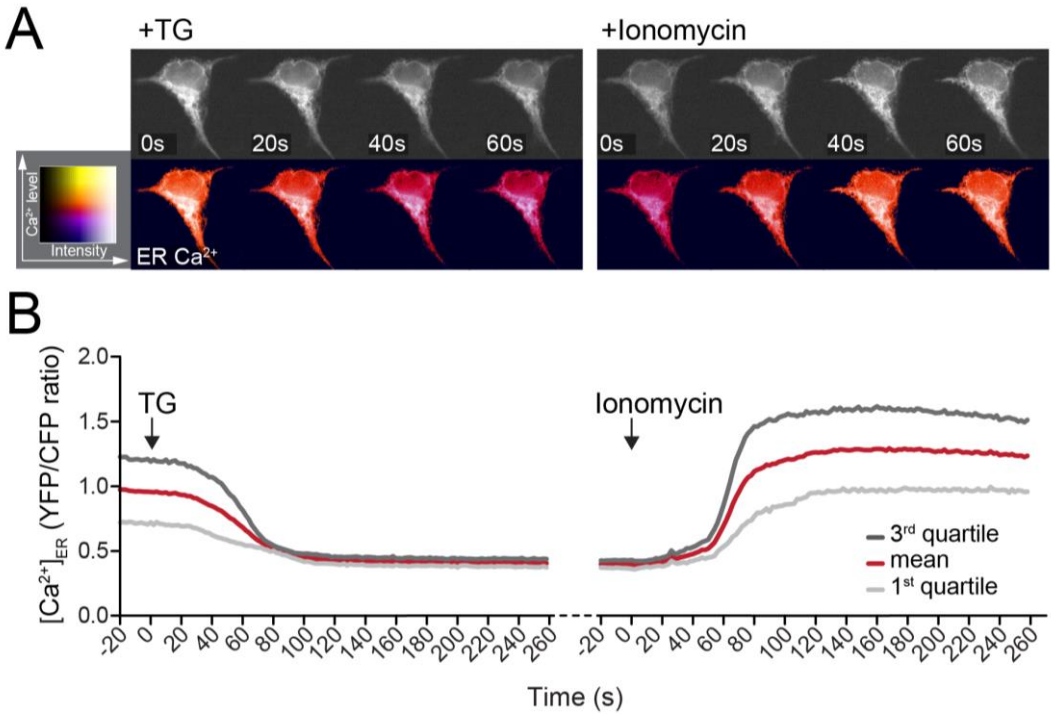

Figure 12: HEK cell ER calcium depletion and replenishment

(**A**) Representative pseudo-coloured ratiometric images of the fast phases of ER calcium depletion and replenishment in a Hek-293 cell with 3 µM thapsigargin (TG) and 10 mM ionomycin + 10 mM $CaCl_2$ (Ionomycin); widefield-epifluorescence microscopy. (**B**) Graphs depict sequential depletion and replenishment of ER calcium; 1st, 3rd quartiles and mean values are shown; recorded and measured with two-second intervals; a total of 14 individual cells in two independent imaging/treatment rounds were analysed.

For in-vitro characterisation of the sensor in Hek-293 cells, pharmacological manipulations were used which can either cause ER calcium depletion by blocking the SERCA (thapsigargin) or can equilibrate calcium concentrations through mem-

branes in the presence of high extracellular calcium and thereby replenish ER calcium (ionomycin + $CaCl_2$). Time-series analyses in Hek-293 cells demonstrated that Twitch2B-54S+ ER can indicate sequential ER-calcium depletion with 3 µM thapsigargin perfusion and ER-calcium replenishment with 10 µM ionomycin + 10 mM $CaCl_2$ perfusion. Graphs obtained from the time-series analysis of 14 individual cells in two independent imaging rounds are demonstrated in Figure 12B. Values are normalised to the mean of the first time-point. A dynamic range of ~ 300% (R_{max}/R_{min}) could be achieved, a value slightly below the dynamic range determined for purified Twitch2B 54S+ sensor (Thestrup et al., 2014), which could be, in part, accounted for by incomplete ER calcium depletion (the concentration, even after blocking the SERCA, is known to remain well over the cytoplasmic concentration in the range of tens of micromolar).

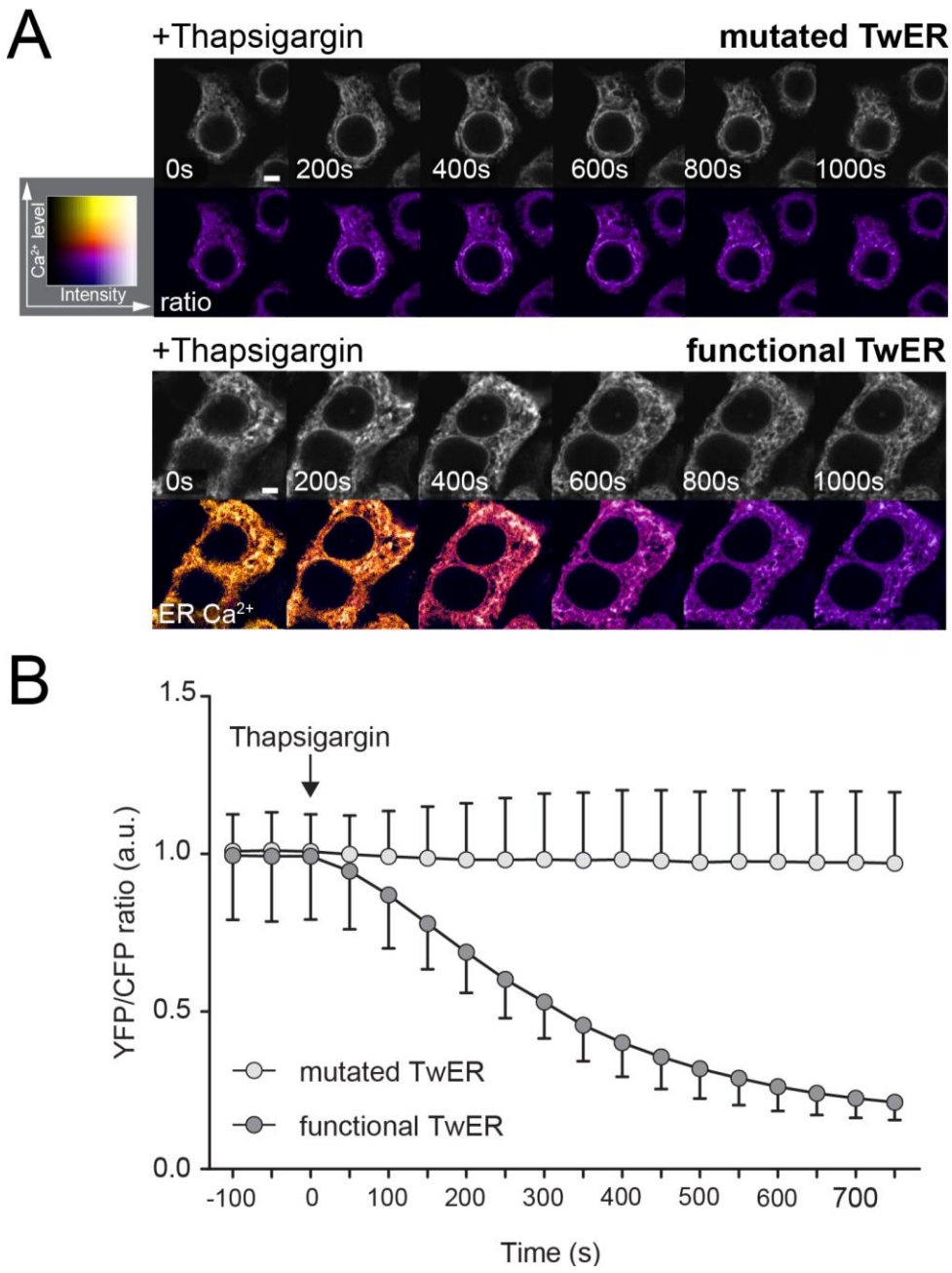

Figure 13: Mutated EF hands Twitch2B control

(**A**) Representative pseudo-coloured ratiometric images of Hek-293 cells transfected with mutated EF hands Twitch 2B ER control plasmid (top) and functional Twitch2B 54S+ ER plasmid (bottom) treated with 5 µM thapsigargin; imaged with 2-photon microscope. YFP channel in upper row, pseudocoloured YFP/CFP ratio in lower row. (**B**) Graphs depict responses of mutated and functional Twitch ER; thapsigargin is added at t=0 s; a total of 37 cells transfected with mutated Twitch2B ER and 39 cells transfected with functional Twitch 2B ER from four independent experiments were analysed. Error bars indicate standard deviation. Scale bars 5 µm.

In order to verify that the sensor actually measures calcium levels, the following control experiment was performed: the calcium-responsive EF hand domains were

replaced by non-functional aliphatic linker domains in pCMV-Twitch2B 54S+ ER, thereby creating pCMV-Twitch2B mutated linker ER (see chapter 3.2.1). In Hek-293 cells, ER calcium depletion with 5 µM thapsigargin does not cause changes in the ratio of the Twitch2B-mutated linker ER protein, while ratios in the functional Twitch2B 54S+ ER decline in the shape of a sigmoidal curve. This is demonstrated in Figure 13. The graph in Figure 13B displays the measurements from 37 pCMV-Twitch2B mutated linker-transfected cells (negative control) and from 39 cells pCMV-Twitch2B 54S+ ER transfected cells (positive control), each in four independent experiments. Thus, changes in the ratio of functional Twitch2B 54S+ ER can reliably be attributed to functional EF-hand domains (i.e. a calcium-dependent process) and not changes of the FPs themselves (e.g. by changes in pH and protonation status).

4.1.3 Generation and screening of Thy1-TwitchER transgenic mice

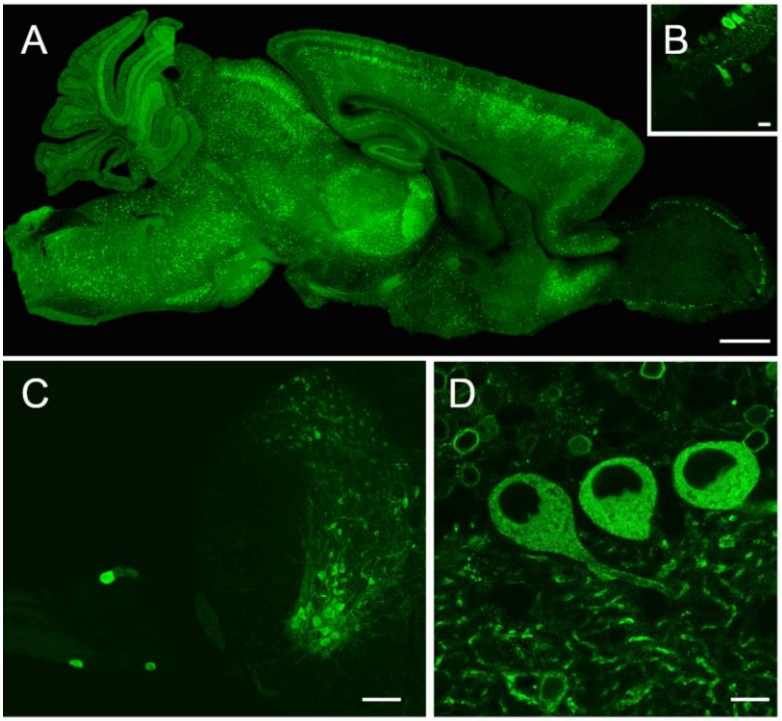

Figure 14: Twitch2B 54 S+ ER expression in Thy1-TwitchER transgenic mouse lines

(**A**-**C**) Confocal overviews of Thy1-TwitchER 481 fixed-tissue screening showing (**A**) a mosaic scan of a sagittal brain section, (**B**) a retinal section and (**C**) a horizontal hemi-section of the spinal cord and an adjacent DRG with sparse subset labelling. (**D**) Twitch2B 54S+ ER positive Purkinje-cells of cerebellar section in Thy1-TwitchER 489 transgenic mouseline. Scale bars are 1 mm in (A), 5 µm in (B), 100 µm in (C) and 10 µm in (D).

After verifying the functionality of the Twitch2B 54 S+ ER sensor in Hek-293 cells, Thy1-TwitchER mice were generated by pronuclear injection of linearised Thy1-Twitch2B 54S+ ER DNA (see chapter 3.2.7). Eleven PCR positive transgenic mouse lines were yielded, which were then subjected to a previously described screening protocol, which involved rib-cage explant ex-vivo imaging (fluorescence in intercostal nerves and NMJs was evaluated), in-vivo imaging of the spinal cord and preparation of brain, spinal cord and DRG slices from PFA-fixed mice (Marinkovic et al., 2015) (see chapter 3.2.8). Two of the lines obtained turned out to be particularly interesting and were selected for continued breeding. Thy1-TwitchER 481 displayed strong expression in both the CNS and PNS in a sparse subset of neurons (Figure 14A-C). Notably, neuronal somata showed significantly brighter fluorescence than their processes, which hints at different luminal ER volumes and complicates axonal ER imaging. The sparse subset labelling of DRG neurons (Figure 14C) is correlated with the subset labelling of axons in the superficial dorsal column, as seen by in-vivo imaging. The subset labelling of axons in the dorsal column facilitates spinal cord in-vivo imaging by making the axons and stages of FAD more easily distinguishable. The second transgenic mouse line, which was kept for continued breeding, was Thy1-TwitchER 489, which featured relatively bright and ‘full’ (~90 % of neurons) expression of the transgene, including expression in cerebellar Purkinje cells (Figure 14D), useful for electrophysiological experiments with cerebellar brain slices. All other lines lacked Purkinje cell expression. Another transgenic mouse line, Thy1-TwitchER 509, was used in several experiments of this thesis (when indicated). However, breeding of this line was later discontinued due to limited breeding space. Thy1-TwitchER 509 is characterised by a subset expression in ~60 % of DRG neurons, which yields a higher labelling density in spinal cord in-vivo imaging. Fluorescence intensity was weak in comparison to Thy1-TwitchER 481, which deteriorated the signal-to-noise ratio.

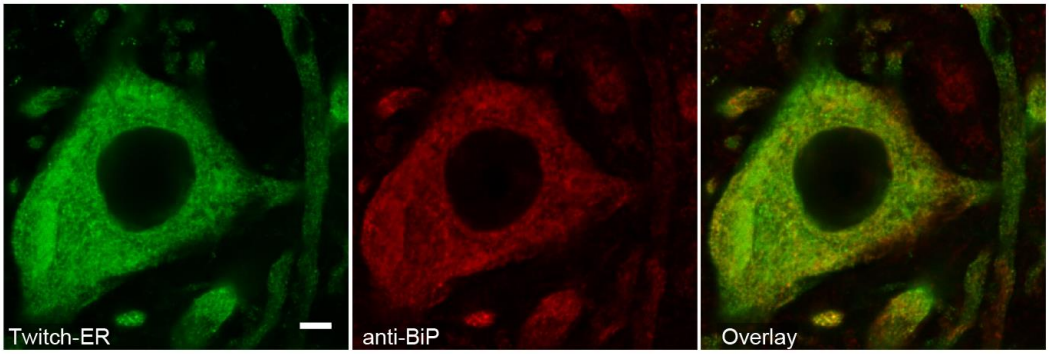

Figure 15: Twitch2B 54 S+ ER colocalisation with GRP78/BiP

Representative confocal image of an immunostained spinal cord sagittal slice, which demonstrates the colocalisation of the ER marker GRP78/BiP (red channel) and Twitch2B 54S+ ER (green channel). Note the GRP78/BiP positive cells in the overlay image, which do not express Twitch2B 54S+ ER. Scale bar 5 µm.

To test whether Twitch 2B 54S+ was correctly localised in the ER, immunostainings of GRP78/BiP were carried out (see chapter 3.2.8). GRP78/BiP has previously been expressed in mouse dorsal-root axons (Stirling et al., 2014). Confocal imaging of stained spinal cord sections revealed that GRP78/BiP colocalises with the calcium indicator Twitch2B 54S+ in the Thy1-TwitchER481 transgenic line in spinal interneurons (Figure 15). Spectral bleed-through between the channels was avoided by choosing a secondary antibody with an infrared emission spectrum and by sequential scanning of single channels (Alexa Fluor 647). GRP78/BiP clearly also stained ER of cells which did not display sensor expression, including glia, while DRG neurons and axons were only weakly stained. Axonal ER tended to be fragmented after 4 % PFA perfusion. Therefore, colocalisation could only be reliably demonstrated in spinal interneurons, where bright GRP78/BiP staining could be observed.

4.1.4 Thy1-TwitchER transgenic mice report intra-ER free calcium levels

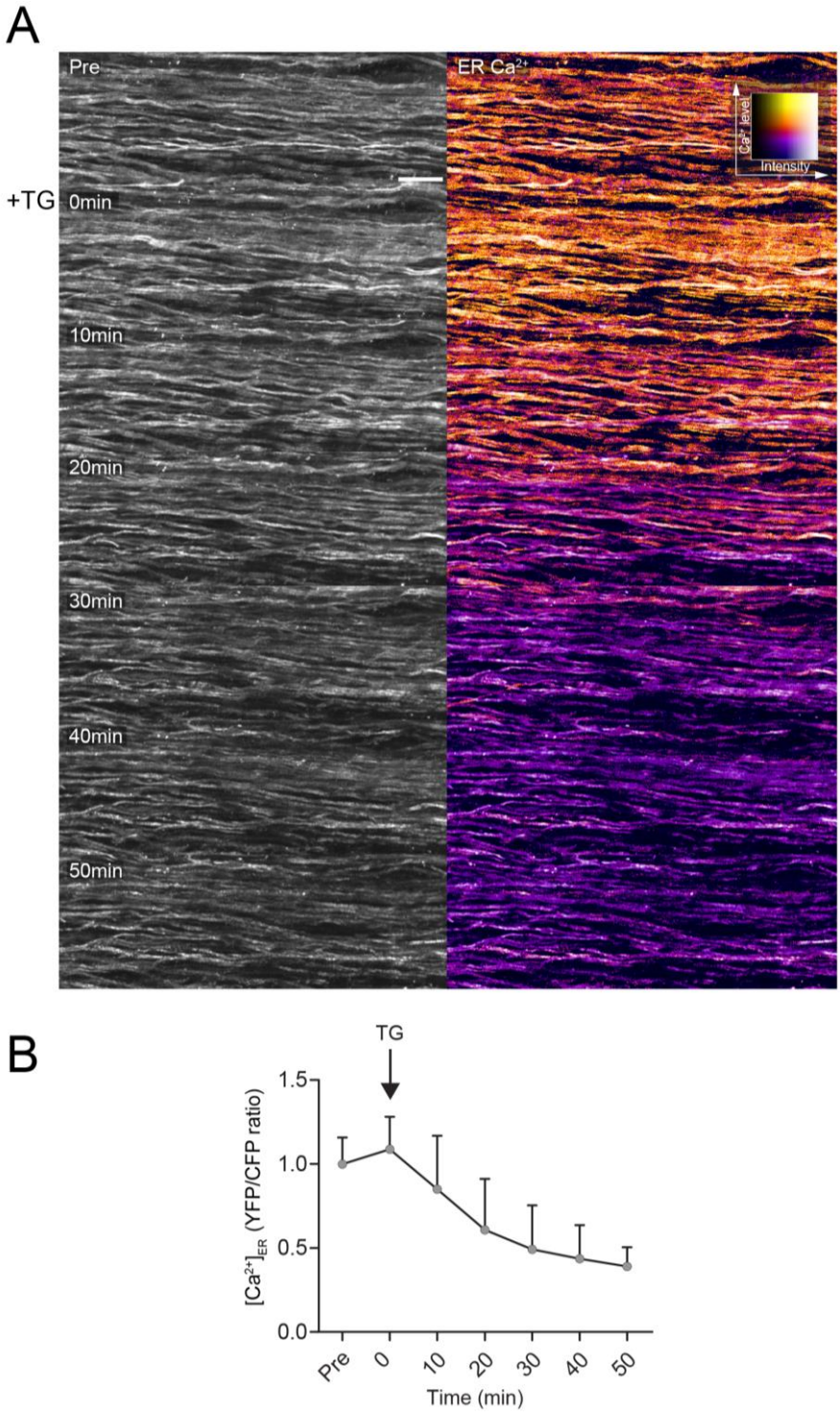

Figure 16: Functional characterisation of the Thy1-TwitchER 481 transgenic mouse line with thapsigargin

(**A**) Representative time series of Thy1-TwitchER 481 spinal cord in-vivo imaging experiment. Continuous 10 µM thapsigargin bath application (SERCA inhibitor) from t=0 onwards. On the left, greyscale YFP channel intensity projections; on the right, corresponding ratiometric (YFP(FRET)/CFP) images. (**B**) Graph obtained from two independent experiments, where a total of 25 axons were tracked over time. Error bars indicate standard deviation.

A pharmacological characterisation ensued the morphological screening of the Thy1-TwitchER 481 transgenic line. Depletion of intra-ER free calcium was achieved by a bath application of 10 µM thapsigargin dissolved in ACSF. DMSO of the stock solution was diluted to 1 % in ACSF. In-vivo imaging of the spinal cord (see chapter 3.2.9) revealed a gradual decline of the YFP(FRET)/CFP-ratio, which is consistent with a higher proportion of calcium-free sensor molecules. Analysis of a total of 25 axons tracked over time in two independent ER depletion experiments demonstrated that after 50 minutes of thapsigargin bath application, all axons were uniformly depleted in their ratios (Figure 16). Superficial axons depleted faster than deeper axons, probably owing to restricted thapsigargin diffusion into the tissue. Compared to Hek293-cell ER calcium depletion, which only requires 1–10 minutes, calcium depletion of the axoplasmic reticulum took significantly longer (~50 min). There could be several explanations for this phenomenon. Firstly, the effective concentration of thapsigargin reaching the axons by diffusion could be lower due to diffusion limitation by the tissue and dilution by interstitial fluids. Secondly, neurons could have a larger total supply of ER calcium, which might diffuse from somatic stores to axons, as long as these are not sufficiently blocked by the SERCA-inhibitor thapsigargin (assuming that axonal ER is continuous with somatic ER). Thirdly, the axonal ER might have less intrinsic calcium leak than somatic ER, which is feasible since axonal ER is SER without translocon pores (as opposed to the abundant RER in somata). Notably, the decrease of ratios also led to a reduced spread, potentially by an equilibration of ER calcium levels at the lowest possible level after pharmacological depletion and by reduced sensor response characteristics at concentrations far below the its K_d-value. Thus, Thy1-TwitchER mice reliably detected and reported relative changes in intra-ER free calcium of the axoplasmic reticulum. This finding confirmed that a sensor with a K_d suitable for measurement, axoplasmic reticulum calcium levels were selected.

4.2 Intra-ER free calcium in paradigms of axonal degeneration

With the generation of the transgenic Thy1-TwitchER mouse lines, a novel tool was at hand to directly visualise changes of calcium in the axoplasmic reticulum. Moreover, we observed an intriguing morphological response pattern: ER vesicularisation following laser-induced axonal injury in AAV mEmeraldER-injected mice. Effects of this vesicularisation process on ER calcium homeostasis could only be

speculated on using structural ER markers, but combined with ER calcium indicators these were open to direct investigation. Since ER calcium dyshomeostasis is discussed and plays an important role in axonal degeneration (see chapter 1.3.5), we further investigated changes of ER calcium as well as the phenomenon of ER vesicularisation in various axonal degeneration paradigms.

4.2.1 ER calcium release occurs late and is not causative for FAD

An important mode of axonal degeneration that has been discovered in EAE is FAD, which is characterised by the succession of morphological degeneration stages. Stage 0 axons are morphologically unaltered, while stage 1 axons are defined by focal axonal swellings (while the axon's continuity is maintained), and stage 2 axons are disrupted in their continuity and fragmented. Stage 1 axons are capable of recovery, while stage 2 axons are irrevocably damaged. The probability of the progression to the next stage is determined by the amount of cytoplasmic calcium. Axons with high cytoplasmic calcium are more prone to undergo FAD and less likely to recover than axons with low/recovered cytoplasmic calcium (see chapter 1.3.1) (Nikić et al., 2011; Witte et al., 2019). In this thesis, the contribution of ER-derived calcium to the detrimental cytoplasmic-calcium rise observed in FAD was evaluated.

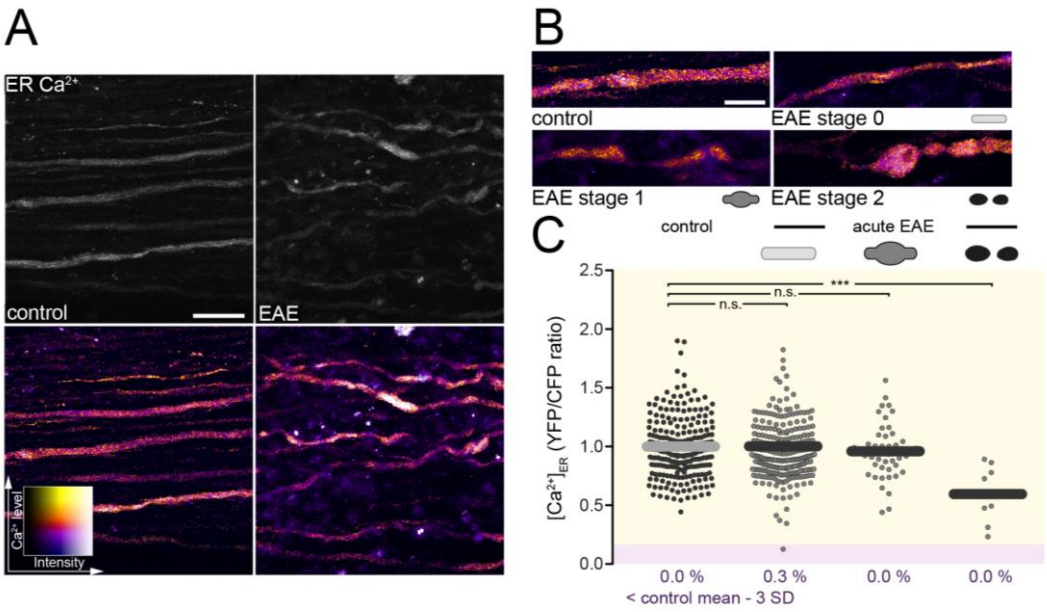

Figure 17: ER calcium in EAE

(**A**) Representative in vivo 2-photon microscopy intensity projections (top, YFP channel) and the corresponding colour-coded ER calcium levels (bottom, YFP/CFP ratio) under control conditions (left) and subsequent to EAE induction, two days after onset (right). The images show the superficial dorsal funiculi of the spinal cord in Thy1-TwitchER 481 mice. (**B**) Exemplary images colour-coded for ER calcium (YFP/CFP ratio) of axons under control conditions (upper left) and axons representative of the morphological FAD stages 0 (upper right), 1 (lower left) and 2 (lower right) 2 days after onset of EAE (**C**) ER calcium of single axons (YFP/CFP ratio normalised to the mean of control axons) in healthy spinal cord and FAD stages in EAE. Grey bars indicate mean values. The percentages indicated below show the proportion of axons with formally depleted $[Ca2+]_{ER}$ < control mean – 3 SD. Mann-Whitney U test control vs. EAE stages 0-2 in n = 6 control mice and n = 4 EAE mice. Scale bars are 25 µm in (A) and 10 µm in (B). n.s P > 0.5, ***P < 0.001. Caption modified from and figure layout adapted from Witte et al. (2019). Experimenter: Alexander Scheiter

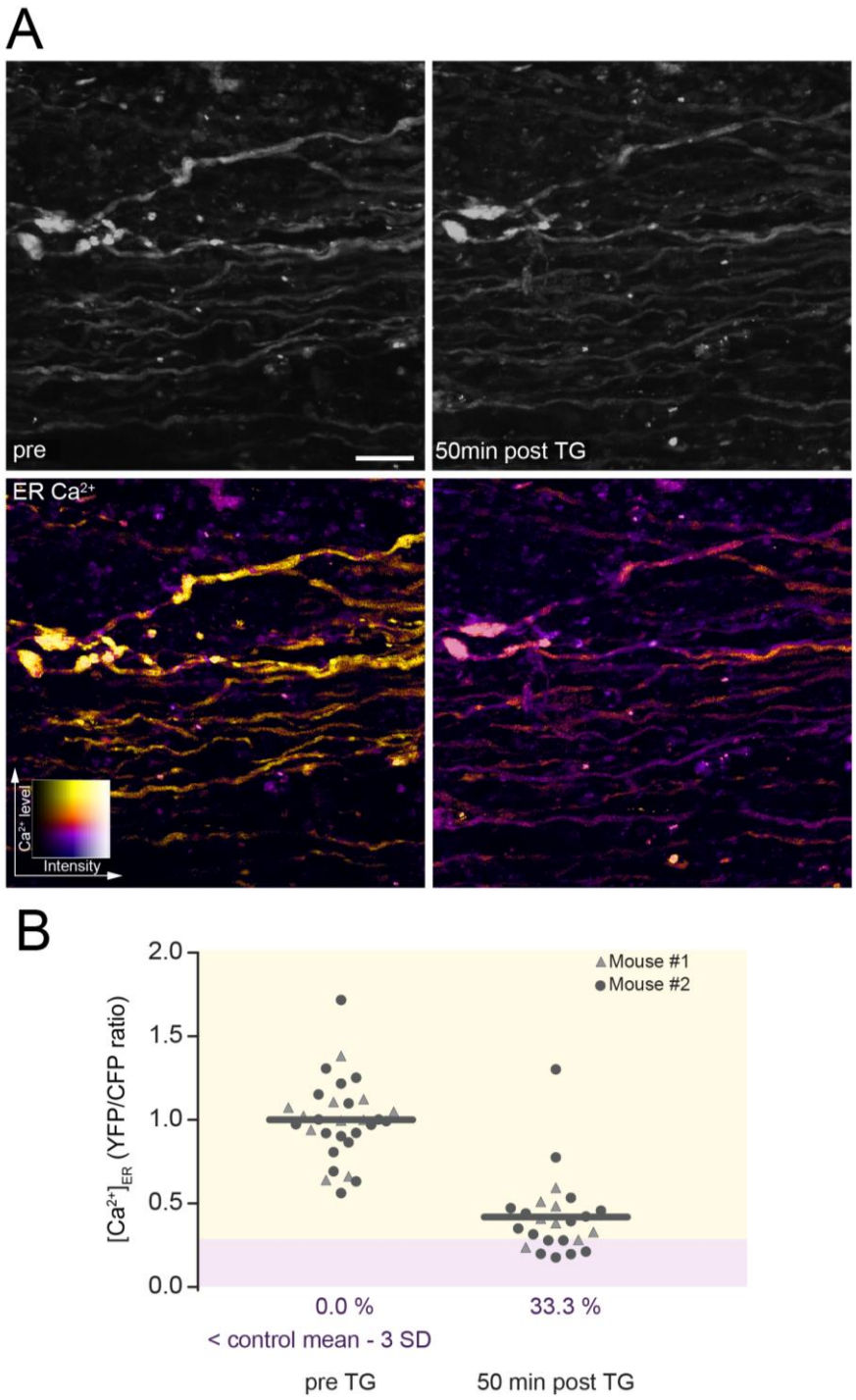

Figure 18: Thapsigargin depletes ER calcium in EAE

(**A**) In vivo 2-photon maximum intensity projection of spinal cord axons of Thy1-TwitchER 481 mice in EAE lesions. Left: pre-10 µM thapsigargin (TG) bath application. Right: 50 min post 10 µM thapsigargin bath application. Top: Greyscale images of YFP channel. Bottom: Ratiometric (YFP(FRET)/CFP) images colour-coded for ER calcium levels ($[Ca2+]_{ER}$). Scale bar 25 µm. (**C**) $[Ca2+]_{ER}$ of single axons. Note that Mouse 1 and 2 belong to different Thy1-TwitchER lines (478 and 481) and were imaged with different detector voltages. Thus, the YFP(FRET)/CFP channel ratio was normalised to the mean of the pre-TG time point for each mouse. Grey bars indicate combined mean values. Percentages (below) show the proportion of axons with formally depleted $[Ca2+]_{ER}$ < control mean – 3 SD.

To this end, ER calcium was measured in spinal axons of healthy Thy1-TwitchER 481 control mice and in axons of acute spinal lesions of Thy1-TwitchER 481 mice induced with EAE (see chapter 3.2.9.2). Four mice with an EAE score ≥ 2 and 6 healthy control mice were imaged. Significant depletion of ER calcium was only detectable in a small fraction of fragmented, i.e. stage 2, axons. This depletion did not reach values below the mean minus three standard deviations but was statistically significant compared to control. The cut-off value of the mean plus three standard deviations had previously been employed for a binary scoring approach in the assessment of cytoplasmic calcium elevations (Witte et al., 2019). Stage 0 control axons did not display a significant decrease of ER calcium, as compared to healthy control axons. Neither did ER calcium in stage 0 axons differ significantly from stage 1 axons (Figure 17). A Mann-Whitney test was employed, testing control axons against stage 0, stage 1 and stage 2 axons in a population based analysis respectively since normal distribution could not be confirmed with the Shapiro-Wilk normality test. These data indicate that ER calcium only depletes in the late, irreversible stage of FAD. Consequently, ER calcium depletion does not predict the fate of axons undergoing FAD, unlike cytoplasmic calcium elevation. Thus, the observed cytoplasmic calcium elevations are not caused by calcium efflux from the ER, the most important organellar calcium store. However, this dataset can only securely assess relative ER calcium depletions in the range of the strong pharmacological depletions caused by thapsigargin, for which a substantial sensor response has been demonstrated in Thy1-Twitch ER 481 mice (chapter 4.1.4). Notably, thapsigargin depletion could also be reliably measured in EAE lesions of two Thy1-TwitchER mice (lines 481 and 478), which affirms the functionality of the Twitch2B 54S+ ER sensor under inflammatory conditions. Fifty minutes post thapsigargin application 33.3% of axons could formally be categorised as depleted, i.e. measured YFP(FRET)/CFP ratios were below the mean minus three standard deviations (Figure 18). Nonetheless, minute changes of ER calcium would likely be obscured due to the large interaxonal spread and due to the employed method of single time-point population analysis. Regarding axonal ER morphology, resolvable ER vesicularisation/fragmentation was not detectable in in FAD.

4.2.2 ER calcium release occurs early in models of LiSCI and spinal cord contusion

Given that neither ER fragmentation nor ER calcium dysregulation (at least prior to the disruption of axonal continuity) was observable in EAE, other paradigms of axonal degeneration were investigated. Since laser lesioning of intercostal nerve axons was shown to induce ER fragmentation in AAV-mEmeraldER-injected mice (see chapter 4.1.1), laser-induced spinal-cord injury (LiSCI) was chosen to search for detectable ER calcium alterations. Breckwoldt et al. (2014) were previously able to image temporal calcium in Thy1-TN-XXL mice following LiSCI. A localised calcium influx spread at a speed of ~3.8 µm/s from the transection site. With regard to this cytoplasmic calcium dysregulation, a concomitant dysregulation of ER calcium seemed likely.

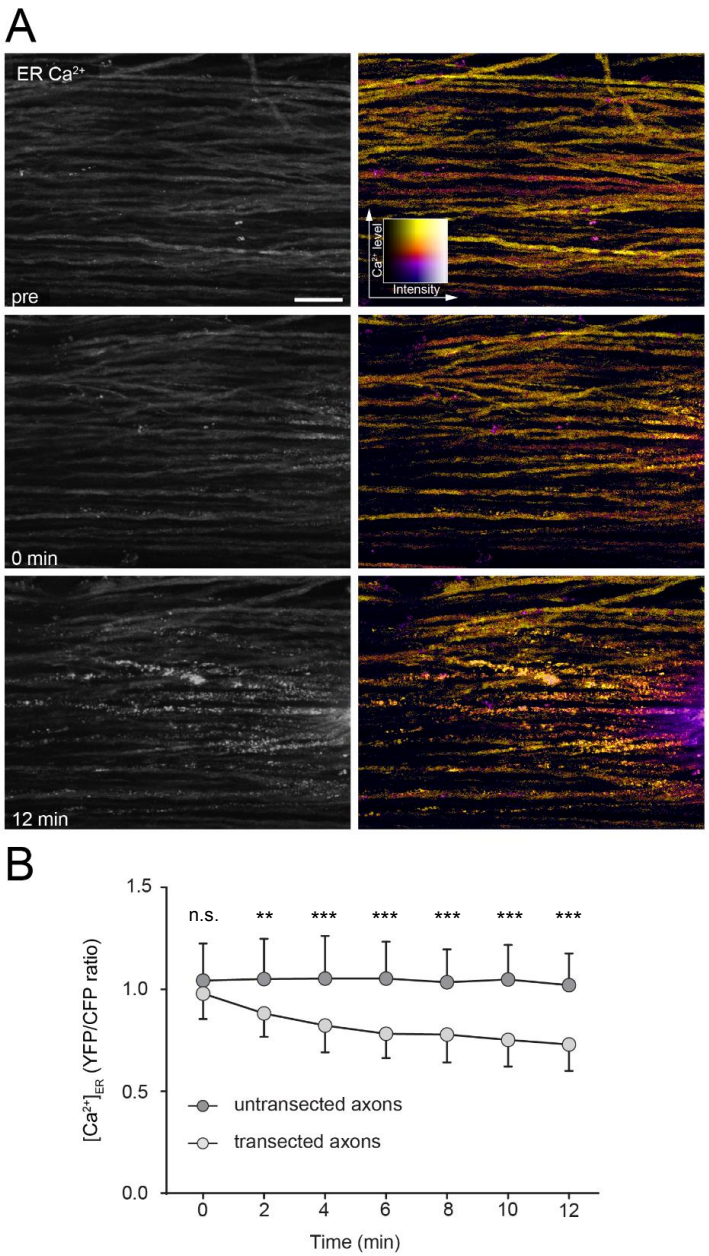

Figure 19: Thy1-TwitchER laser transections

(**A**) In-vivo 2-photon maximum intensity projection of spinal-cord axons of Thy1-TwitchER 509 mice at time points pre-laser lesion, 0 min post-laser lesion, and 12 min post-laser lesion. Left: Greyscale images of YFP channel. Right: Ratiometric (YFP(FRET)/CFP) images colour-coded for ER calcium levels ($[Ca2+]_{ER}$). Laser lesion site partly included on right edge. Scale bar 25 µm. (**B**) Graph contrasts $[Ca^{2+}]_{ER}$ time courses of a total of 37 transected axons2 $[Ca^{2+}]_{ER}$ to a total of 18 untransected axons obtained from five Thy1-TwitchER 509 mice beginning at time point of 0 min post-contusion. Error bars indicate standard deviation. Unpaired t-test control transected vs. untransected except for 4 minutes time point transected vs. untransected Mann-Whitney U test. n.s $P > 0.5$, $^{**}P < 0.01$, $^{***}P < 0.001$

Following LiSCI in Thy1-TwitchER 509 mice (see chapter 3.2.9.3), ER fragmentation occurred in severed axons and spread to a maximum distance of ~300 µm from

the transection site at the end of the observation period (12 minutes post-transection). The $[Ca^{2+}]_{ER}$ time course of a total of 37 transected axons was compared to a total of 18 untransected axons obtained from 5 Thy1-TwitchER 509 mice (Figure 19). Transected axons were differentiated from non-transected axons by the occurrence of resolvable ER fragmentation. Untransected axons were chosen not to traverse the lesion site (which was detectable by strong autofluorescence). The ROI for $[Ca^{2+}]_{ER}$ measurements was selected to be within a range of a 100 µm from the transection site. In the case of transected axons, the ROI was traversed by an ER fragmentation front. Z-stacks were acquired at two-minute intervals for a total of 12 minutes following LiSCI. $[Ca^{2+}]_{ER}$ was measurably reduced in transected axons compared to non-transected axons and the decrease persisted for the total time of observation (12 minutes). The ratios of transected axons were significantly different from non-transected axons at all time points except for the first time point immediately after transection using unpaired t-tests or a Mann-Whitney test (for the 4 minutes time point, where normal distribution could not be confirmed with the Shapiro-Wilk normality test).

Regions of morphologically intact ER calcium had already displayed ER calcium depletion, so it remained unclear whether the fragmentation process per se was causative for the observed ER calcium depletion. However, it cannot be ruled out that visually intact axonal ER was, in fact, disrupted in its continuity at a submicroscopic level. The observed depletion of $[Ca^{2+}]_{ER}$ was small in comparison to the effect of the thapsigargin-mediated depletion. A possible explanation could be that the electrochemical gradient for ER-calcium release is reduced by excessive calcium influx to the cytoplasm from the extracellular space.

With respect to this potential limitation of ER calcium release in laser transections, the paradigm of spinal-cord contusion was chosen to study $[Ca^{2+}]_{ER}$ dynamics. Williams et al. (2014) previously demonstrated that cytoplasmic calcium dysregulation occurs in a spinal-cord contusion model. Axolemmal mechanopores were discovered to be an important port of calcium entry. Raised cytoplasmic calcium levels increased the degeneration probability. Intriguingly, many axons with increased calcium recovered homeostasis without intervention (see chapter 1.3.4). Thus, the spinal-cord contusion model offers a ‘window of opportunity’ for therapeutic interventions, where axons still remain a recoverable state (in contrast to axonal transections, where the axonal fate is set). It can be speculated that the cytoplasmic calcium

elevations in the contusion model are less pronounced than in direct axonal transection and maintain the steep physiological gradient for ER calcium release – which might, in turn, contribute to a further detrimental cytoplasmic calcium rise.

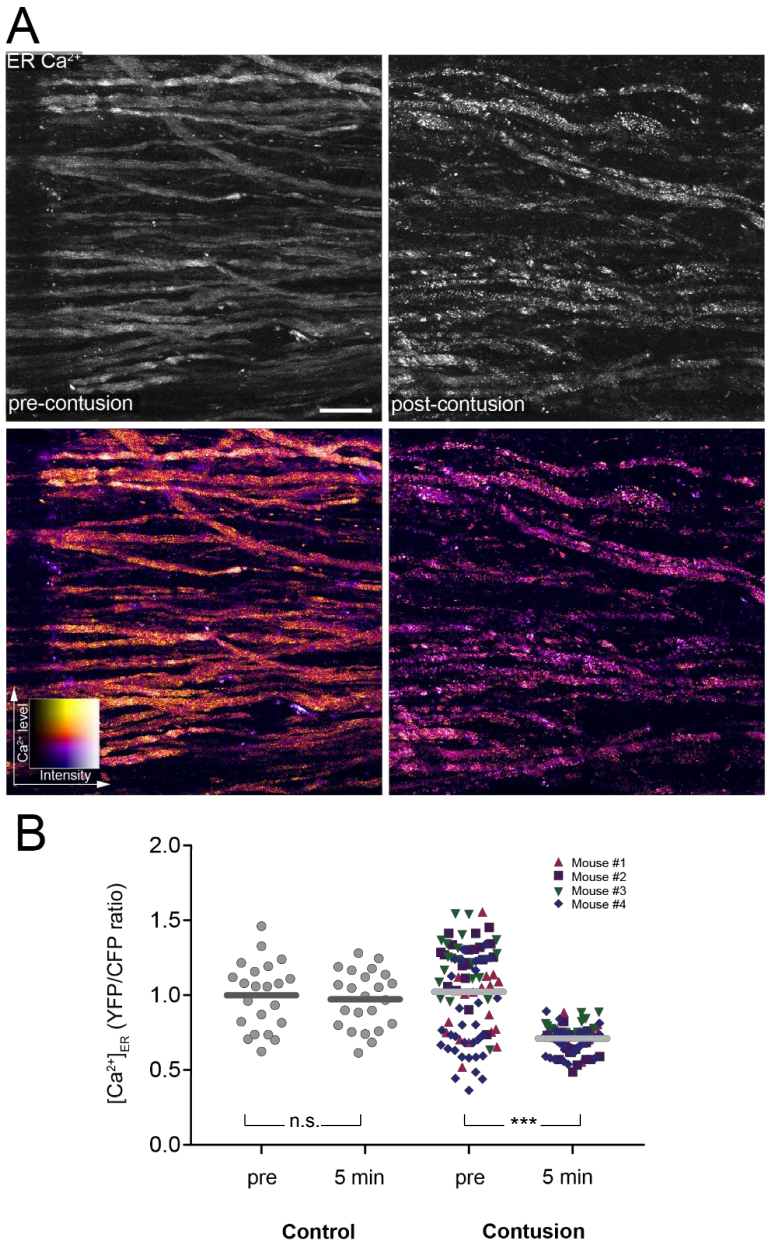

Figure 20: ER calcium in contusion model

(**A**) In-vivo 2-photon maximum intensity projection of spinal-cord axons of Thy1-TwitchER 509 mice at time points pre-contusion (left) and five min post-contusion (right). Top: Greyscale images of YFP channel. Bottom: Ratiometric (YFP(FRET)/CFP) images colour-coded for ER calcium levels ($[Ca2+]_{ER}$). Scale bar 25 µm. (**B**) Graph depicts axonal $[Ca^{2+}]_{ER}$ measurements of a control Thy1-TwitchER 509 mouse before and after a five-min waiting interval, as opposed to $[Ca^{2+}]_{ER}$ from 4 contused Thy1-TwitchER 509 mice pre-contusion and five min post-contusion. Bars indicate mean value. Unpaired t-test control pre vs. control 5 min. Mann-Whitney U test pre-contusion vs. 5 min post-contusion. n.s $P > 0.5$, ***$P < 0.001$

Contusions were carried out as outlined in chapter 3.2.9.4 in a total of four Thy1-TwitchER 509 mice. A comparison of pre- and ~5-min post-contusion 2-photon

stacks revealed that resolvable ER fragmentation occurred in a large proportion of contused axons, while $[Ca^{2+}]_{ER}$ was homogeneously depleted in all contused axons. The decrease of $[Ca^{2+}]_{ER}$ was found to be statistically significant in a population-based analysis including all contused mice pre- compared to post-contusion using a Mann-Whitney test, while the ratios of the control mouse axons were not significantly altered using an unpaired t-test according to the results of the Shapiro-Wilk normality test (Figure 20). The pre-contusion data displayed a large spread, which was attributable to one mouse (Mouse #4), which might have accidentally been pre-contused during the laminectomy. As a control, a Thy1-TwitchER 509 mouse was repeatedly recorded in five-minute intervals in order to exclude phototoxicity or photobleaching mediated changes of the YFP(FRET)/CFP ratio. The control did not show a significant change of reported $[Ca^{2+}]_{ER}$. When testing per animal with Mann-Whitney tests all contused mice except for Mouse #4 had significantly decreased sensor ratios 5 minutes after contusion compared to the pre-contusion time point.

The homogeneity of $[Ca^{2+}]_{ER}$ depletion was in stark contrast to the changes which had previously been observed in cytoplasmic calcium levels. Cytoplasmic calcium levels differed between axons and predicted their fate (Williams et al., 2014). Since all axons display a similar extent of $[Ca^{2+}]_{ER}$ depletion, it is unlikely that these are causative for cytoplasmic calcium elevations observed in Thy1-TN-XXL in only a fraction of axons. Notably, the experimental procedures had been carefully adapted to the protocol of Williams et al. (2014) (identical contusion device, contusion forces, imaging procedures and surgery technique). Thus, only a fraction of axons should undergo axonal degeneration due to the contusion damage. It appears that the events of $[Ca^{2+}]_{ER}$ depletion and ER fragmentation are not fatal to spinal axons and can recover completely. In fact, the homogeneity of these events' appearance indicates they happen in a regulated fashion, which could even be speculated to play a protective role.

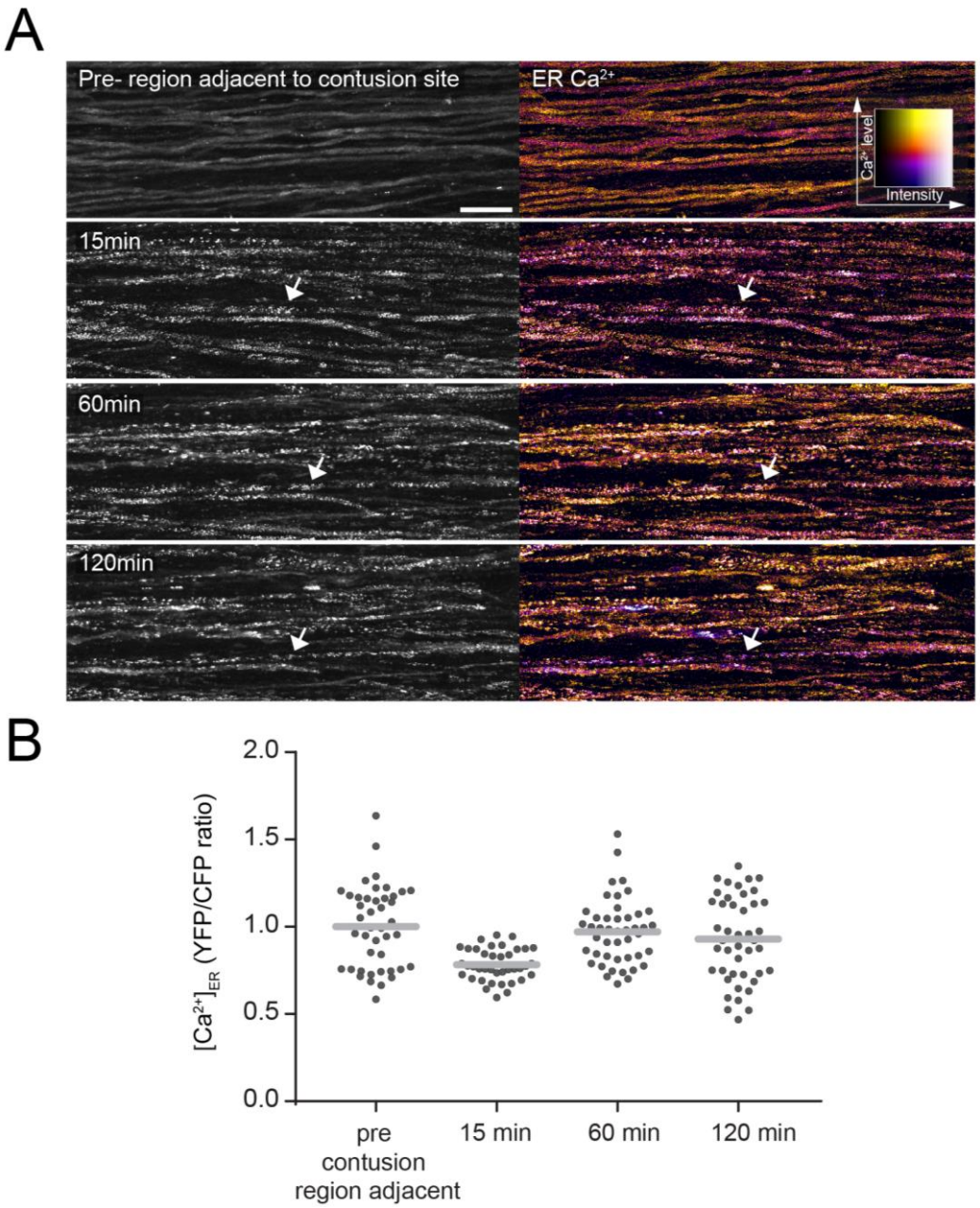

Figure 21: Temporal dynamics of ER calcium in contusion model

(**A**) In-vivo 2-photon maximum intensity projection of spinal-cord axons of Thy1-TwitchER 509 mice at time points pre-contusion, 15, 60 and 120 min post-contusion. Left: Greyscale images of YFP channel. Right: Ratiometric (YFP(FRET)/CFP) images colour-coded for ER calcium levels ($[Ca2+]_{ER}$). Arrows indicate an example axon with initially depleted $[Ca2+]_{ER}$ (15 min), which later replenishes (60 min), before depleting again (120 min). Scale bar 25 µm. (**B**) Graph depicts axonal $[Ca^{2+}]_{ER}$ measurements of a single contused Thy1-TwitchER 509 mouse pre-contusion ,15, 60 and 120 min post-contusion.

In another contusion experiment, which was, however, carried out in only one Thy1-TwitchER 509 mouse, $[Ca^{2+}]_{ER}$ was tracked over time (Figure 21). Following the expected initial $[Ca^{2+}]_{ER}$ depletion, the time-series analysis revealed a recovery

$[Ca^{2+}]_{ER}$ to pre-contusion values after ~1 hour, while at ~2 hours post-contusion, several axons dropped to low $[Ca^{2+}]_{ER}$. Moreover, many axons managed to reconstitute ER continuity. The finding that YFP(FRET)/CFP ratios can recover (and deplete again) strengthens the finding of initial $[Ca^{2+}]_{ER}$ depletion. Since ratios can behave dynamically, it is unlikely that the initial depletion is imitated by confounding factors, e.g. blood, which might selectively obscure YFP channel intensity. Nevertheless, these findings should be interpreted with caution, as the experiment was only conducted once. Subsequent repetition of contusion time-series analyses by Jonas Lehmitz, the successor for the axonal ER calcium project, substantiated the findings of initial ER-calcium depletion with subsequent recovery in spinal-cord contusions (see chapter 5.2.2).

In conclusion, $[Ca^{2+}]_{ER}$ alterations and ER fragmentation have been discovered in two axonal degeneration paradigms: LiSCI and spinal-cord contusion. Importantly, ER-fragmentation and $[Ca^{2+}]_{ER}$ alterations concur and represent a stereotypical response pattern to mechanical axonal injury with little variation between axons. The discovery of axonal $[Ca^{2+}]_{ER}$ changes and structural ER responses in traumatic injury emphasises the lack of these response patterns in EAE, where ER calcium levels remain stable until the axon has completely disintegrated and ER fragmentation cannot be resolved.

To conclude, $[Ca^{2+}]_{ER}$ alterations and ER fragmentation have been discovered in two axonal degeneration paradigms: LiSCI and spinal cord contusion. Importantly, ER-fragmentation and $[Ca^{2+}]_{ER}$ alterations concur and represent a stereotypical response pattern to mechanical axonal injury with little variation between axons. The discovery of axonal $[Ca^{2+}]_{ER}$ changes and structural ER responses in traumatic injury emphasizes the lack of these response patterns in EAE, where ER calcium levels remain stable until the axon has completely disintegrated and ER fragmentation cannot be resolved.

5 Discussion

5.1 Imaging intra-ER free calcium in single axons: Accomplishments and limitations

In this thesis, a novel tool was generated, which allowed measurement of axonal intra-ER free calcium for the first time: the Thy1-TwitchER transgenic mouse line. By means of in-vivo 2-photon microscopy, direct axonal imaging of the spinal cord's superficial dorsal column was achieved. Moreover, axonal ER morphology could be assessed for the first time in vivo (both by injecting the structural marker AAV-mEmeraldER and by imaging the Thy1-TwitchER transgenic mouse line), which revealed a unique response pattern to traumatic axonal injury: ER fragmentation. In this chapter, the pitfalls and potentials of axonal ER imaging and intra-ER free calcium measurements will be discussed in depth.

5.1.1 Insights from structural imaging of axonal ER

The structural marker AAV-mEmeraldER was used as proof of principle to demonstrate that axonal ER can be successfully labelled and imaged with FPs. This was an important prerequisite to evaluate the feasibility of generating a transgenic mouse line expressing a calcium indicator in the ER. The calreticulin signalling sequence, in combination with the KDEL retention sequence, were used in the AAV-mEmeraldER construct, since these had previously been employed successfully to target and image dendritic ER in a Thy-1 EGFP ER transgenic line by Kucharz et al. (2011b). In chapter 4.1.1, we demonstrate that the AAV-mEmeraldER labelling pattern matched the expectations for ER labelling: in confocal imaging of fixed spinal-cord sections, nuclear envelope- and RER sheet-like structures were noted. Furthermore, the confocal and widefield imaging of explants prepared from AAV-mEmeraldER-injected mice revealed a dynamic network of tubules, with prominent subsurface structures and periodical thinning of the network corresponding to the nodes of Ranvier. Although localisation to the ER has not been verified by immunostainings for AAV-mEmeraldER injections (as it has been done in the case of Thy1-TwitchER mice), the morphological features observed correspond to electron-microscopic depictions of axonal and somatic ER reported in literature (Terasaki, 2018; Wu et al., 2017; Yin et al., 2016). Moreover, the morphological pattern yielded

was identical to the morphology of Thy1-TwitchER transgenic mice, where ER localisation was validated by the co-localisation of the ER marker GRP78/BiP and the calcium indicator Twitch2B 54S+ ER.

What remains questionable is the identity of the fast-moving 'comets', which were incidentally observed in AAV mEmerald ER mice. Notably, similar distally bound and fast-moving vesicular structures were occasionally visible in Thy1-TwitchER transgenic mice, where they were often associated with depleted ER calcium levels. These could represent mere proteinaceous aggregates (FPs have a tendency for aggregation when they are expressed at high levels) or vesicles transported by fast-axonal transport. In the latter case, the observed 'comets' could very well represent an axonal ER sub-compartment, which is not continuous with the tubular axonal ER, and might serve distinct functions, such as the rapid supply of ER resident proteins to distal axonal regions.

The ER fragmentation, or vesicularisation process, observed in laser transections of AAV-mEmeraldER-injected mouse explants was a particularly intriguing finding. ER fragmentation had previously been reported as an ER response pattern, in response to excitotoxicity and ischemia in dendrites (see chapter 1.2.5). In this thesis, ER fragmentation was established as a consistent response to traumatic ER injury, including laser transections and contusions. As in dendritic non-traumatic paradigms, ER fragmentation in axons was demonstrated to be reversible in the case of spinal-cord contusions. Thus, ER fragmentation is not fatal to axons, and a coping program must exist. Given the regularity at which ER fragmentation occurs, one might speculate that it could even serve as a protective response to traumatic and non-traumatic injury mechanisms – for example, by limiting the ER stress response by restricting the diffusion of local luminal proteins.

5.1.2 Assessing the chosen ER calcium indicator

A primary focus of GECI engineering throughout the last years has been to enhance GECI sensitivity in order to resolve calcium fluctuations in the nanomolar range. This enabled researchers to measure cytoplasmic-calcium transients elicited by single-action potentials (Tang et al., 2011). Contrarily, the generation of probes with lower calcium affinities which are necessary for measurements of calcium in high-calcium organelles, such as the ER, has long been an orphaned field of research. However, with recent implications of organellar calcium in physiology and pathophysiology,

interest in low-affinity GECIs has revived and has yielded a number of valuable new tools, including CEPIA and GAP1 calcium indicators, which have both been validated for intra-ER free calcium measurements. (Rodriguez-Garcia et al., 2014; Suzuki et al., 2014). Using G-CEPIAer, it has been possible to visualise dendritic synaptic activity-evoked ER calcium dynamics in cerebellar slices (Okubo et al., 2015). erGAP1 also allowed ex-vivo measurements of ER Ca^{2+} release in acute hippocampal slices triggered by cholinergic receptors. Moreover, sarcoplasmic reticulum calcium oscillations could be recorded in transgenic flies (Navas-Navarro et al., 2016), which only represented the second report of imaging ER calcium dynamics in an in-vivo setting. Previously, the first report of in-vivo endoplasmic reticulum calcium imaging had visualised SR calcium decrease following muscle twitches in mice expressing the ER-targeted cameleon-family indicator D1ER (Rudolf, Magalhães & Pozzan, 2006).

Thus, there was only a limited literature foundation on in-vivo ER calcium imaging, which, moreover, had only been achieved previously in somatic ER. This complicated the choice of a suitable sensor for in-vivo intra-ER free calcium measurements in neuronal processes. At the beginning of this thesis, the concentration of ER calcium in the axonal endoplasmic reticulum could only be speculated on. Favourably, de Juan-Sanz et al. (2017) carried out the first solid calculations of intra-ER free calcium in primary dissociated hippocampal neurons, where a mean concentration of ~150 µM was determined for somata. Furthermore, they demonstrated that axonal ER calcium was not significantly different from somatic ER calcium, as expected from the assumption of ER continuity. The calculations were based on the measured fluorescence-intensity changes of several ER-GCaMP variants with different calcium affinities upon ionomycin-mediated saturation, assuming the pre-determined in-vitro characteristics of the sensors. Notably, neuronal ER calcium varied significantly between cells, reflecting different states of activity. Nevertheless, it remained unclear whether ER calcium in the neuronal population of interest (DRG neurons) in vivo is located in a similar range. According to Palmer et al. (2011), an ideal sensor's K_d-value should be located in the range of ± 5 times the resting concentration, which represents the steep part of the binding curve, in order to be capable of measuring small concentration changes. Given that Twitch2B 54S+ displays a K_d-value of 174.0 µM, it would meet this criterion, even in cases of ER calcium concentrations significantly higher than the ~150 µM assumed by Juan-Sanz

et al. (2017). However, this K_d-value was determined by calcium titrations of purified sensor protein in a cuvette using fluorescence spectrophotometry (Thestrup et al., 2014), which does not take into account influences of the in-vivo setting and the modifications added to the sensor for ER targeting. While the N-terminal signalling peptide is cleaved upon translocation to the ER, the C-terminal KDEL-peptide remains and can, in theory, alter the sensor's structure and calcium affinity. Also determined in the cuvette, Twitch2B 54S+ displays a dynamic range (ΔR/R) of 320% (Thestrup et al., 2014), which is larger than the dynamic range of the cytoplasmic calcium sensor CerTN-L15 (95%); previously, this was successfully employed for in-vivo calcium imaging of cytoplasmic calcium in EAE (Heim et al., 2007; Schumacher, 2015). The amount of putative ER calcium change was unknown, so that a high dynamic range would, in theory, allow researchers to resolve comparatively small relative differences. Further advantages, which led to the choice of Twitch 2B 54S+, include its characteristic of being a FRET-based ratiometric sensor, which can help cancel out movement artefacts in an in-vivo setting and enable one time-point imaging. In fact, it comprises two fluorescent proteins with a high quantum yield and high photostability, mCerulean3 and cpVenus^{CD}. Furthermore, the single functional EF-hand toadfish Troponin C-minimal domain linker leads to quasi-linear response kinetics over a large range in vitro (Thestrup et al., 2014) (see chapter 1.4.2).

Expressed in Hek-293 cells, Twitch 2B 54S+ ER responded to pharmacological depletion (administration of the SERCA-blocker thapsigargin) and replenishment (administration of ionomycin in a high calcium milieu) of the endoplasmic reticulum as expected. It displayed a dynamic range of ~300 %, similar to the dynamic range of 320%, determined in cuvette measurements for Twitch 2B 54S+ (Thestrup et al., 2014). This similarity of dynamic ranges indicates that the addition of the KDEL retention sequence did not lead to a marked alteration of the sensor's properties. Given that the N-terminal signalling peptide should be cleaved upon import to the endoplasmic reticulum, it can be assumed that this modification does not alter the sensor's properties.

Notably, signals obtained with FRET-based GECIs can be perturbed by a variety of environmental factors, which include temperature, pH, chloride and magnesium; these can affect either the fluorophores or the troponin-derived calcium-responsive element (Grienberger & Konnerth, 2012). Apart from temperature, which was tightly

regulated by a temperature-control system in case of the cell experiments, the other parameters were not directly accounted for. Regarding pH, mCerlulean3 has an acid-dissociation constant (pK_a) of 4.7 and mVenus has a pK_a-value of 6 (Bajar, Wang, Zhang, Lin & Chu, 2016), which is important to consider when imaging in acidic environments, such as the Golgi apparatus (Wu et al., 2000). De Juan-Sanz et al. (2017) measured ER pH changes in neuronal somata using ER-pHluorin in response to 500 µM ionomycin application and reported a pH increase from 7.25 to 7.68. Such an alkalinisation is unlikely to impact the fluorophores. Advances in FP development have reduced chloride and magnesium sensitivity (Griesbeck, Baird, Campbell, Zacharias & Tsien, 2001). However, the influence of chloride and magnesium concentration shifts on the Twitch2B 54S+ ER ratio cannot be ruled out completely. At least in the case of thapsigargin ER depletion, it is unlikely that the sensor's fluorophores were perturbed by other environmental influences, since the ratio of the mutated EF hand control sensor remained stable, which indicates that the observed drop in ratios is caused primarily by the calcium-sensitive domain (see chapter 4.1.2).

5.1.3 Remarks on the yielded transgenic lines

Several Thy1-TwitchER transgenic lines were yielded, of which Thy1-TwitchER 509, Thy1-TwitchER 489 and Thy1-TwitchER 481 were used in this thesis (see chapter 4.1.3). Thy1-TwitchER 481 mice were characterised by relatively bright sensor expressions in the superficial dorsal column. A rather small proportion of predominantly thick axons was labelled. In contrast, Thy1-TwitchER 509 displayed a larger proportion of labelled superficial dorsal column axons, which, however, required higher-laser intensities to generate sufficient emission light. Thy1-TwitchER 489 mice were selected primarily because of the full labelling pattern, which is useful for imaging NMJs in triangularis sterni explants and because of the sensor expression detected in Purkinje cells, which can be used for electrophysiological studies in cerebellar slices.

The sensor's brightness in axons was sufficient for in-vivo imaging of the spinal cord. As determined for the Thy1-TwitchER 509 line, signal-to-noise ratios of ~3 could be achieved for CFP, while signal-to-noise ratios of ~8 were obtained for YFP using optimised detection settings (GaAsP1 detector voltage of 640 V for CFP; GaAsP2 detector voltage of 500 V for YFP). For the cytoplasmic calcium GECI transgenic

line CerTN an optimum signal-to-noise ratio of ~4 for both CFP and YFP channel was previously reported and CerTN was successfully used for in-vivo imaging of the spinal cord (Schumacher, 2015). The relatively low baseline signal-to-noise ratios of the CFP channel can be explained by the quenching of the donor's fluorescence by FRET under high ER-calcium conditions. The low CFP signal-to noise ratio combined with intraER free calcium variations between different axons putatively account for the large spread of baseline ratios observed in the Thy1-TwitchER transgenic lines. Inter-neuronal ER calcium variations have previously been reported (de Juan-Sanz et al., 2017). Thus, ER calcium is not as tightly maintained at a fixed baseline level as cytoplasmic calcium, which displays minimal interaxonal spread (Schumacher, 2015). The larger interaxonal ER calcium spread precludes the detection of smaller ratio changes in population-based analyses. However, the tracking of relative intra-ER free calcium changes of single axons in response to the application of the SERCA inhibitor thapsigargin were solidly achieved. In addition to a decrease in ratios, a reduction of the interaxonal spread was observed, which points to an equilibration of ER calcium levels between individual axons (see chapter 4.1.3). This finding indicates that the sensor's properties are unlikely to be perturbed in single axons. Possible perturbations leading to an interaxonal ratio spread despite a maximum ER calcium depletion could have been sensor concentration-dependent FRET or depth-dependent attenuation of individual channels' signals.

An effective co-localisation of the Twitch 2B 54S+ sensor with the ER-resident chaperone GRP78/BiP was demonstrated using immunostainings of spinal neurons. However, immunostainings of dorsal column axons were not obtained, since 4% PFA perfusion fixation led to a fragmentation of axonal ER, potentially because of the short period of ischemia and ionic dyshomeostasis during the period of PBS flushing preceding PFA injection (see chapter 1.2.5). Moreover, the GRP78/BiP antibody used did not yield a sufficiently strong staining of dorsal column axons. The co-localisation of GRP78/BiP and the Twitch 2B 54S+ sensor in somata of DRG neurons could be successfully demonstrated using an adapted staining protocol with optimised antibody incubation times by subsequent work by my colleague Jonas Lehmitz (Witte et al., 2019). Considering that the Twitch 2B 54S+ ER sensor reports high calcium levels, which are unlikely to be reached in other cellular compartments than the ER, and that no significant cytoplasmic sensor fluorescence can be detected following ER fragmentation (a state in which the cytoplasm can be clearly

differentiated from vesicularised ER compartments), a high targeting efficiency of the sensor can be assumed.

To assess the novelty of the generated Thy1-TwitchER transgenic lines, it can be said that at that time, the only other reported transgenic mice expressing an ER calcium indicator were mice expressing the excitation ratiometric erGAP1 under the control of the ubiquitous promoter CAG-GS, which also showed neuronal expression (Rodriguez-Garcia et al., 2014). Obvious advantages of the Thy1-TwitchER lines are the emission ratiometric property of the Twitch 2B 54S+ sensor, which can be imaged with commonly available CFP/YFP FRET filter sets, the neuron-specific expression achieved by the Thy1-promoter and the superior brightness of the incorporated fluorophores, which enabled in-vivo imaging of ER calcium in axons for the first time.

5.2 Discussing the role of intra-ER free calcium in paradigms of axonal degeneration

In this thesis, several important new insights were gleaned on the behaviour of intra-ER free calcium levels in three different paradigms of axonal degeneration: ER calcium in neuroinflammatory EAE lesions only declined in late stages of FAD (making it an unlikely early effector), while ER calcium following LiSCI and spinal-cord contusions responded with an early and generalised decrease in conjunction with ER fragmentation. Remarkably, these phenomena were completely reversible in the spinal-cord contusion model. Different modes of axonal degeneration, e.g. toxic, ischemic, neuroinflammatory or mechanical insults, can bear striking resemblances in terms of executed molecular pathways. Dysfunctional axonal transport, mitochondrial disturbance and increased intra-axonal calcium are considered to be the key convergence points of all axonal degeneration programs (Coleman, 2005). The strikingly diverse behaviour of ER contrasts to the stereotypically observed increase of cytoplasmic calcium and adds a new component of diversity to the concepts of ‘commonality amid diversity’ (Coleman, 2005) for axon-degeneration mechanisms.

5.2.1 Identifying the source of detrimental calcium influx in EAE

Axon loss is a pathognomonic feature of MS and its animal model, EAE, and determines the extent of disability in patients. Hence, it is imperative to analyse the process of axonal degeneration and identify the molecular pathways involved. A multitude of pathological features are observable in EAE, which include mitochondrial dysfunction (decrease of the mitochondrial membrane potential and morphological alteration), axonal beading and impaired cytoskeletal and axonal transport function (Nikić et al., 2011; Sorbara, Misgeld & Kerschensteiner, 2012). However, in order to assess the therapeutic value of any of these changes, it is of paramount importance to determine the sequence of events – to reveal which event is simply an epiphenomenon of the initiated degeneration cascade and which event is truly causative. A newly discovered pathological feature that can already be detected in stage 0 axons, is a long-lasting cytoplasmic calcium increase. Retained high cytoplasmic calcium is predictive of FAD progression (Schumacher, 2015). In contrast, the reconstitution of normal cytoplasmic calcium levels favours a morphological recovery of axons. This was a particularly interesting finding, since it indicated that FAD was not a cul-de-sac but rather offers a time window for therapeutic intervention. Despite the lack of direct scientific evidence, it is tempting to consider this cytoplasmic calcium rise as a primary, upstream event in the degeneration cascade of EAE. In fact, axonal swellings could be explained by the calcium-dependent activation of calpains, which can degrade the cytoskeleton (George et al., 1995; Yang et al., 2013). Moreover, calcium accumulates in the mitochondrial matrix at high cytoplasmic calcium levels. Excessive mitochondrial calcium uptake can lead to mitochondrial dysfunction and the initiation of cell-death programs (e.g. via MPTP formation) (Pivovarova & Andrews, 2010). Consequently, the assumption of calcium as an early effector in the FAD cascade is plausible. Notably, cytoplasmic calcium elevations have also been found to be fate-determining following transection and contusion injuries (Adalbert et al., 2012; Vargas, Yamagishi, Tessier-Lavigne & Sagasti, 2015; Williams et al., 2014). Assessing whether ER calcium release contributes significantly to the cytoplasmic calcium elevations in EAE was one of the main objectives of this thesis. Next I will therefore discuss the contribution of different calcium sources to axon degeneration in neuroinflammatory lesions.

5.2.1.1 ER calcium release

By means of the newly developed ratiometric calcium reporter mouse line Thy1-TwitchER 481, ER calcium was accessible to direct measurement for the first time. The sensor expression was sufficient to image the limited ER volume in single axons in active EAE lesions. Measurements of $[Ca^{2+}]_{ER}$ in the different stages of FAD showed neither a significant difference between $[Ca^{2+}]_{ER}$ of healthy control axons and stage 0 axons, nor a significant difference between $[Ca^{2+}]_{ER}$ in stage 0 and stage 1 axons in EAE lesions. Only $[Ca^{2+}]_{ER}$ of irreversibly damaged stage 2 axons differed significantly from $[Ca^{2+}]_{ER}$ in stage 1 axons (see chapter 4.2.1). The latter finding served as an important internal control, since it could be expected that energetic failure upon complete axonal fragmentation would lead to a depletion of ER calcium due to a reduction of SERCA activity. Notably, not all stage 2 axons showed a clear decrease in $[Ca^{2+}]_{ER}$, which again could be explained by an equilibration of cytoplasmic calcium and, subsequently, ER calcium to extracellular calcium concentrations. Stage 2 axons have lost their structural continuity and are thus considered inaccessible to therapeutic interventions. The dataset depicted contains data from four Thy1-TwitchER 481 with induced EAE and six healthy Thy1-TwitchER 481 control mice. The EAE experiments were later repeated by Jonas Lehmitz and yielded a total of seven control and seven EAE mice; they reached the same conclusions as the dataset acquired for this thesis. An important addition acquired by the dataset of Jonas Lehmitz was the caffeine-induced depletion of $[Ca^{2+}]_{ER}$ at the end of each experiment. Caffeine depletion led to a robust decrease of ER calcium even below the arbitrary value of mean – 3 standard deviations in both EAE and control mice (the mean + 3 standard deviations was used for binary scoring for cytoplasmic calcium levels) (Witte et al., 2019). Likewise, in this thesis, thapsigargin application on EAE lesions decreased $[Ca^{2+}]_{ER}$ of one-third of axons below the value of the mean – 3 standard deviations after 50 minutes. The measurement of ER depletion indicates that the responsiveness of the sensor is maintained in EAE lesions. A drawback of the Thy1-TwitchER 481 transgenic line is that it preferentially labels larger-calibre axons compared to the Thy1-CerTN line used for cytoplasmic-calcium imaging. Since smaller axons are more prone to undergo FAD, it is harder to find degenerating axons than in the Thy1-CerTN line. Additionally, labelling is overall sparser than in Thy1-CerTN line.

It could be argued that the depletion of ER calcium could occur only temporarily and might not be as prolonged as the observed cytoplasmic-calcium elevations. Thus, a single time-point analysis might be insufficient to detect such temporarily restricted events. However, when Jonas Lehmitz analysed single axons over 15 min in 30 second intervals, no significant ER calcium fluctuations were observable in axons traversing EAE lesions. Another point to consider is that small $[Ca^{2+}]_{ER}$ changes would likely be overlooked in the population-based analysis approach used in this thesis, due to the relatively high interaxonal variation in $[Ca^{2+}]_{ER}$. Nevertheless, large $[Ca^{2+}]_{ER}$ variations in the dimension of caffeine or thapsigargin-mediated depletion were robustly detected in the population-based analysis approach and can be excluded for stage 0 and stage 1 axons in EAE lesions.

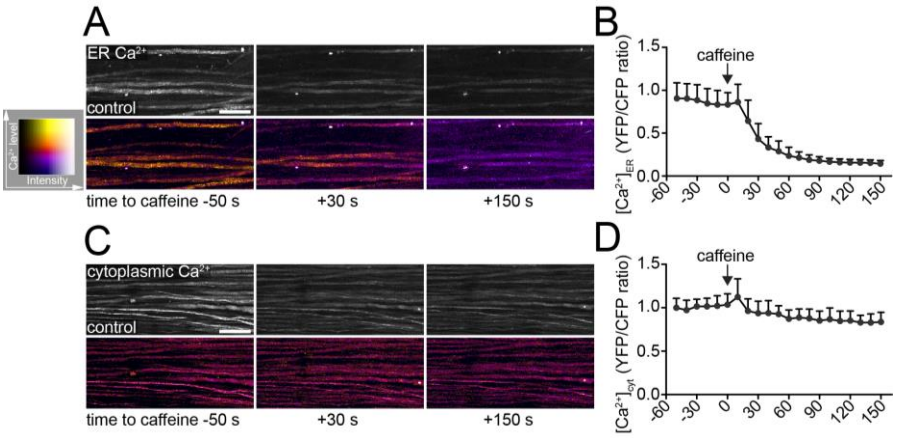

Figure 22: Caffeine effect on $[Ca^{2+}]_{ER}$ and $[Ca^{2+}]_{cyt}$

(**A, C**) Intensity projections of healthy spinal cord dorsal funiculi (YFP channel, top) and colour-coded calcium levels (YFP/CFP ratio, bottom) of $[Ca2+]_{ER}$ in (**A**), i.e. in Thy1-TwitchER mice and $[Ca2+]_{cyt}$ in (**C**), i.e. in Thy1-CerTN-L15 mice. Time-lapse images before and after application of 50 mM caffeine. (**B, D**) Graphs of respective experiments illustrated as mean ± SD (n=26 axons in B, 46 axons in D). Data normalised to mean values of initial measurements. Scale bars = 25 µm. Figure adapted from and caption modified from Witte et al. (2019). Experimenter: Jonas Lehmitz.

In addition to the absence of large $[Ca^{2+}]_{ER}$ transients, another line of argumentation can be pursued. Jonas Lehmitz determined whether $[Ca^{2+}]_{ER}$ release, when it occurs, measurably changes cytoplasmic-calcium levels. To this end, a substance was required that can rapidly deplete ER calcium in a spinal cord in in-vivo imaging setting (contrary to thapsigargin which needs ~1 hour for complete ER store depletion). Caffeine, a reported voltage-independent activator of all three RyR subtypes (Thomas & Williams, 2012), depleted $[Ca^{2+}]_{ER}$ to the lower measurement limit of

Twitch2B 54S+ ER within three minutes. In contrast, caffeine application on spinal cords of Thy1-CerTN cytoplasmic calcium reporter mice did not lead to a marked increase of cytoplasmic calcium (Witte et al., 2019) (Figure 22). Thus, even the rapid ER calcium depletion caused by caffeine is insufficient to increase cytoplasmic axonal calcium to an extent measurable with the CerTN calcium sensor. Albeit surprising, a recent report by de Juan-Sanz et al. (2017) has yielded very similar results in vitro. By using the cytoplasmic intensiometric indicator GCaMP6f with a K_d-value of 375 nM, these researchers were able to measure the calcium transients elicited by the application of the SERCA-inhibitor cyclopiazonic acid (CPA) in the dendrites of dissociated hippocampal neurons. The CPA-induced cytoplasmic calcium increase in dendrites corresponded to an elevation of 11.8 nM, which is similar to the cytoplasmic-calcium elevation measured for a single action potential (9.6 nM). In axons, no significant cytoplasmic-calcium increase following CPA treatment could be detected. Juan-Sanz et al. (2017) concluded that both dendritic and axonal ER occupy only a small volume percentage and thus – despite the high $[Ca^{2+}]_{ER}$ concentration of ~150 µm – store only small absolute amounts of calcium, while axonal ER had to be even sparser than dendritic ER. Although the in-vivo imaging approach in this thesis lacks the resolution to visualise the axonal ER network and determine its percentage of axonal volume, confocal imaging revealed a steep intensity gradient in the labelling of neuronal somatic ER and axonal ER. The lower-labelling intensity of axonal ER compared to the somato-dendritic department suggests a smaller volume fraction. Based on these results, a significant contribution of ER-derived calcium to the constant cytoplasmic calcium elevations in FAD can be ruled out.

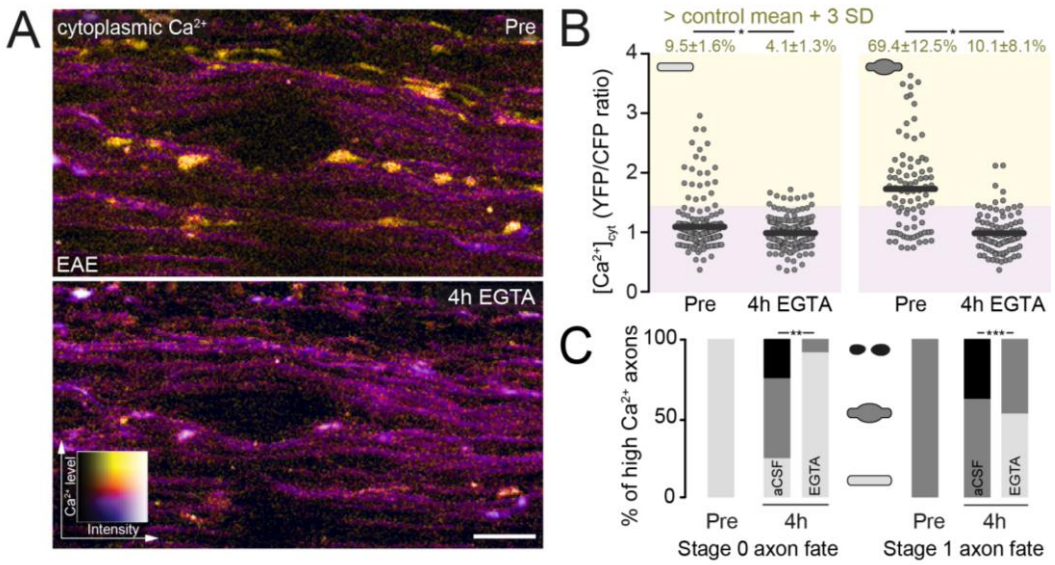

Figure 23: Removal of extracellular Ca^{2+} reverses cytoplasmic Ca^{2+} accumulation and prevents axon degeneration

(**A**) 2-photon in-vivo intensity projections of the spinal cord dorsal funiculus in an EAE mouse. The upper image displays colour-coded cytoplasmic calcium levels before, the lower image after 4 hours of EGTA calcium chelation. (**B**) Cytoplasmic calcium levels separately displayed for morphological stage 0 axons (left) and stage 1 axons (right) before and after chelation of extracellular calcium after 4 hours of EGTA incubation. The percentages of axons with cytoplasmic calcium ratios > 3 times the standard deviation of control mean (± SEM) is noted on top and the corresponding range is depicted in yellow. Statistical testing per animal in n=5 control and n=5 EAE mice, paired t-test. (**C**) Tracing the axonal fate of stage 0 axons (left) and stage 1 axons (right) with and without EGTA calcium chelation after 4 hours (chi-square test). Scale bar in A = 25 µm. *P < 0.05; **P < 0.01; ***P < 0.001. Figure adapted from and caption modified from Witte et al. (2019). Experimenter: Christoph Mahler

In addition, an essential experiment performed by my colleague Christoph Mahler clearly implicated extracellular calcium – which is around ten-thousand-fold higher than in the cytoplasm – as the predominant source for the cytoplasmic-calcium elevation in FAD. Superfusion of neuroinflammatory lesions with the calcium chelator EGTA was capable of reconstituting intraaxonal calcium level and prevented axonal degeneration (Figure 23). However, this experiment alone is insufficient to rule out an additional influence of $[Ca^{2+}]_{ER}$. For example, SOCE could result from a depletion of ER stores (Jun Wu et al., 2016), which would mitigate a calcium influx from the extracellular space. In this scenario $[Ca^{2+}]_{ER}$ depletion would be accentuated by a triggered extracellular calcium influx via ORAI channels. However, cytoplasmic-calcium measurements in Thy1-CerTN mice treated with the RyR agonist caffeine

showed no detectable late-phase cytoplasmic calcium increase, which could be attributed to SOCE.

5.2.1.2 Influx of extracellular calcium

While the results of this thesis rendered the ER an unlikely contributor to the observed elevations of cytoplasmic calcium, a pathway for the entry of calcium from the extracellular space could be established by parallel work in the Kerschensteiner laboratory. Various groups had proposed the reversal of Na^+/Ca^{2+} exchanger and calcium influx through plasma-membrane calcium channels and glutamate excitotoxicity as putative mechanisms for the increase of cytoplasmic calcium in axonal degeneration (Friese, Schattling & Fugger, 2014; Mahad, Trapp & Lassmann, 2015). However, parallel experiments performed by Christoph Mahler clearly indicated that the opening of glutamate receptors mediated by the agonist glutamic acid was insufficient to cause a distinct cytoplasmic-calcium increase in axons. Notably, however, a cytoplasmic-calcium increase could very well be elicited in neuronal somata, which served as an important internal positive control confirming a sufficient diffusion and concentration of glutamic acid. In addition, a protective effect of bepridil, an inhibitor of the Na^+/Ca^{2+} exchanger, on FAD progression was not observable (Witte et al., 2019).

After ruling out calcium release from internal stores and calcium influx via glutamate receptors or the Na^+/Ca^{2+} exchanger, the importance of nanoscale ruptures in the plasma membrane was evaluated. These ruptures had previously been described as source of increased detrimental cytoplasmic calcium in traumatic neuronal injuries, namely in a model of spinal-cord contusion (Williams et al., 2014). Experiments employing different macromolecules of different sizes with a fluorescent tag, which included 0.8 kD cadaverine or 3, 10 and 70 kD dextran, clearly demonstrated a permeability of a subset of axons (especially stage 1 and 2 axons, but also a significant proportion of normal-appearing axons) to these dyes in the EAE. Contrarily, healthy animals displayed persistent exclusion of the dye from the axoplasm. Importantly, dextrans of the size of 70 kD remained excluded from the axoplasm in EAE, suggesting a size of less than 10 nm of the assumed membrane pores. The dye-uptake correlated positively with calcium-uptake in an in-vivo experiment with subdurally fluorescently tagged cadaverine-injected EAE mice on a single axon level (Witte et al., 2019).

These results clearly suggest that membrane disruption constitutes a primary pathway of calcium entry into the axoplasm from the extracellular space. Evidently the question arises how these nanoruptures are formed and consequently resealed. One possibility is that they are mere 'mechanopores' as a result of axonal swelling and a disruption of the cytoskeleton. While a disruption of the membrane by sheer mechanical force seemed plausible in the spinal-cord contusion experiments performed by Williams et al. (2014), in the context of EAE, the fact that the axonal swellings often occur after an initial increase of cytoplasmic calcium content precludes this interpretation. Thus, another scenario of a possible disruption of the plasma membrane by toxic mediators should be discussed. Candidates for toxic mediators are reactive oxygen species, which can result in lipid peroxidation (Di Domenico, Tramutola & Butterfield, 2017). Further possibilities are secreted phospholipases and damage that could be directly inflicted by immune cells. Finally, the immune system could directly harm the membrane by means of the membrane attack complex or perforin (Witte et al., 2019). Apparently when the plasma membrane is disrupted, internal lipid bilayers, such as the ER membrane, are also at risk. However, ER fragmentation was observable neither in stage 0 nor 1 axons. Only Stage 2 axons regularly showed signs of a disrupted ER network. This finding should be interpreted with caution, since there could still be architectural ER alterations at the sub-microscopic level. Still, even if internal lipid bilayers were also affected, the amount of calcium sequestered in the ER would still not be capable of inducing the rise of cytoplasmic calcium observed in EAE as it was delineated above.

5.2.2 Analysing the depletion ER calcium in traumatic axonal injury

This thesis first described the occurrence of ER fragmentation in axons following traumatic mechanical injury. Previously, ER fragmentation in an in-vivo setting had only been observed in dendrites in response to cardiac arrest and ischemia (Kucharz et al., 2011b). Kurcharz et al. (2011b) have already described the reversible nature of the process of ER fragmentation, a finding which could also be reproduced for acute traumatic injury to ER of the spinal cord, albeit in only one exemplary experiment, which had, for reasons of temporal constraints, not been further pursued by me. However, repetition of the proposed longitudinal experiment by Jonas Lehmitz in a total of five mice over a time course of 125 min post-contusion clearly demonstrated the reversibility of ER fragmentation following contusion injury (Figure

24). Here, the initial evaluation of microscopically visible fragmentation revealed ER fragmentation rates of ~80–90% immediately post-contusion, which gradually dropped to an ER fragmentation rate of ~60–70% after two hours of recovery. Tracing single axons visually, over time, confirmed the occurrence of ER fragmentation recovery. The drop of ER calcium – ensuing spinal-cord contusion that could be established in this thesis – was again observed by Jonas Lehmitz. Importantly, like ER fragmentation, ER calcium recovered over the course of time. The drop of ER calcium was ubiquitous and independent of the ER fragmentation state. The homogeneity of the ER calcium depletion and fragmentation following a defined contusion injury indicates that these processes do not constitute a fate-determining axonal alteration, unlike the individual axonal cytoplasmic calcium increase observed by Williams et al. (2014). However, neither by laser transection nor by contusion experiments could a threshold be reached, which would only lead to a decrease of ER calcium in only a subset of axons (while ER fragmentation was observed in the vast majority of axons and also only spared a few axons). Thus, a fate-tracing approach, as it had been applied by Williams et al. (2014), was neither feasible nor reasonable, since in order to elicit a sufficient ratio of degenerating axons, a sufficient force needs to be applied. One candidate for a fate-tracing experiment would, however, be a secondary depletion of ER calcium after initial recovery, which had only been observed in a small subset of axons (see chapter 4.2.2). Even if these events could be reproduced in a greater number, the question would still remain as to whether the second drop of ER calcium observed constitutes an important step of the degeneration cascade or a mere epiphenomenon of axonal demise and energy failure. The latter can be deemed more likely, since the secondary drop of ER calcium has only been observed very late (after 120 minutes), while the cytoplasmic-calcium increase happens almost instantaneously following axonal injury. Even if ER calcium release and ER fragmentation cannot be attributed to have a prominent role in the axonal degeneration cascade, the temporal variability observed can act as an important positive control to the TwitchER mouse line generated, since it can rule out that the observed changes of sensor ratios are merely artefactual – for example, due to the photo bleaching of one preferential FP or occlusion of only a portion of the signal by bleeding at the contusion site. Thus, the changes observed in ratio are most likely genuine, with the restrictions of genetically encoded calcium sensors discussed in chapter 4.1.2 applying.

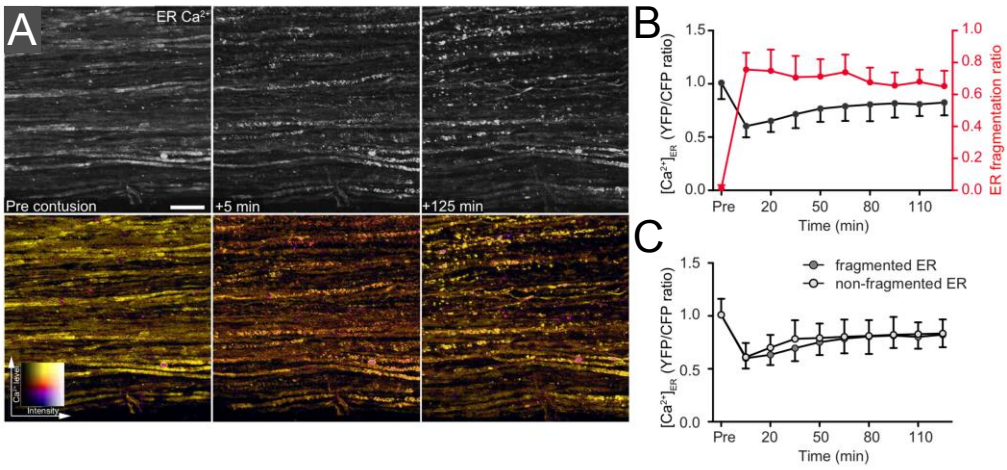

Figure 24: ER calcium and fragmentation rate following spinal cord contusion

(**A**) 2-photon in-vivo intensity projections (top: YFP channel, bottom: colour-coded YFP/CFP ratio) of the dorsal spinal funiculus of Thy1-TwitchER 481 mice before (left) and sequentially after (middle and right) contusion injury. (**B**) Graph displays the ER calcium levels before (Pre) and sequentially after contusion in black (mean minus standard deviation) and the corresponding ER fragmentation rate in red (mean plus standard deviation). Images acquired in 15 minutes intervals in n=5 mice. (**C**) Respective YFP/CFP ratios separately displayed for axons with and without overt ER fragmentation. Dark grey as mean plus and light grey as mean minus standard deviation. Scale bar in A = 25 µm. Figure adapted from and caption modified from Witte et al. (2019). Experimenter: Jonas Lehmitz.

5.3 Concluding remarks and outlook

This thesis has yielded a novel transgenic mouse line, which allowed for the measurement of intra-ER free calcium in vivo for the first time. This was achieved by targeting the expression of the genetically encoded ratiometric low-affinity calcium indicator Twitch2B 54 S+ to the neuronal endoplasmic reticulum. While G-CEPIA1ER has been successfully employed to measure ER calcium in murine slice cultures (Okubo et al., 2015), the intesiometric property of this sensor precluded its application for the 2-photon spinal cord in-vivo imaging technique (Misgeld, Nikic & Kerschensteiner, 2007). By means of this novel transgenic mouseline, large calcium transients elicited by the SERCA inhibitor thapsigargin could be potently and reliably visualised in an in-vivo imaging setting. Changes of a similar extent were undetectable in a population-based analysis in EAE, which demonstrated that ER calcium

dysregulation does not contribute to the process of focal axonal degeneration. However, in the paradigms of laser transection and spinal-cord contusion injury, a global axonal response of ER calcium release, in conjunction with the process of ER fragmentation in a large subset of axons, was observed. In the context of spinal-cord contusion, both ER fragmentation and ER calcium release were partially reversible over a time course of two hours (as it was later confirmed by my colleague Jonas Lehmitz). ER fragmentation following mechanical injury was a completely novel finding. Furthermore, calcium imaging of the process of ER fragmentation had not been achieved before. It appears that ER calcium depletion often concurs with ER fragmentation; however, fragmented ER can also retain high calcium levels. Initial ER fragmentation and ER calcium depletion are not fate-determining factors in axonal degeneration, since they occur in the majority of axons in the paradigm of spinal-cord contusion, of which only a small proportion are subject to later demise. Thus, changes of ER continuity and ER calcium content can be ruled out as main effectors of axonal degeneration in EAE, as well as traumatic axonal injury. Nonetheless, these dynamic changes of an organelle pose a to date largely unknown cellular response mechanism that warrants further examination. Given the importance of the endoplasmic reticulum concerning ion homeostasis, cellular-stress responses and protein trafficking (Verkhratsky, 2005), a continuous or long-lasting disintegration of its structure might severely impair cellular function. Thus, an approach to monitor the differential capacity of single neurites to re-establish ER continuity over a time course of two hours or longer paired with a survival analysis appears promising. If ER fragmentation and subsequent ER fusion could be established as a fate-determining factor in long-term axonal survival, the recent work of Kucharz et al. (2018) could be of great interest. Kucharz et al. (2018) managed to shed light on the molecular mechanisms of ER fragmentation and fusion. Not only did they demonstrate that ER fission can be caused in vivo in the paradigm of cortical spreading depolarisation, but they also found that physiological stimuli, such as whisker stimulation, can evoke ER fission detectable by fluorescence recovery after photobleaching. ER fission coincided with a loss of synaptic activity and could be inhibited by pharmacological inhibition of N-methyl-D-aspartate receptors and by inhibition of the downstream effector of Ca2 + /calmodulin-dependent protein kinase II. ER fusion was, in turn, impaired by dynamin GTPases inhibition.

With emergent molecular insights into the process of ER fragmentation and fusion and the tools developed in this thesis for imaging ER structural and functional dynamics, exciting new avenues are opened for future research regarding the axoplasmic reticulum and its role in neurodegeneration.

6 References

Abdul-Majid, K. B., Jirholt, J., Stadelmann, C., Stefferl, A., Kjellen, P., Wallstrom, E., … Harris, R. A. (2000). Screening of several H-2 congenic mouse strains identified H-2(q) mice as highly susceptible to MOG-induced EAE with minimal adjuvant requirement. *Journal of Neuroimmunology*, *111*(1–2), 23–33.

Adalbert, R., Morreale, G., Paizs, M., Conforti, L., Walker, S. A., Roderick, H. L., … Coleman, M. P. (2012). Intra-axonal calcium changes after axotomy in wild-type and slow Wallerian degeneration axons. *Neuroscience*, *225*, 44–54. https://doi.org/10.1016/j.neuroscience.2012.08.056

Akerboom, J., Carreras Calderon, N., Tian, L., Wabnig, S., Prigge, M., Tolo, J., … Looger, L. L. (2013). Genetically encoded calcium indicators for multi-color neural activity imaging and combination with optogenetics. *Frontiers in Molecular Neuroscience*, *6*, 2. https://doi.org/10.3389/fnmol.2013.00002

Alberts B, Johnson A, L. J. (2002). *Molecular Biology of the Cell. 4th edition*. ew York: Garland Science.

Bajar, B. T., Wang, E. S., Zhang, S., Lin, M. Z. & Chu, J. (2016). A guide to fluorescent protein FRET pairs. *Sensors (Switzerland)*, *16*(9), 1–24. https://doi.org/10.3390/s16091488

Barrientos, S. A., Martinez, N. W., Yoo, S., Jara, J. S., Zamorano, S., Hetz, C., … Court, F. A. (2011). Axonal Degeneration Is Mediated by the Mitochondrial Permeability Transition Pore. *Journal of Neuroscience*, *31*(3), 966–978. https://doi.org/10.1523/JNEUROSCI.4065-10.2011

Berridge, M. J. (2002). The endoplasmic reticulum : a multifunctional signaling organelle, *32*, 235–249. https://doi.org/10.1016/S0143-4160(02)00182-3

Berridge, M. J. (2016). The Inositol Trisphosphate/Calcium Signaling Pathway in Health and Disease. *Physiological Reviews*, *96*(4), 1261–1296. https://doi.org/10.1152/physrev.00006.2016

Bewersdorf, J. (2017). In vivo Mechanismen des axonalen Kalziumeinstroms im Tiermodell der Multiplen Sklerose.

Bitsch, A., Schuchardt, J., Bunkowski, S., Kuhlmann, T. & Bruck, W. (2000). Acute axonal injury in multiple sclerosis. Correlation with demyelination and inflammation. *Brain : A Journal of Neurology*, *123 (Pt 6*, 1174–1183.

Booth, D. M., Enyedi, B., Geiszt, M., Várnai, P. & Hajnóczky, G. (2016). Redox Nanodomains Are Induced by and Control Calcium Signaling at the ER-Mitochondrial Interface. *Molecular Cell*, *63*(2), 240–248. https://doi.org/10.1016/j.molcel.2016.05.040

Brandman, O., Liou, J., Park, W. S. & Meyer, T. (2007). STIM2 is a Feedback Regulator that Stabilizes Basal Cytosolic and Endoplasmic Reticulum Ca(2+) Levels. *Cell*, *131*(7), 1327–1339. https://doi.org/10.1016/j.cell.2007.11.039

Breckwoldt, M. (2014). Imaging of mitochondrial redox signals in neuronal physiology and pathology, 1–113.

Breckwoldt, M. O., Franz, M. J. P., Bradley, P. M., Marinkovi, P., Williams, P. R., Brill, M. S., … Misgeld, T. (2014). Multiparametric optical analysis of

mitochondrial redox signals during neuronal physiology and pathology in vivo. *Nat Med*, *20*(5), 555–560. https://doi.org/10.1038/nm.3520

Cabral-Miranda, F. & Hetz, C. (2017). ER stress in neurodegenerative disease: from disease mechanisms to therapeutic interventions. *Endoplasmic Reticulum Stress in Diseases*, *4*(1), 11–26. https://doi.org/10.1515/ersc-2017-0002

Caroni, P. (1997). Overexpression of growth-associated proteins in the neurons of adult transgenic mice. *J Neurosci Methods*, *71*(1), 3–9. Retrieved from http://www.ncbi.nlm.nih.gov/pubmed/9125370

Carreras-Sureda, A., Pihán, P. & Hetz, C. (2017). Calcium signaling at the endoplasmic reticulum: Fine-tuning stress responses. *Cell Calcium*, *70*(April 2017), 24–31. https://doi.org/10.1016/j.ceca.2017.08.004

Ching- Yuen, L. J. (1963). Electron microscopy of Wallerian degeneration. *Journal of Comparative Neurology*, *120*(1), 65–79. https://doi.org/10.1002/cne.901200107

Christman, C. W., Grady, M. S., Walker, S. A., Holloway, K. L. & Povlishock, J. T. (1994). Ultrastructural Studies of Diffuse Axonal Injury in Humans. *Journal of Neurotrauma*, *11*(2), 173–186. https://doi.org/10.1089/neu.1994.11.173

Coleman, M. (2005). Axon degeneration mechanisms: commonality amid diversity. *Nature Reviews. Neuroscience*, *6*(11), 889–898. https://doi.org/10.1038/nrn1788

Compston, A. & Coles, A. (2008). Multiple sclerosis. *Lancet (London, England)*, *372*(9648), 1502–1517. https://doi.org/10.1016/S0140-6736(08)61620-7

Conforti, L., Gilley, J. & Coleman, M. P. (2014). Wallerian degeneration : an emerging axon death pathway linking injury and disease. *Nature Publishing Group*, *15*(6), 394–409. https://doi.org/10.1038/nrn3680

de Brito, O. M. & Scorrano, L. (2008). Mitofusin 2 tethers endoplasmic reticulum to mitochondria. *Nature*, *456*, 605. Retrieved from http://dx.doi.org/10.1038/nature07534

de Juan-Sanz, J., Holt, G. T., Schreiter, E. R., de Juan, F., Kim, D. S. & Ryan, T. A. (2017). Axonal Endoplasmic Reticulum Ca2+Content Controls Release Probability in CNS Nerve Terminals. *Neuron*, *93*(4), 867–881.e6. https://doi.org/10.1016/j.neuron.2017.01.010

DeLuca, G. C., Ebers, G. C. & Esiri, M. M. (2004). Axonal loss in multiple sclerosis: a pathological survey of the corticospinal and sensory tracts. *Brain : A Journal of Neurology*, *127*(Pt 5), 1009–1018. https://doi.org/10.1093/brain/awh118

Di Domenico, F., Tramutola, A. & Butterfield, D. A. (2017). Role of 4-hydroxy-2-nonenal (HNE) in the pathogenesis of alzheimer disease and other selected age-related neurodegenerative disorders. *Free Radical Biology and Medicine*, *111*, 253–261. https://doi.org/10.1016/J.FREERADBIOMED.2016.10.490

Dotson, D. G. & Putkey, J. A. (1993). Differential recovery of Ca2+ binding activity in mutated EF-hands of cardiac troponin C. *The Journal of Biological Chemistry*, *268*(32), 24067–24073.

Dziedzic, T., Metz, I., Dallenga, T., König, F. B., Müller, S., Stadelmann, C. & Brück, W. (2010). Wallerian degeneration: A major component of early axonal pathology in multiple sclerosis. *Brain Pathology*, *20*(5), 976–985.

https://doi.org/10.1111/j.1750-3639.2010.00401.x

Eddleman, C. S., Ballinger, M. L., Smyers, M. E., Fishman, H. M. & Bittner, G. D. (1998). Endocytotic formation of vesicles and other membranous structures induced by Ca2+ and axolemmal injury. *The Journal of Neuroscience : The Official Journal of the Society for Neuroscience*, *18*(11), 4029–4041.

Edelstein, A. D., Tsuchida, M. A., Amodaj, N., Pinkard, H., Vale, R. D. & Stuurman, N. (2014). Advanced methods of microscope control using μManager software. *Journal of Biological Methods; Vol 1, No 2 (2014)*. Retrieved from http://www.jbmethods.org/jbm/article/view/36/29

Ehrenberg, M. (2008). *Scientific Background on the Nobel Prize in Chemistry 2008: The green fluorescent protein: discovery, expression and development*. Retrieved from https://www.nobelprize.org/nobel_prizes/chemistry/laureates/2008/advanced-chemistryprize2008.pdf

English, A. R. & Voeltz, G. K. (2013a). Endoplasmic reticulum structure and interconnections with other organelles. *Cold Spring Harbor Perspectives in Biology*, *5*(4), 1–16. https://doi.org/10.1101/cshperspect.a013227

English, A. R. & Voeltz, G. K. (2013b). Rab10 GTPase regulates ER dynamics and morphology. *Nature Cell Biology*, *15*(2), 169–178. https://doi.org/10.1038/ncb2647

Feng, G., Mellor, R. H., Bernstein, M., Keller-peck, C., Nguyen, Q. T., Wallace, M., … Sanes, J. R. (2000). Imaging neuronal subsets in transgenic mice expressing multiple spectral variants of GFP. *Neuron*, *28*(1), 41–51. Retrieved from http://www.ncbi.nlm.nih.gov/pubmed/11086982

Friese, M. A., Schattling, B. & Fugger, L. (2014). Mechanisms of neurodegeneration and axonal dysfunction in multiple sclerosis. *Nature Reviews Neurology*, *10*, 225. Retrieved from https://doi.org/10.1038/nrneurol.2014.37

Furuichi, T., Simon-Chazottes, D., Fujino, I., Yamada, N., Hasegawa, M., Miyawaki, A., … Mikoshiba, K. (1993). Widespread expression of inositol 1,4,5-trisphosphate receptor type 1 gene (Insp3r1) in the mouse central nervous system. *Receptors & Channels*, *1*(1), 11–24.

George, E. B., Glass, J. D. & Griffin, J. W. (1995). Axotomy-induced axonal degeneration is mediated by calcium influx through ion-specific channels. *The Journal of Neuroscience*, *15*(10), 6445 LP-6452. Retrieved from http://www.jneurosci.org/content/15/10/6445.abstract

Gerasimenko, J. V., Petersen, O. H. & Gerasimenko, O. V. (2014). Monitoring of intra-ER free Ca 2+. *Wiley Interdisciplinary Reviews: Membrane Transport and Signaling*, *3*(3), 63–71. https://doi.org/10.1002/wmts.106

Gerdts, J., Brace, E. J., Sasaki, Y., DiAntonio, A. & Milbrandt, J. (2015). SARM1 activation triggers axon degeneration locally via NAD+ destruction. *Science*, *348*(6233), 453 LP-457. Retrieved from http://science.sciencemag.org/content/348/6233/453.abstract

Gerdts, J., Summers, D. W., Milbrandt, J. & DiAntonio, A. (2016). Axon Self-Destruction: New Links among SARM1, MAPKs, and NAD+ Metabolism. *Neuron*, *89*(3), 449–460. https://doi.org/10.1016/j.neuron.2015.12.023

Gerdts, J., Summers, D. W., Sasaki, Y., DiAntonio, A. & Milbrandt, J. (2013).

Sarm1-Mediated Axon Degeneration Requires Both SAM and TIR Interactions. *The Journal of Neuroscience*, *33*(33), 13569 LP-13580. Retrieved from http://www.jneurosci.org/content/33/33/13569.abstract

Gilley, J. & Coleman, M. P. (2010). Endogenous Nmnat2 Is an Essential Survival Factor for Maintenance of Healthy Axons. *PLOS Biology*, *8*(1), e1000300. Retrieved from https://doi.org/10.1371/journal.pbio.1000300

Glass, J. D., Schryer, B. L. & Griffin, J. W. (1994). Calcium- Mediated Degeneration of the Axonal Cytoskeleton in the Ola Mouse. *Journal of Neurochemistry*, *62*(6), 2472–2475. https://doi.org/doi:10.1046/j.1471-4159.1994.62062472.x

Grienberger, C. & Konnerth, A. (2012). Imaging Calcium in Neurons. *Neuron*, *73*(5), 862–885. https://doi.org/10.1016/j.neuron.2012.02.011

Griesbeck, O., Baird, G. S., Campbell, R. E., Zacharias, D. A. & Tsien, R. Y. (2001). Reducing the environmental sensitivity of yellow fluorescent protein. Mechanism and applications. *J Biol Chem*, *276*(31), 29188–29194. https://doi.org/10.1074/jbc.M102815200

Griesbeck, O., Baird, G. S., Campbell, R. E., Zacharias, D. A. & Tsien, R. Y. (2001). Reducing the Environmental Sensitivity of Yellow Fluorescent Protein, *276*(31), 29188–29194. https://doi.org/10.1074/jbc.M102815200

Haines, J. D., Inglese, M. & Casaccia, P. (2011). Axonal Damage in Multiple Sclerosis. *The Mount Sinai Journal of Medicine, New York*, *78*(2), 231–243. https://doi.org/10.1002/msj.20246

Hayashi, A., Kasahara, T., Iwamoto, K., Ishiwata, M., Kametani, M., Kakiuchi, C., … Kato, T. (2007). The role of brain-derived neurotrophic factor (BDNF)-induced XBP1 splicing during brain development. *The Journal of Biological Chemistry*, *282*(47), 34525–34534. https://doi.org/10.1074/jbc.M704300200

Heim, N., Garaschuk, O., Friedrich, M. W., Mank, M., Milos, R. I., Kovalchuk, Y., … Griesbeck, O. (2007). Improved calcium imaging in transgenic mice expressing a troponin C-based biosensor. *Nature Methods*, *4*(2), 127–129. https://doi.org/10.1038/nmeth1009

Hemmer, B., Kerschensteiner, M. & Korn, T. (2015). Role of the innate and adaptive immune responses in the course of multiple sclerosis. *The Lancet. Neurology*, *14*(4), 406–419. https://doi.org/10.1016/S1474-4422(14)70305-9

Henderson, M. J., Baldwin, H. A., Werley, C. A., Boccardo, S., Whitaker, L. R., Yan, X., … Harvey, B. K. (2015). A low affinity GCaMP3 variant (GCaMPer) for imaging the endoplasmic reticulum calcium store. *PLoS ONE*, *10*(10), 1–17. https://doi.org/10.1371/journal.pone.0139273

Hetz, C., Chevet, E. & Harding, H. P. (2013). Targeting the unfolded protein response in disease. *Nature Reviews Drug Discovery*, *12*(9), 703–719. https://doi.org/10.1038/nrd3976

Hetz, C., Chevet, E. & Oakes, S. A. (2015). Proteostasis control by the unfolded protein response. *Nature Cell Biology*, *17*(7), 829–838. https://doi.org/10.1038/ncb3184

Hetz, C. & Mollereau, B. (2014). Disturbance of endoplasmic reticulum proteostasis in neurodegenerative diseases. *Nature Reviews Neuroscience*, *15*(4), 233–249. https://doi.org/10.1038/nrn3689

Higo, T., Hamada, K., Hisatsune, C., Nukina, N., Hashikawa, T., Hattori, M., …

Mikoshiba, K. (2010). Mechanism of ER Stress-Induced Brain Damage by IP3 Receptor. *Neuron*, *68*(5), 865–878. https://doi.org/10.1016/j.neuron.2010.11.010

Hill, C. S., Coleman, M. P. & Menon, D. K. (2016). Traumatic Axonal Injury: Mechanisms and Translational Opportunities. *Trends in Neurosciences*, *39*(5), 311–324. https://doi.org/10.1016/j.tins.2016.03.002

Hoopfer, E. D., McLaughlin, T., Watts, R. J., Schuldiner, O., O'Leary, D. D. M. & Luo, L. (2006). Wld^{s} Protection Distinguishes Axon Degeneration following Injury from Naturally Occurring Developmental Pruning. *Neuron*, *50*(6), 883–895. https://doi.org/10.1016/j.neuron.2006.05.013

Hu, J., Shibata, Y., Zhu, P.-P., Voss, C., Rismanchi, N., Prinz, W. A., … Blackstone, C. (2009). A Class of Dynamin-like GTPases Involved in the Generation of the Tubular ER Network. *Cell*, *138*(3), 549–561. https://doi.org/10.1016/j.cell.2009.05.025

Ingraham, H. A., Lawless, G. M. & Evans, G. A. (1986). The mouse Thy-1.2 glycoprotein gene: complete sequence and identification of an unusual promoter. *Journal of Immunology (Baltimore, Md. : 1950)*, *136*(4), 1482–1489.

John, L. M., Lechleiter, J. D. & Camacho, P. (1998). Differential modulation of SERCA2 isoforms by calreticulin. *Journal of Cell Biology*, *142*(4), 963–973. https://doi.org/10.1083/jcb.142.4.963

Johnson, V. E., Stewart, J. E., Begbie, F. D., Trojanowski, J. Q., Smith, D. H. & Stewart, W. (2013). Inflammation and white matter degeneration persist for years after a single traumatic brain injury. *Brain*, *136*(1), 28–42. Retrieved from http://dx.doi.org/10.1093/brain/aws322

Johnson, V. E., Stewart, W. & Smith, D. H. (2013). Axonal pathology in traumatic brain injury. *Experimental Neurology*, *246*, 35–43. https://doi.org/10.1016/j.expneurol.2012.01.013

Kaneko, S., Wang, J., Kaneko, M., Yiu, G., Hurrell, J. M., Chitnis, T., … He, Z. (2006). Protecting axonal degeneration by increasing nicotinamide adenine dinucleotide levels in experimental autoimmune encephalomyelitis models. *The Journal of Neuroscience : The Official Journal of the Society for Neuroscience*, *26*(38), 9794–9804. https://doi.org/10.1523/JNEUROSCI.2116-06.2006

Kapoor, R., Davies, M., Blaker, P. A., Hall, S. M. & Smith, K. J. (2003). Blockers of sodium and calcium entry protect axons from nitric oxide-mediated degeneration. *Annals of Neurology*, *53*(2), 174–180. https://doi.org/10.1002/ana.10443

Kerschensteiner, M., Reuter, M. S., Lichtman, J. W. & Misgeld, T. (2008). Ex vivo imaging of motor axon dynamics in murine triangularis sterni explants. *Nat. Protocols*, *3*(10), 1645–1653. https://doi.org/10.1038/nprot.2008.160

Kerschensteiner, M., Schwab, M. E., Lichtman, J. W. & Misgeld, T. (2005). In vivo imaging of axonal degeneration and regeneration in the injured spinal cord. *Nat Med*, *11*(5), 572–577. https://doi.org/10.1038/nm1229

Khurana, I. (2006). *Characteristics of muscle excitability and contractility* (1st edition). Elsevier.

Kimata, Y. & Kohno, K. (2011). Endoplasmic reticulum stress-sensing mechanisms in yeast and mammalian cells. *Current Opinion in Cell Biology*,

23(2), 135–142. https://doi.org/https://doi.org/10.1016/j.ceb.2010.10.008

Kimball, S. R. & Jefferson, L. S. (1992). Regulation of protein synthesis by modulation of intracellular calcium in rat liver. *The American Journal of Physiology*, *263*(5 Pt 1), E958-64. https://doi.org/10.1152/ajpendo.1992.263.5.E958

Kleele, T., Marinkovic, P., Williams, P. R., Stern, S., Weigand, E. E., Engerer, P., … Misgeld, T. (2014). An assay to image neuronal microtubule dynamics in mice. *Nat Commun*, *5*, 4827. https://doi.org/10.1038/ncomms5827

Kucharz, K., Krogh, M., Ng, A. N. & Toresson, H. (2009). NMDA receptor stimulation induces reversible fission of the neuronal endoplasmic reticulum. *PLoS One*, *4*(4), e5250. https://doi.org/10.1371/journal.pone.0005250

Kucharz, K. & Lauritzen, M. (2018). CaMKII-dependent endoplasmic reticulum fission by whisker stimulation and during cortical spreading depolarization. *Brain*, *141*(4), 1049–1062. https://doi.org/10.1093/brain/awy036

Kucharz, K., Wieloch, T. & Toresson, H. (2011a). Potassium-induced structural changes of the endoplasmic reticulum in pyramidal neurons in murine organotypic hippocampal slices. *J Neurosci Res*, *89*(8), 1150–1159. https://doi.org/10.1002/jnr.22646

Kucharz, K., Wieloch, T. & Toresson, H. (2011b). Rapid Fragmentation of the Endoplasmic Reticulum in Cortical Neurons of the Mouse Brain *in situ* Following Cardiac Arrest. *Journal of Cerebral Blood Flow & Metabolism*, *31*(8), 1663–1667. https://doi.org/10.1038/jcbfm.2011.37

Kucharz, K., Wieloch, T. & Toresson, H. (2013). Fission and Fusion of the Neuronal Endoplasmic Reticulum. *Translational Stroke Research*, *4*(6), 652–662. https://doi.org/10.1007/s12975-013-0279-9

Kuhlmann, T., Lingfeld, G., Bitsch, A., Schuchardt, J. & Bruck, W. (2002). Acute axonal damage in multiple sclerosis is most extensive in early disease stages and decreases over time. *Brain : A Journal of Neurology*, *125*(Pt 10), 2202–2212.

Kühnel, W. (2003). *Color Atlas of Cytology, Histology, and Microscopic Anatomy*.

Lahiri, S., Toulmay, A. & Prinz, W. A. (2015). Membrane contact sites, gateways for lipid homeostasis. *Current Opinion in Cell Biology*, *33*, 82–87. https://doi.org/10.1016/j.ceb.2014.12.004

Lassmann, H. (2013). Pathology and disease mechanisms in different stages of multiple sclerosis. *Journal of the Neurological Sciences*, *333*(1–2), 1–4. https://doi.org/10.1016/j.jns.2013.05.010

Lee, J. Y., Taghian, K. & Petratos, S. (2014). Axonal degeneration in multiple sclerosis: Can we predict and prevent permanent disability? *Acta Neuropathologica Communications*, *2*(1), 1–16. https://doi.org/10.1186/s40478-014-0097-7

Li, F., Hayashi, T., Jin, G., Deguchi, K., Nagotani, S., Nagano, I., … Abe, K. (2005). The protective effect of dantrolene on ischemic neuronal cell death is associated with reduced expression of endoplasmic reticulum stress markers. *Brain Research*, *1048*(1–2), 59–68. https://doi.org/10.1016/j.brainres.2005.04.058

Li, S. & Stys, P. K. (2000). Mechanisms of ionotropic glutamate receptor-mediated excitotoxicity in isolated spinal cord white matter. *The Journal of*

Neuroscience : The Official Journal of the Society for Neuroscience, *20*(3), 1190–1198.

Li, S., Yang, L., Selzer, M. E. & Hu, Y. (2013). Neuronal endoplasmic reticulum stress in axon injury and neurodegeneration. *Ann Neurol*, *74*(6), 768–777. https://doi.org/10.1002/ana.24005

Lichtman, J. W. & Fraser, S. E. (2001). The neuronal naturalist: watching neurons in their native habitat. *Nature Neuroscience*, *4*, 1215. Retrieved from http://dx.doi.org/10.1038/nn754

Lomax, R. B., Camello, C., Van Coppenolle, F., Petersen, O. H. & Tepikin, A. V. (2002). Basal and physiological Ca2+ leak from the endoplasmic reticulum of pancreatic acinar cells. Second messenger-activated channels and translocons. *Journal of Biological Chemistry*, *277*(29), 26479–26485. https://doi.org/10.1074/jbc.M201845200

Lunn, E. R., Perry, V. H., Brown, M. C., Rosen, H. & Gordon, S. (1989). Absence of Wallerian Degeneration does not Hinder Regeneration in Peripheral Nerve. *European Journal of Neuroscience*, *1*(1), 27–33. https://doi.org/10.1111/j.1460-9568.1989.tb00771.x

Luo, L. & O'Leary, D. D. M. (2005). Axon retraction and degeneration in development and disease. *Annual Review of Neuroscience*, *28*, 127–156. https://doi.org/10.1146/annurev.neuro.28.061604.135632

Ma, M., Ferguson, T. A., Schoch, K. M., Li, J., Qian, Y., Shofer, F. S., … Neumar, R. W. (2013). Calpains mediate axonal cytoskeleton disintegration during Wallerian degeneration. *Neurobiology of Disease*, *56*, 34–46. https://doi.org/https://doi.org/10.1016/j.nbd.2013.03.009

Mack, T. G. A., Reiner, M., Beirowski, B., Mi, W., Emanuelli, M., Wagner, D., … Coleman, M. P. (2001a). Wallerian degeneration of injured axons and synapses is delayed by a Ube4b/Nmnat chimeric gene. *Nature Neuroscience*, *4*, 1199. Retrieved from http://dx.doi.org/10.1038/nn770

Mack, T. G. A., Reiner, M., Beirowski, B., Mi, W., Emanuelli, M., Wagner, D., … Coleman, M. P. (2001b). Wallerian degeneration of injured axons and synapses is delayed by a Ube4b/Nmnat chimeric gene. *Nature Neuroscience*, *4*, 1199.

Mahad, D. H., Trapp, B. D. & Lassmann, H. (2015). Pathological mechanisms in progressive multiple sclerosis. *The Lancet Neurology*, *14*(2), 183–193. https://doi.org/10.1016/S1474-4422(14)70256-X

Mank, M. & Griesbeck, O. (2008). Genetically encoded calcium indicators. *Chemical Reviews*, *108*(5), 1550–1564. https://doi.org/10.1021/cr078213v

Marinkovic, P., Godinho, L. & Misgeld, T. (2015). Generation and Screening of Transgenic Mice with Neuronal Labeling Controlled by Thy1 Regulatory Elements. *Cold Spring Harb Protoc*, *2015*(10), pdb top087668. https://doi.org/10.1101/pdb.top087668

Martone, M. E., Zhang, Y., Simpliciano, V. M., Carragher, B. 0. & Ellisman, M. H. (1993). Three-Dimensional Visualization of the Smooth Reticulum in Purkinje Cell Dendrites Endoplasmic. *The Journal of Neuroscience*, *13*(11), 4636–4646. Retrieved from http://www.jneurosci.org/content/13/11/4636.long

Matute, C. (1998). Characteristics of acute and chronic kainate excitotoxic damage to the optic nerve. *Proceedings of the National Academy of Sciences of the*

United States of America, *95*(17), 10229–10234. Retrieved from http://www.ncbi.nlm.nih.gov/pmc/articles/PMC21490/

Medana, I. M. & Esiri, M. M. (2003). Axonal damage: a key predictor of outcome in human CNS diseases. *Brain : A Journal of Neurology*, *126*(Pt 3), 515–530.

Miller, B. F., Keles, E., Tien, L., Zhang, J., Kaplan, D., Lo, E. H. & Whalen, M. J. (2014). The Pharmacokinetics and Pharmacodynamics of Kollidon VA64 Dissociate its Protective Effects from Membrane Resealing after Controlled Cortical Impact in Mice. *Journal of Cerebral Blood Flow & Metabolism*, *34*(8), 1347–1353. https://doi.org/10.1038/jcbfm.2014.89

Miller, B. R., Press, C., Daniels, R. W., Sasaki, Y., Milbrandt, J. & DiAntonio, A. (2009). A dual leucine kinase–dependent axon self-destruction program promotes Wallerian degeneration. *Nature Neuroscience*, *12*, 387. Retrieved from http://dx.doi.org/10.1038/nn.2290

Misgeld, T. (2011). Lost in elimination: mechanisms of axonal loss. *E-Neuroforum*, *2*(2), 21–34. https://doi.org/10.1007/s13295-011-0017-2

Misgeld, T. & Kerschensteiner, M. (2006). In vivo imaging of the diseased nervous system. *Nat Rev Neurosci*, *7*(6), 449–463. https://doi.org/10.1038/nrn1905

Misgeld, T., Nikic, I. & Kerschensteiner, M. (2007). In vivo imaging of single axons in the mouse spinal cord. *Nat Protoc*, *2*(2), 263–268. https://doi.org/10.1038/nprot.2007.24

Miyawaki, A., Griesbeck, O., Heim, R. & Tsien, R. Y. (1999). Dynamic and quantitative Ca2+ measurements using improved cameleons. *Proceedings of the National Academy of Sciences*, *96*(5), 2135–2140. https://doi.org/10.1073/pnas.96.5.2135

Miyawaki, A., Llopis, J., Heim, R., McCaffery, J. M., Adams, J. A., Ikura, M. & Tsien, R. Y. (1997). Fluorescent indicators for Ca2+based on green fluorescent proteins and calmodulin. *Nature*, *388*, 882. Retrieved from http://dx.doi.org/10.1038/42264

Mori, F., Fukaya, M., Abe, H., Wakabayashi, K. & Watanabe, M. (2000). Developmental changes in expression of the three ryanodine receptor mRNAs in the mouse brain. *Neuroscience Letters*, *285*(1), 57–60.

Morris, R. (1992). Thy-1, the enigmatic extrovert on the neuronal surface. *BioEssays : News and Reviews in Molecular, Cellular and Developmental Biology*, *14*(10), 715–722. https://doi.org/10.1002/bies.950141014

Murphy, D. B. & Davidson, M. W. (2012). Fluorescence Imaging of Dynamic Molecular Processes. In *Fundamentals of Light Microscopy and Electronic Imaging* (pp. 233–263). Wiley-Blackwell. https://doi.org/10.1002/9781118382905.ch12

Nagai, T., Yamada, S., Tominaga, T., Ichikawa, M. & Miyawaki, A. (2004). Expanded dynamic range of fluorescent indicators for Ca(2+) by circularly permuted yellow fluorescent proteins. *Proceedings of the National Academy of Sciences of the United States of America*, *101*(29), 10554–10559. https://doi.org/10.1073/pnas.0400417101

Nakai, J., Ohkura, M. & Imoto, K. (2001). A high signal-to-noise Ca(2+) probe composed of a single green fluorescent protein. *Nature Biotechnology*, *19*(2), 137–141. https://doi.org/10.1038/84397

Navas-Navarro, P., Rojo-Ruiz, J., Rodriguez-Prados, M., Ganfornina, M. D.,

Looger, L. L., Alonso, M. T. & García-Sancho, J. (2016). GFP-Aequorin Protein Sensor for Ex Vivo and in Vivo Imaging of Ca2+ Dynamics in High-Ca2+ Organelles. *Cell Chemical Biology*, *23*(6), 738–745. https://doi.org/10.1016/j.chembiol.2016.05.010

Neukomm, L. J. & Freeman, M. R. (2014). Diverse cellular and molecular modes of axon degeneration. *Trends in Cell Biology*, *24*(9), 515–523. https://doi.org/10.1016/j.tcb.2014.04.003

Nikić, I., Merkler, D., Sorbara, C., Brinkoetter, M., Kreutzfeldt, M., Bareyre, F. M., … Kerschensteiner, M. (2011). A reversible form of axon damage in experimental autoimmune encephalomyelitis and multiple sclerosis. *Nat Med*, *17*(4), 495–499. https://doi.org/10.1038/nm.2324

Okubo, Y., Mikami, Y., Kanemaru, K. & Iino, M. (2018). Role of endoplasmic reticulum-mediated Ca^{2+} signaling in neuronal cell death. *Antioxidants & Redox Signaling*, 1–11. https://doi.org/10.1089/ars.2018.7498

Okubo, Y., Suzuki, J., Kanemaru, K., Nakamura, N., Shibata, T. & Iino, M. (2015). Visualization of Ca2+ Filling Mechanisms upon Synaptic Inputs in the Endoplasmic Reticulum of Cerebellar Purkinje Cells. *Journal of Neuroscience*, *35*(48), 15837–15846. https://doi.org/10.1523/JNEUROSCI.3487-15.2015

Ontaneda, D., Cohen, J. A. & Amato, M. P. (2017). Clinical outcome measures for progressive MS trials. *Multiple Sclerosis*, *23*(12), 1627–1635. https://doi.org/10.1177/1352458517729465

Osterloh, J. M., Yang, J., Rooney, T. M., Fox, A. N., Adalbert, R., Powell, E. H., … Freeman, M. R. (2012). dSarm/Sarm1 Is Required for Activation of an Injury-Induced Axon Death Pathway. *Science*, *337*(6093), 481 LP-484. Retrieved from http://science.sciencemag.org/content/337/6093/481.abstract

Ouardouz, M., Coderre, E., Basak, A., Chen, A., Zamponi, G. W., Hameed, S., … Stys, P. K. (2009). Glutamate receptors on myelinated spinal cord axons: I. glur6 kainate receptors. *Annals of Neurology*, *65*(2), 151–159. https://doi.org/10.1002/ana.21533

Ouardouz, M., Coderre, E., Zamponi, G. W., Hameed, S., Yin, X., Trapp, B. D. & Stys, P. K. (2009). Glutamate receptors on myelinated spinal cord axons: II. AMPA and GluR5 receptors. *Ann Neurol*, *65*(2), 160–166. https://doi.org/10.1002/ana.21539

Ouardouz, M., Nikolaeva, M. A., Coderre, E., Zamponi, G. W., McRory, J. E., Trapp, B. D., … Stys, P. K. (2003). Depolarization-induced Ca2+ release in ischemic spinal cord white matter involves L-type Ca2+ channel activation of ryanodine receptors. *Neuron*, *40*(1), 53–63. https://doi.org/10.1016/j.neuron.2003.08.016

Paillusson, S., Stoica, R., Gomez-Suaga, P., Lau, D. H. W., Mueller, S., Miller, T. & Miller, C. C. J. (2016). There's Something Wrong with my MAM; the ER-Mitochondria Axis and Neurodegenerative Diseases. *Trends in Neurosciences*, *39*(3), 146–157. https://doi.org/10.1016/j.tins.2016.01.008

Palmer, A. E., Jin, C., Reed, J. C. & Tsien, R. Y. (2004). Bcl-2-mediated alterations in endoplasmic reticulum Ca2+ analyzed with an improved genetically encoded fluorescent sensor. *Proceedings of the National Academy of Sciences*, *101*(50), 17404–17409. https://doi.org/10.1073/pnas.0408030101

Palmer, A. E., Qin, Y., Park, J. G. & McCombs, J. E. (2011). Design and

application of genetically encoded biosensors. *Trends in Biotechnology*, *29*(3), 144–152. https://doi.org/10.1016/j.tibtech.2010.12.004

Patrikios, P., Stadelmann, C., Kutzelnigg, A., Rauschka, H., Schmidbauer, M., Laursen, H., … Lassmann, H. (2006). Remyelination is extensive in a subset of multiple sclerosis patients. *Brain : A Journal of Neurology*, *129*(Pt 12), 3165–3172. https://doi.org/10.1093/brain/awl217

Patron, M., Raffaello, A., Granatiero, V., Tosatto, A., Merli, G., Stefani, D. De, … Rizzuto, R. (2013). The mitochondrial calcium uniporter (MCU): Molecular identity and physiological roles. *Journal of Biological Chemistry*, *288*(15), 10750–10758. https://doi.org/10.1074/jbc.R112.420752

Penas, C., Guzmán, M. S., Verdú, E., Forés, J., Navarro, X. & Casas, C. (2007). Spinal cord injury induces endoplasmic reticulum stress with different cell-type dependent response. *Journal of Neurochemistry*, *102*(4), 1242–1255. https://doi.org/10.1111/j.1471-4159.2007.04671.x

Peter, W. & David, R. (2011). The Unfolded Protein Response. *Science*, *1*(7), 1–3.

Pitt, D., Werner, P. & Raine, C. S. (2000). Glutamate excitotoxicity in a model of multiple sclerosis. *Nature Medicine*, *6*(1), 67–70. https://doi.org/10.1038/71555

Pivovarova, N. B. & Andrews, S. B. (2010, September). Calcium-dependent mitochondrial function and dysfunction in neurons. *The FEBS Journal*. https://doi.org/10.1111/j.1742-4658.2010.07754.x

Porter, K. R. (1953). Observations on a submicroscopic basophilic component of cytoplasm. *The Journal of Experimental Medicine*, *97*(5), 727–750.

Porter, K. R., Claude, A. & Fullam, E. F. (1945). A study of tissue culture cells by electron micoscopy. *The Journal of Experimental Medicine*, *81*(3), 233 LP-246.

Povlishock, J. T. (1992). Traumatically induced axonal injury: pathogenesis and pathobiological implications. *Brain Pathology (Zurich, Switzerland)*, *2*(1), 1–12.

Qi, X., Hosoi, T., Okuma, Y., Kaneko, M. & Nomura, Y. (2004). Sodium 4-phenylbutyrate protects against cerebral ischemic injury. *Molecular Pharmacology*, *66*(4), 899–908. https://doi.org/10.1124/mol.104.001339

Raeymaekers, L. & Larivière, E. (2011). Vesicularization of the endoplasmic reticulum is a fast response to plasma membrane injury. *Biochemical and Biophysical Research Communications*, *414*(1), 246–251. https://doi.org/10.1016/j.bbrc.2011.09.065

Ramirez, O. A. & Couve, A. (2011). The endoplasmic reticulum and protein trafficking in dendrites and axons. *Trends in Cell Biology*, *21*(4), 219–227. https://doi.org/10.1016/j.tcb.2010.12.003

Reeves, T. M., Greer, J. E., Vanderveer, A. S. & Phillips, L. L. (2010). Proteolysis of submembrane cytoskeletal proteins ankyrin-G and αII-spectrin following diffuse brain injury: A role in white matter vulnerability at nodes of ranvier. *Brain Pathology*, *20*(6), 1055–1068. https://doi.org/10.1111/j.1750-3639.2010.00412.x

Rigaud, M., Gemes, G., Weyker, P. D., Cruikshank, J. M., Kawano, T., Wu, H.-E. & Hogan, Q. H. (2009). Axotomy depletes intracellular calcium stores in primary sensory neurons. *Anesthesiology*, *111*(2), 381–392.

https://doi.org/10.1097/ALN.0b013e3181ae6212

Roderick, H. L., Lechleiter, J. D. & Camacho, P. (2000). Cytosolic phosphorylation of calnexin controls intracellular Ca2+ oscillations via an interaction with SERCA2b. *Journal of Cell Biology*, *149*(6), 1235–1247. https://doi.org/10.1083/jcb.149.6.1235

Rodriguez-Garcia, A., Rojo-Ruiz, J., Navas-Navarro, P., Aulestia, F. J., Gallego-Sandin, S., Garcia-Sancho, J. & Alonso, M. T. (2014). GAP, an aequorin-based fluorescent indicator for imaging Ca2+ in organelles. *Proceedings of the National Academy of Sciences of the United States of America*, *111*(7), 2584–2589. https://doi.org/10.1073/pnas.1316539111

Romanelli, E., Sorbara, C. D., Nikic, I., Dagkalis, A., Misgeld, T. & Kerschensteiner, M. (2013). Cellular , subcellular and functional in vivo labeling of the spinal cord using vital dyes, *8*(3), 481–490. https://doi.org/10.1038/nprot.2013.022

Ross, W. N. (2012). Understanding calcium waves and sparks in central neurons. *Nature Reviews Neuroscience*, *13*(March), 157–168. https://doi.org/10.1038/nrn3168

Rowland, A. A. & Voeltz, G. K. (2012). Endoplasmic reticulum-mitochondria contacts: function of the junction. *Nat Rev Mol Cell Biol*, *13*(10), 607–625. https://doi.org/10.1038/nrm3440

Rudolf, R., Magalhães, P. J. & Pozzan, T. (2006). Direct in vivo monitoring of sarcoplasmic reticulum Ca2+ and cytosolic cAMP dynamics in mouse skeletal muscle. *Journal of Cell Biology*, *173*(2), 187–193. https://doi.org/10.1083/jcb.200601160

Ruschel, J., Hellal, F., Flynn, K. C., Dupraz, S., Elliott, D. A., Tedeschi, A., … Bradke, F. (2015). Systemic administration of epothilone B promotes axon regeneration after spinal cord injury. *Science*, *348*(6232), 347 LP-352. Retrieved from http://science.sciencemag.org/content/348/6232/347.abstract

Samtleben, S., Jaepel, J., Fecher, C., Andreska, T., Rehberg, M. & Blum, R. (2013). Direct Imaging of ER Calcium with Targeted-Esterase Induced Dye Loading (TED). *Journal of Visualized Experiments*, (75), 1–17. https://doi.org/10.3791/50317

Sasaki, Y. & Milbrandt, J. (2010). Axonal degeneration is blocked by nicotinamide mononucleotide adenylyltransferase (Nmnat) protein transduction into transected axons. *Journal of Biological Chemistry*, *285*(53), 41211–41215. https://doi.org/10.1074/jbc.C110.193904

Saxena, S. & Caroni, P. (2007). Mechanisms of axon degeneration: From development to disease. *Progress in Neurobiology*, *83*(3), 174–191. https://doi.org/https://doi.org/10.1016/j.pneurobio.2007.07.007

Schindl, R., Muik, M., Fahrner, M., Derler, I., Fritsch, R., Bergsmann, J. & Romanin, C. (2009). Recent progress on STIM1 domains controlling Orai activation. *Cell Calcium*, *46*(4), 227–232. https://doi.org/10.1016/j.ceca.2009.08.003

Schumacher, A. M. (2015). *Die Rolle von Kalzium bei der axonalen Schädigung im Tiermodell der Multiplen Sklerose.* Ludwig-Maximilians-Universität München.

Schwarz, D. S. & Blower, M. D. (2016). The endoplasmic reticulum: Structure, function and response to cellular signaling. *Cellular and Molecular Life*

Sciences, *73*(1), 79–94. https://doi.org/10.1007/s00018-015-2052-6

Shibata, Y., Shemesh, T., Prinz, W. A., Palazzo, A. F., Kozlov, M. M. & Rapoport, T. A. (2010). Mechanisms Determining the Morphology of the Peripheral ER. *Cell*, *143*(5), 774–788. https://doi.org/10.1016/j.cell.2010.11.007

Shibata, Y., Voeltz, G. K. & Rapoport, T. A. (2006). Essay Rough Sheets and Smooth Tubules, (C), 435–439. https://doi.org/10.1016/j.cell.2006.07.019

Smith, K. J. (2007). Sodium channels and multiple sclerosis: roles in symptom production, damage and therapy. *Brain Pathology (Zurich, Switzerland)*, *17*(2), 230–242. https://doi.org/10.1111/j.1750-3639.2007.00066.x

Smith, K. J., Kapoor, R., Hall, S. M. & Davies, M. (2001). Electrically active axons degenerate when exposed to nitric oxide. *Annals of Neurology*, *49*(4), 470–476.

Sorbara, C. D., Wagner, N. E., Ladwig, A., Nikic, I., Merkler, D., Kleele, T., … Kerschensteiner, M. (2014). Pervasive axonal transport deficits in multiple sclerosis models. *Neuron*, *84*(6), 1183–1190. https://doi.org/10.1016/j.neuron.2014.11.006

Sorbara, C. D., Wagner, N. E., Ladwig, A., Nikic, I., Merkler, D., Kleele, T., … Marinkovi, P. (2014). Pervasive axonal transport deficits in multiple sclerosis models. *Neuron*, *84*(6), 1183–1190. https://doi.org/10.1016/j.neuron.2014.11.006

Sorbara, C., Misgeld, T. & Kerschensteiner, M. (2012). In vivo imaging of the diseased nervous system: an update. *Curr Pharm Des*, *18*(29), 4465–4470. Retrieved from http://www.ncbi.nlm.nih.gov/pubmed/22612742

Spacek, J. & Harris, K. M. (1997). Three-Dimensional Organization of Smooth Endoplasmic Reticulum in Hippocampal CA1 Dendrites and Dendritic Spines of the Immature and Mature Rat. *The Journal of Neuroscience*, *17*(1), 190 LP-203. Retrieved from http://www.jneurosci.org/content/17/1/190.abstract

Spira, M., Ruthi, O., Ada, D. & Daniel, G. (2003). Critical calpain- dependent ultrastructural alterations underlie the transformation of an axonal segment into a growth cone after axotomy of cultured Aplysia neurons. *Journal of Comparative Neurology*, *457*(3), 293–312. https://doi.org/doi:10.1002/cne.10569

Staal, J. A., Dickson, T. C., Gasperini, R., Liu, Y., Foa, L. & Vickers, J. C. (2010). Initial calcium release from intracellular stores followed by calcium dysregulation is linked to secondary axotomy following transient axonal stretch injury. *Journal of Neurochemistry*, *112*(5), 1147–1155. https://doi.org/10.1111/j.1471-4159.2009.06531.x

Steward, O. (1997). mRNA Localization in Neurons: Minireview A Multipurpose Mechanism? *Neuron*, *18*, 9–12.

Stirling, D. P., Cummins, K., Wayne Chen, S. R. & Stys, P. (2014). Axoplasmic reticulum Ca(2+) release causes secondary degeneration of spinal axons. *Annals of Neurology*, *75*(2), 220–229. https://doi.org/10.1002/ana.24099

Stirling, D. P. & Stys, P. K. (2010). Mechanisms of axonal injury: internodal nanocomplexes and calcium deregulation. *Trends Mol Med*, *16*(4), 160–170. https://doi.org/10.1016/j.molmed.2010.02.002

Stys, P. K. (1998). Anoxic and Ischemic Injury of Myelinated Axons in CNS White Matter: From Mechanistic Concepts to Therapeutics. *Journal of Cerebral*

Blood Flow & Metabolism, *18*(1), 2–25. https://doi.org/10.1097/00004647-199801000-00002

Suzuki, J., Kanemaru, K. & Iino, M. (2016). Genetically Encoded Fluorescent Indicators for Organellar Calcium Imaging. *Biophysical Journal*, *111*(6), 1119–1131. https://doi.org/10.1016/j.bpj.2016.04.054

Suzuki, J., Kanemaru, K., Ishii, K., Ohkura, M., Okubo, Y. & Iino, M. (2014). Imaging intraorganellar Ca2+ at subcellular resolution using CEPIA. *Nat Commun*, *5*(May), 4153. https://doi.org/10.1038/ncomms5153

Svoboda, K., Denk, W., Kleinfeld, D. & Tank, D. W. (1997). In vivo dendritic calcium dynamics in neocortical pyramidal neurons. *Nature*, *385*, 161. Retrieved from http://dx.doi.org/10.1038/385161a0

Tamsett, T. J., Picchione, K. E. & Bhattacharjee, A. (2009). NAD+ Activates K Na Channels in Dorsal Root Ganglion Neurons, *29*(16), 5127–5134. https://doi.org/10.1523/JNEUROSCI.0859-09.2009

Tang, S., Wong, H.-C. C., Wang, Z.-M. M., Huang, Y., Zou, J., Zhuo, Y., … Yang, J. J. (2011). Design and application of a class of sensors to monitor Ca2+ dynamics in high Ca2+ concentration cellular compartments. *Proceedings of the National Academy of Sciences*, *108*(39), 16265–16270. https://doi.org/10.1073/pnas.1103015108

Taylor, A. M., Blurton-Jones, M., Rhee, S. W., Cribbs, D. H., Cotman, C. W. & Jeon, N. L. (2005). A microfluidic culture platform for CNS axonal injury, regeneration and transport. *Nature Methods*, *2*, 599. Retrieved from http://dx.doi.org/10.1038/nmeth777

Terasaki, M. (2018). Axonal endoplasmic reticulum is very narrow. *Journal of Cell Science*, *131*(4), jcs210450. https://doi.org/10.1242/jcs.210450

Terasaki, M., Slater, N. T., Fein, A., Schmidek, A. & Reese, T. S. (1994). Continuous network of endoplasmic reticulum in cerebellar Purkinje neurons. *Proceedings of the National Academy of Sciences*, *91*(16), 7510–7514. https://doi.org/10.1073/pnas.91.16.7510

Thestrup, T., Litzlbauer, J., Bartholomäus, I., Mues, M., Russo, L., Dana, H., … Griesbeck, O. (2014). Optimized ratiometric calcium sensors for functional in vivo imaging of neurons and T lymphocytes. *Nature Methods*, *11*(2), 175–182. https://doi.org/10.1038/nmeth.2773

Thomas, N. & Williams, A. (2012). Pharmacology of ryanodine receptors and Ca2+-induced Ca2+ release. *Wiley Interdisciplinary Reviews: Membrane Transport and Signaling*, *1*(4), 383–397. https://doi.org/10.1002/wmts.34

Trapp, B. D., Peterson, J., Ransohoff, R. M., Rudick, R., Mörk, S. & Bö, L. (1998). Axonal Transection in the Lesions of Multiple Sclerosis. *New England Journal of Medicine*, *338*(5), 278–285. https://doi.org/10.1056/NEJM199801293380502

Tsukita, S. & Ishikawa, H. (1976). Three-dimensional distribution of smooth endoplasmic reticulum in myelinated axons. *Journal of Electron Microscopy*, *25*(3), 141–149. Retrieved from http://dx.doi.org/10.1093/oxfordjournals.jmicro.a050013

Vargas, M. E., Yamagishi, Y., Tessier-Lavigne, M. & Sagasti, A. (2015). Live Imaging of Calcium Dynamics during Axon Degeneration Reveals Two Functionally Distinct Phases of Calcium Influx. *Journal of Neuroscience*,

35(45), 15026–15038. https://doi.org/10.1523/JNEUROSCI.2484-15.2015

Veldwijk, M. R., Topaly, J., Laufs, S., Hengge, U. R., Wenz, F., Zeller, W. J. & Fruehauf, S. (2002). Development and optimization of a real-time quantitative PCR-based method for the titration of AAV-2 vector stocks. *Molecular Therapy : The Journal of the American Society of Gene Therapy*, *6*(2), 272–278.

Verkhratsky, A. (2005). Physiology and pathophysiology of the calcium store in the endoplasmic reticulum of neurons. *Physiological Reviews*, *85*(1), 201–279. https://doi.org/10.1152/physrev.00004.2004

Vidal, M., Morris, R., Grosveld, F. & Spanopoulou, E. (1990). Tissue-specific control elements of the Thy-1 gene. *The EMBO Journal*, *9*(3), 833–840. Retrieved from http://www.ncbi.nlm.nih.gov/pmc/articles/PMC551743/

Villegas, R., Martinez, N. W., Lillo, J., Pihan, P., Hernandez, D., Twiss, J. L. & Court, F. A. (2014). Calcium release from intra-axonal endoplasmic reticulum leads to axon degeneration through mitochondrial dysfunction. *J Neurosci*, *34*(21), 7179–7189. https://doi.org/10.1523/JNEUROSCI.4784-13.2014

Voeltz, G. K., Rolls, M. M. & Rapoport, T. A. (2002). EMBO reports Structural organization of the endoplasmic reticulum, *3*(10), 944–950.

Wang, J. T., Medress, Z. A. & Barres, B. A. (2012). Axon degeneration: Molecular mechanisms of a self-destruction pathway. *Journal of Cell Biology*, *196*(1), 7–18. https://doi.org/10.1083/jcb.201108111

Wang, S. S., Denk, W. & Häusser, M. (2000). Coincidence detection in single dendritic spines mediated by calcium release. *Nature Neuroscience*, *3*(12), 1266–1273. https://doi.org/10.1038/81792

Westrate, L. M., Lee, J. E., Prinz, W. A. & Voeltz, G. K. (2015). Form Follows Function : The Importance of Endoplasmic Reticulum Shape. https://doi.org/10.1146/annurev-biochem-072711-163501

Wilkins, A. & Scolding, N. (2008). Protecting axons in multiple sclerosis. *Multiple Sclerosis*, *14*(8), 1013–1025. https://doi.org/10.1177/1352458508091370

Williams, P. R., Marincu, B. N., Sorbara, C. D., Mahler, C. F., Schumacher, A. M., Griesbeck, O., … Misgeld, T. (2014). A recoverable state of axon injury persists for hours after spinal cord contusion in vivo. *Nat Commun*, *5*, 5683. https://doi.org/10.1038/ncomms6683

Witte, M. E., Schumacher, A.-M., Mahler, C. F., Bewersdorf, J. P., Lehmitz, J., Scheiter, A., … Kerschensteiner, M. (2019). Calcium Influx through Plasma-Membrane Nanoruptures Drives Axon Degeneration in a Model of Multiple Sclerosis. *Neuron*, *101*(4), 615–624.e5. https://doi.org/10.1016/j.neuron.2018.12.023

Wu, J., Prole, D. L., Shen, Y., Lin, Z., Gnanasekaran, A., Liu, Y., … Campbell, R. E. (2014). Red fluorescent genetically encoded Ca 2+ indicators for use in mitochondria and endoplasmic reticulum. *Biochemical Journal*, *464*(1), 13–22. https://doi.org/10.1042/BJ20140931

Wu, J., Ryskamp, X. D. A., Liang, X., Egorova, P., Zakharova, X. O. & Hung, G. (2016). Enhanced Store-Operated Calcium Entry Leads to Striatal Synaptic Loss in a Huntington ' s Disease Mouse Model, *36*(1), 125–141. https://doi.org/10.1523/JNEUROSCI.1038-15.2016

Wu, M. M., Llopis, J., Adams, S., Mccaffery, J. M., Kulomaa, M. S., Machen, T. E.,

… Tsien, R. Y. (2000). Organelle pH studies using targeted avidin and fluorescein – biotin. *Chemistry & Biology*, Volume 7, Issue 3, 197 - 209. https://doi.org/10.1016/S1074-5521(00)00088-0

Wu, Y., Whiteus, C., Xu, C. S., Hayworth, K. J., Weinberg, R. J., Hess, H. F. & De Camilli, P. (2017). Contacts between the endoplasmic reticulum and other membranes in neurons. *Proceedings of the National Academy of Sciences*, *114*(24), E4859–E4867. https://doi.org/10.1073/pnas.1701078114

Yamauchi, T., Sakurai, M., Abe, K., Matsumiya, G. & Sawa, Y. (2007). Impact of the endoplasmic reticulum stress response in spinal cord after transient ischemia. *Brain Research*, *1169*, 24–33. https://doi.org/https://doi.org/10.1016/j.brainres.2007.06.093

Yang, J., Weimer, R. M., Kallop, D., Olsen, O., Wu, Z., Renier, N., … Tessier-Lavigne, M. (2013). Regulation of axon degeneration after injury and in development by the endogenous calpain inhibitor calpastatin. *Neuron*, *80*(5), 1175–1189. https://doi.org/10.1016/j.neuron.2013.08.034

Yang, J., Wu, Z., Renier, N., Simon, D. J., Uryu, K., Park, D. S., … Tessier-Lavigne, M. (2015). Pathological Axonal Death through a MAPK Cascade that Triggers a Local Energy Deficit. *Cell*, *160*(1), 161–176. https://doi.org/10.1016/j.cell.2014.11.053

Yin, X., Kidd, G. J., Ohno, N., Perkins, G. A., Ellisman, M. H., Bastian, C., … Trapp, B. D. (2016). Proteolipid protein-deficient myelin promotes axonal mitochondrial dysfunction via altered metabolic coupling. *Journal of Cell Biology*, *215*(4), 531–542. https://doi.org/10.1083/jcb.201607099

Zhao, Y., Araki, S., Wu, J., Teramoto, T., Chang, Y. F., Nakano, M., … Campbell, R. E. (2011). An expanded palette of genetically encoded Ca(2)(+) indicators. *Science*, *333*(6051), 1888–1891. https://doi.org/10.1126/science.1208592

Ziv, N. E. & Spira, M. E. (1993). Spatiotemporal Distribution of Ca2+ Following Axotomy and Throughout the Recovery Process of Cultured Aplysia Neurons. *European Journal of Neuroscience*, *5*(6), 657–668. https://doi.org/10.1111/j.1460-9568.1993.tb00531.x

Zündorf, G. & Reiser, G. (2011). Calcium Dysregulation and Homeostasis of Neural Calcium in the Molecular Mechanisms of Neurodegenerative Diseases Provide Multiple Targets for Neuroprotection. *Antioxidants & Redox Signaling*, *14*(7), 1275–1288. https://doi.org/10.1089/ars.2010.3359

7 Acknowledgements

First, I would like to thank my supervisors, Prof. Martin Kerschensteiner (LMU) and Prof. Thomas Misgeld (TUM), for the unique opportunity to do research in their laboratories and for their vigorous support. I truly appreciated the environment of great creativity which nurtured my interest in the field of neurodegeneration and multiple sclerosis. The introduction and pursuit of my own ideas was always encouraged and valued, which was a substantial source of motivation for me. Having two supervisors with their combined expertise paved the way to a successful project. I benefitted noticeably from their analytical and rigorous way of conducting science. From the beginning, I enjoyed working on the carefully chosen scientific topic, particularly because of the previous inspiring achievements of my colleagues Maarten Witte, Adrian-Minh Schumacher, Christoph Mahler and Jan Bewersdorf. I am especially grateful for their friendship and support and for the continuous, lively scientific discussions we had. I am also grateful for the extraordinary support of all members of the two laboratories. I would like to especially thank Caroline Fecher, Selin Kenet, Charlène Granier, Peter Bradley, Elisa Romanelli, Delphine Theodorou and Giuseppe Locatelli for introducing me to the numerous methods used in this paper. I would also like to thank Dr. Florence Bareyre and Dr. Leanne Godinho for their exceptional advice and help concerning molecular cloning. I am grateful to Ronald Naumann for performing the successful pronucleus injections and delivering the founder lines in person. Jonas Lehmitz continued the ER project after I went back to medical school; I am indebted to him for the great vigour with which he continued pursuing the project, thereby contributing substantially to its success. It was an enormous pleasure to work together with him as friends, and our discussions were always inspiring and fruitful.

Finally, I cannot thank enough Andrea and my family for their endearing and unconditional support.

8 Curriculum vitae

Persönliche Angaben	
Name	Scheiter, Alexander Julian
Staatsbürgerschaft	Deutsch
Geburtsdatum und -ort	14.12.1991, Herrenberg

Klinische Ausbildung	
	Facharztweiterbildung: ○ ab 02/19: Institut für Pathologie, Universität Regensburg Praktisches Jahr: ○ 07/18 – 10/18: Pathologie, Klinikum Rechts der Isar, TU München ○ 03/18 – 06/18: Innere Medizin, Klinikum Bogenhausen, München ○ 11/17 – 03/18: Chirurgie, Klinikum Bogenhausen, München Famulaturen: ○ 02/17: Ambulanz Klinische Neuroimmunologie, LMU München ○ 08/15: Allgemeinmedizin, Dres. Kadauke, Sindelfingen ○ 07/15: Neurologie, kbo-Isar-Amper-Klinikum München-Ost, Haar ○ 08/14: Radioonkologie, LMU München

Forschung	
Ab 2019	Arbeitsgruppe experimentelle Tumorpathologie, Universität Regensburg, AG Calvisi
2015 – 2019	Medizinische Doktorarbeit: ○ Institut für Klinische Neuroimmunologie, LMU, AG Kerschensteiner ○ 10/15 – 10/16: Vollzeittätigkeit
2012 – 2013	Studentische Hilfskraft: ○ Untersuchungen zum Calbindin ○ Betreuung des Laborpraktikums ○ Institut für Physiologie - Molekulare Neurophysiologie, LMU, AG Meyer

Akademische Ausbildung	
2011 – 2018	Medizinstudium: ○ Gesamtnote: 1,33 ○ Klinischer Abschnitt: – Technische Universität München – 11/18: Dritter Abschnitt der Ärztlichen Prüfung – Note: 1,0 – 10/17: Zweiter Abschnitt der Ärztlichen Prüfung Note: 2,0 ○ Vorklinischer Abschnitt: – Ludwig-Maximilians-Universität München – 08/13: Erster Abschnitt der Ärztlichen Prüfung Note: 1,0
2002 – 2011	Abitur: ○ Gymnasium Unterrieden Sindelfingen ○ Note: 1,1
Stipendium	
2017 - 2018	Deutschlandstipendium TUM
Veröffentlichungen	
2019	Witte, M. E., Schumacher, A.-M., Mahler, C. F., Bewersdorf, J. P., Lehmitz, J., Scheiter, A., Sánchez, P., Williams, P. R., Griesbeck, O., Naumann, R., Misgeld, T., Kerschensteiner, M. (2019). Calcium Influx through Plasma-Membrane Nanoruptures Drives Axon Degeneration in a Model of Multiple Sclerosis. Neuron, 101(4), 615–624.e5. https://doi.org/10.1016/j.neuron.2018.12.023
September 2016	Abstract und Poster (Axoplasmic reticulum calcium dynamics), EMBO Workshop Organelle Contact Sites, Domus de Maria, Italien

9 Affidavit / Eidesstattliche Versicherung

LMU LUDWIG-MAXIMILIANS-UNIVERSITÄT MÜNCHEN

Promotionsbüro
Medizinische Fakultät

MMRS MUNICH MEDICAL RESEARCH SCHOOL

Eidesstattliche Versicherung

Scheiter, Alexander Julian

Name, Vorname

Ich erkläre hiermit an Eides statt,

dass ich die vorliegende Dissertation mit dem Titel

Die Dynamik des axoplasmatischen Retikulums in Modellen der Neuroinflammation und des spinalen Traumas

selbständig verfasst, mich außer der angegebenen keiner weiteren Hilfsmittel bedient und alle Erkenntnisse, die aus dem Schrifttum ganz oder annähernd übernommen sind, als solche kenntlich gemacht und nach ihrer Herkunft unter Bezeichnung der Fundstelle einzeln nachgewiesen habe.

Ich erkläre des Weiteren, dass die hier vorgelegte Dissertation nicht in gleicher oder in ähnlicher Form bei einer anderen Stelle zur Erlangung eines akademischen Grades eingereicht wurde.

Neustadt an der Donau, 19.05.2020

Ort, Datum

Alexander Julian Scheiter

Unterschrift Doktorand